

Travelling Fires Methodology and Probabilistic Design of Structures

Mohammad HEIDARI

Imperial College London

Department of Mechanical Engineering

A thesis submitted for the degree of

Doctor of Philosophy

2021

Supervised by Prof. Guillermo Rein

Copyright

Mohammad Heidari, 2021

All rights reserved

Declaration of Originality

I declare that this thesis and the work described within have been completed solely by Mohammad Heidari under the supervision of Prof. Guillermo Rein. Where others have contributed or other sources are quoted, full references are given.

Mohammad Heidari

2021

Copyright Declaration

The copyright of this thesis rests with the author and is made available under a Creative Commons Attribution Non-Commercial No Derivatives licence. Researchers are free to copy, distribute or transmit the thesis on the condition that they attribute it, that they do not use it for commercial purposes and that they do not alter, transform, or build up on it. For any reuse or redistribution, researchers must make clear to others the licence terms of this work.

To my partner Mathilde.

Abstract

Travelling Fires Methodology and Probabilistic Design of Structures

by

Mohammad HEIDARI

Doctor of Philosophy in Mechanical Engineering

Imperial College London, 2021

Supervised by Prof. Guillermo Rein

Fire is a hazard and a building's structure must be designed to maintain their structural stability when exposed to fire. Fire safety design of structures can be done following the prescriptive codes or carrying out a performance-based design. Prescriptive fire design codes describe how buildings should be built to fulfil generic fire resistance requirements depending on their use, height, or compartment area. Performance fire design allows derivation of structural fire resistance of buildings by characterizing the fire dynamics within a compartment and analysing the thermal and mechanical response of the structures.

Travelling fires methodology (TFM) characterises the fire dynamics for the performance-based design of large compartments, which assumes that as fires burn, they travel along the compartment floor as flames spread. TFM is a design tool based on several assumptions. This thesis revisits and addresses its near field assumptions and applies a probabilistic model to assess the reliability of a structural element exposed to travelling fires and the uniform temperature fire. This work studies the horizontal flame extension under the ceiling, which affects duration of the heating exposure of the structural members and their load-bearing capacity. This study reformulates the TFM in terms of heat fluxes rather than temperatures, allowing for a more formal treatment of heat transfer. The Hasemi, Wakamatsu and Lattimer empirical expressions of heat flux from flames were applied for the near field. The analysis showed that the near field length with flame extension (fTFM) is between 1.5 and 6.5 times longer than without flame extension meaning that more structural elements are affected by

the direct impact of the flame. The highest peak heat flux is obtained for small fires sizes, using flame extension and the Wakamatsu expression.

The observations and findings from two travelling fire experiments, x-TWO.1 and x-TWO.2, conducted inside a very large compartment with an area of 380 m² in Poland, are presented. A uniform continuous wood crib along 29 m of the 35 m compartment provided the fuel load density of 345 MJ/m² in x-TWO.1 and 273 MJ/m² in x-TWO.2. In both experiments, the fire was observed to travel with clear leading and trailing edges and flashover was not observed. Flame spread was accelerating in x-TWO.1 and at a constant rate in x-TWO.2. The non-uniform distributions of temperatures are remarkably different from the conditions typically assumed in other scenarios/standards and could therefore lead to different failure times and mechanisms.

A detailed sensitivity study was carried out for the main input parameters in the uniform temperature fire methodology, and in the heat transfer calculations. This was done to assess the sensitivity of structural element response to input parameter uncertainty. The sensitivity analysis identified the most influential input parameters for the structure and the range of values for each input parameter for which the design is structurally safe.

To study comprehensively the structural fire design of open plan compartments and modern buildings, a simple probabilistic methodology was applied. Probabilistic approach defined the reliability of a fire-affected structure following the uniform fire condition methodology and FTFM methodology, while accounting for uncertainties in input parameters. The probabilistic analysis allowed quantification of the reliability of a structural element in terms of the likelihood of collapse for different fire scenarios. This study demonstrates that both sensitivity and probabilistic analyses can provide a comprehensive understanding of the factors affecting the structural fire resistance of a building and can further inform detailed fire safety and structural analysis. This work presented in this thesis is dealing with design purposes of non-combustible structures.

Acknowledgement

I would like to thank my supervisor and confidant Prof. Guillermo Rein for his insightful guidance. Our meeting in your office, in Paris, calls, and emails during this Ph.D. were extremely important in the development of this study. Your constant encouragement, optimism, intelligence led me here. I have learned a lot from you. My special thanks for your generous support and advice since I have been your student in my master's degree. I am looking forward to our future collaborations.

I am extremely grateful for the support of CERIB in funding this research. I would like to thank you, Fabienne Robert, Christophe Tessier, and Gilles Bernardeau for making this all happen. Thanks to all CERIB colleagues who supported this work during these years.

In particular, my sincere thanks go to Fabienne, who had an indispensable role in the development of this project. Your tremendous support and encouragement, patience, and kindness directed me here. You have been always available for our conversations and provided me incredible guidance during this project, but also during my uncertain times. It has been a real pleasure to exchange and work closely with you.

The expert advice and inspiring discussions with Christophe, even after work, have been precious during these years. Thanks for all your encouragement and having faith in me.

I would like to thank my industrial supervisor, Panos Kotsovinos for providing ideas and enthusiastic conversations. Your 'Eureka moment', support, and our meetings (held even next to Niagara fall) helped to form this work. We missed our metro stations a few times during the deep discussions, but the fruitful results are here in this work. I am looking forward to future collaborations.

x-TWO and x-ONE experiments were a great experience for me, for which I would like to appreciate the team members of the experiments. Thank you Egle, Matt and Harry who kindly proofread my work, Francesco, Nieves, Eirik, Nils, Wojciech, Piotr, Darek, Piotr, Izabella, Franz, Yuqi, Chloe, Rahul, Sebastien, and polish firefighters.

Julien, Philippe, Cecile, Jean-Christophe, Sarah, Nico, and all nice friends have provided comfort, support, and inspiration throughout my studies, so thanks to them!

I am very grateful to all my family in Iran and France for all you have done for me and for giving me such incredible support- thank you!

And most importantly, I would like to thank Mathilde for her presence and her patience. You have been an absolutely incredible partner throughout these years. You were my home supervisor who patiently listened to me and encouraged me during the last four years. Our discussions during the walk in the woods of Petites Dalles were always inspiring. You have done so much for me in terms of all the little things, but also the big ones. For that, I am extremely grateful and incredibly happy to have you in my life.

Table of Contents

Declaration of Originality	ii
Copyright Declaration	iii
Abstract	v
Acknowledgement	vii
Table of Contents	ix
Nomenclature	xii
Preface	xvi
Chapter 1	1
Introduction	1
1.1 Fire and Structure	1
1.2 Fire Methodology for Small Compartments	3
1.3 Fire Methodology for Very Large Compartments.....	6
1.4 Motivation	9
1.5 Outline of Thesis	10
Chapter 2	12
Probabilistic Study of the Resistance of a Simply-supported Reinforced Concrete Slab, according to a Eurocode Parametric Fire	12
2.1 Introduction	13
2.2 Methodology.....	14
2.3 Case Study	19
2.4 Design Fire	21
2.5 Parametric Sensitivity Study using OAT	23
2.5.1 Characteristic Fire Load Density.....	23
2.5.2 Fire Fighting Measures Index	25
2.5.3 Axis Distance of Reinforcement	26
2.5.4 Opening Factor	27

2.5.5	Concrete Density	27
2.5.6	Other Parameters.....	28
2.6	Probabilistic Assessment of Structural Fire Safety	29
2.7	Results of the Monte Carlo Analysis and Discussion	32
2.8	Conclusion.....	34
Chapter 3	37
Flame Extension and the Near Field under the Ceiling for Travelling Fires Inside Large Compartments	37
3.1	Introduction	38
3.2	Flame Extension in Compartment Fires.....	39
3.3	Travelling Fires with Flame Extension.....	43
3.3.1	Background to TFM	43
3.3.2	TFM with Flame Extension (fTFM)	44
3.3.3	Heat Flux Boundary Condition	49
3.4	Comparison for a Generic Structure	50
3.4.1	Heat Flux and Flame Extension Length	52
3.4.2	Thermal Analysis	58
3.5	Conclusion.....	62
Chapter 4	65
Probabilistic Thermal Analysis of a Concrete Compartment Subjected to Travelling Fires with Flame Extension and Parametric Fires	65
4.1	Introduction	65
4.2	Methodology.....	66
4.3	Case Study.....	69
4.4	Probabilistic Analysis and Results	70
4.5	Conclusion.....	76
Chapter 5	78
Effect of Fuel Load on Fire Dynamics in Very Large and Open-Plan Compartment: x-TWO.....		78

5.1	Introduction	79
5.2	The x-TWO Building	80
5.3	Fire Protection of the Structure	81
5.4	Ventilation.....	81
5.5	Fuel Load	82
5.6	Instrumentations and Data Collection	85
5.7	Experimental Results	88
5.7.1	Observations and Fire Characteristics.....	88
5.7.2	Fire Spread	90
5.7.3	Gas Temperature.....	94
5.8	Comparison Between x-TWO and Design Fires	100
5.9	Conclusion.....	102
Chapter 6	104
Conclusions and future work	104
6.1	Conclusions	104
6.2	Future Work.....	108
References	109
Appendix	120

Nomenclature

A_f	surface area of the floor [m^2]
A_t	total surface area of the enclosure [m^2]
A_v	total vertical opening on all walls [m^2]
H_{eq}	weighted average of window heights on the wall [m]
O	opening factor [$m^{1/2}$]
b	thermal inertia of the enclosure boundary [$Ws^{1/2}/m^2Km$]
m	combustion factor
$q_{f,d}$	design fire load density related to the surface area A_f [MJ/m^2]
$q_{f,k}$	characteristic fire load density for an office building
$q_{t,d}$	design fire load density related to the total surface area A_t [MJ/m^2]
δ_n	factor for different active firefighting measures
δ_{q1}	factor for fire activation risk due to the size of the compartment
δ_{q2}	factor for fire activation risk due to the type of occupancy
D	diameter of the fire [m]
d	thickness of insulation [m]
F	surface area of member [m^2]
H	ceiling height above fire source [m]
h	convective coefficient [W/m^2]
K	concrete conductivity [Wm/K]
L	length of the compartment [m]
L_H	horizontal flame length along the ceiling [m]
L_f	length of the fire [m]

L_t^*	dimensionless length of the fire
Q	heat release rate [W]
Q^*	dimensionless heat release related to height H of the compartment
Q_D^*	dimensionless heat release related to the diameter D of the fire
Q_L^*	dimensionless heat release related to fire length L of fire at time t
Q''	heat release rate per unit area [W/m^2]
q_f	fuel load density [J/m^2]
q_c''	received heat flux to the ceiling [kW/m^2]
q_{net}''	net heat flux [kW/m^2]
q_{rad}''	net heat flux to unit surface area due to radiation [kW/m^2]
q_{con}''	net heat flux to unit surface area due to convection [kW/m^2]
q_g''	gauge heat flux [kW/m^2]
r	horizontal distance between the centerline axis of the fire and a point along the ceiling
s	flame spread rate [m/s]
s_{min}	maximum fire spread rate [m/s]
s_{max}	minimum fire spread rate [m/s]
T_f	fire temperature [$^{\circ}C$]
T_s	surface temperature [$^{\circ}C$]
T_g	gas temperature [$^{\circ}C$]
T_{∞}	ambient temperature [$^{\circ}C$]
T_{ff}	far field temperature [$^{\circ}C$]
T_{nf}	near field fire temperature [$^{\circ}C$]
T_i^t	concrete temperature at instantaneous time t and location i [$^{\circ}C$]
t	time [s]

t_b	local burning time [s]
t_t	total fire duration [s]
V	volume of steel per length [m ³]
W	width of the compartment [m]
x	location of interest in the compartment [m]
x'	location of the leading edge of the fire relative to the end of the compartment where fire started [m]
y	normalized distance along ceiling
z'	virtual origin of fire [m]
\emptyset	view factor
ε_f	emissivity of the flame of the fire
ε_s	surface emissivity
ΔT_m	change in steel member temperature
Δt	time step [s]
Δx	element length [m]
c	specific heat [J/kgK] (i: insulation, s: steel; c: concrete)
ρ	density [kg/m ³] (i: insulation, s: steel; c: concrete)
σ	Stephan Boltzmann constant (=5.67·10 ⁻⁸ [W/m ² K ⁴])

Abbreviations

EC	Eurocode
fTFM	Travelling fires methodology with flame extension
iTFM	Improved travelling fires methodology
OAT	One-at-a-time
RTM	Maximum rebar temperature in concrete
TFM	Travelling fires methodology
x-TWO.1	x-TWO Part 1
x-TWO.2	x-TWO Part 2

Preface

The material is presented as follows in this thesis:

Chapter 1 is a brief introduction to the fire and structure, specifying the motivations and objectives of this thesis.

Chapter 2 presents the application of the traditional fire methodology with uniform temperature in current codes (i.e., EC 1-1-2 parametric fire) on a concrete slab. This chapter performs a sensitivity analysis to the main parameters in the fire methodology with uniform temperature and in the heat transfer calculations using a one-at-a-time (OAT) method. This chapter applies a probabilistic approach to determine the reliability of a structural element exposed to fire. This chapter is based on:

Heidari, M., Robert, F., Lange, D., and Rein, G., 2019. *Probabilistic Study of the Resistance of a Simply-Supported Reinforced Concrete Slab According to Eurocode Parametric Fire*. **Fire Technology** 55, 1377–1404. <https://doi.org/10.1007/s10694-018-0704-4>.

Chapter 3 presents the detailed development of the methodology of travelling fires with flame extension, “fTFM”. The methodology is applied to an open-plan generic office compartment of 960 m² floor area. This chapter is based on:

Heidari, M., Kotsovinos, P., and Rein, G., 2020. *Flame extension and the near field under the ceiling for travelling fires inside large compartments*, **Fire and Materials.**, vol. 44, no. 3, pp. 423–436, [https://doi: 10.1002/fam.2773](https://doi:10.1002/fam.2773).

Chapter 4 presents how the fTFM methodology, which was developed in this thesis, can be applied probabilistically. The chapter studies probabilistically the reliability of a fire-affected structure following the uniform fire condition methodology and fTFM methodology. This chapter is intended to be published in a journal (a draft is being prepared for publication in a journal).

Chapter 5 presents the observation and results of the x-TWO traveling fire experiment that I led in 2019 in Poland. This was the largest compartment fire ever done in the history of compartment fires. The experiment provided valuable data in traveling fire dynamics. A part of this experiment has been published as (a draft is being prepared for publication of the full paper in a journal):

Heidari, M., Rackauskaite, E., Bonner, M., Christensen, E., Morat, S., Mitchell, H., Kotsovinos, P., Turkowski, P., Wegrzynski, W., Tofilo, P., and Rein, G., 2020. *Fire experiments inside a very large and open-plan compartment: x-TWO*. Proceeding of the *11th International Conference on Structures in Fire (SiF2020)*, 2020. Brisbane, QLD Australia: The University of Queensland.

Heidari, M., Rackauskaite, E., Christensen E., Bonner M., Morat, S., Mitchell, H., Kotsovinos, P., Turkowski, P., Wegrzynski, W., Tofilo, P., and Rein, G., 2021. *Effect of Fuel Load on Fire Dynamics in Very Large and Open-Plan Compartment: x-TWO experiments*, **Fire and Technology** (A draft is ready for submission).

Chapter 6 is a conclusion for this thesis and presents recommended future work.

Appendix provides the sensitivity analysis results performed in Chapter 2.

Other Publications

The following scholarly output has also been produced as an outcome of this research:

Conference Oral Presentations:

Probabilistic Study of the Resistance of a Simply-Supported Reinforced Concrete Slab according to Eurocode Parametric Fire, **Workshop on probabilistic methods in structural fire engineering**, SP Technical Research Institute of Sweden, October 20-21, 2016.

Revisiting the Near-field formulation of Travelling Fires in Very Large Compartments, **The 15th International Interflam Conference**, University of Nottingham, UK, July 2019.

Fire experiments inside a very large and open-plan compartment: x-TWO. **11th International Conference on Structures in Fire (SiF2020)**, 30 November - 2 December 2020. Brisbane, QLD Australia: The University of Queensland.

Conference Papers:

Heidari, M., Kotsovinos, P., Rein, G., *Revisiting the Near-field formulation of Travelling Fires in Very Large Compartments*, **The 15th International Interflam Conference**, University of Nottingham, UK, July 2019.

Heidari, M., Rackauskaite, E., Bonner, M., Christensen, E., Morat, S., Mitchell, H., Kotsovinos, P., Turkowski, P., Wegrzynski, W., Tofilo, P., and Rein, G., *Fire experiments inside a very large and open-plan compartment: x-TWO*. **11th International Conference on Structures in Fire (SiF2020)**, Online, 30 November - 2 December 2020. Brisbane, QLD Australia: The University of Queensland.

Chapter 1

Introduction

1.1 Fire and Structure

Structural materials lose strength and expand at high temperatures [1], [2]. As a result, structural elements could lose their stability and ability to resist the load-bearing when exposed to fire. This can result in the collapse of a structure putting into threat the life safety of occupants and fire-fighters since structural stability is the last protective measure. Some recent incidents of partial or complete fire-induced structural collapses of buildings are: Garley Building (Hong Kong, 1996), Interstate Tower (California, 1988), One Meridian Plaza (Philadelphia, 1999), World trade center (New York, 2001), Windsor Tower (Spain, 2005), Plasco Building (Tehran, 2017), as illustrated in Figure 1.1.



Garley Building



Interstate Tower



One Meridian Plaza



World trade center



Windsor Tower



Plasco Building

Figure 1.1 Examples of fire-induced collapse of buildings.

Therefore, to limit the risk to the occupants and firefighters, *“the construction works must be designed and build in such a way, that in the event of an outbreak of fire, the generation and spread of fire and smoke within the works are limited, and the load-bearing resistance of the construction can be assumed for a specified period of time and the spread of fire to neighbouring construction works is limited”* [3]. The full duration of fire should be considered for the structural fire design when the temperature-time curve accounts for the cooling phase. These are the example of the essential requirement for the limitation of fire risks to the occupants and rescue teams, as stated in Eurocode 1991-1-2 (EC 1-1-2) (General actions - Actions on structures exposed to fire) and Construction Products Directive 89/106/EEC [3].

Fire safety design of structures can be done following the prescriptive codes or performing a performance-based design to show the compliance of a structure with the essential requirements.¹

Prescriptive design codes simply describe how buildings should be built to fulfil generic fire resistance requirements depending on their use and other characteristics, such as height or compartment area. The prescriptive approaches have been developed assuming a simple fire scenario in a small compartment. Therefore, this approach sets limitations to the building (e.g., maximum compartment area), which is a challenge (or not applicable) for the architectural design innovations with typical examples being very large open compartments, buildings with atriums, or glazing façades.

As alternative way to achieve the aforementioned essential requirement is through performance-based design and first principles structural fire engineering. The performance-based design allows the derivation of structural fire resistance of buildings based on a first principles approach by characterizing the fire dynamics within a compartment and the structure's subsequent thermal and mechanical response.

The first step is thus to determine the fire dynamics (i.e., thermal action, temperature) inside the compartment fire. The thermal action to which the structural elements are being exposed can be defined in the form of temperature-time or heat flux-time curves. These curves are used as boundary conditions for the heat transfer calculation and the mechanical analysis of structural members under

¹ Performance-based fire design is emerging in most jurisdictions though some countries are restricted to objective based codes. Which are based on alternative solutions, or performance-based fire design, being demonstrated as equivalent if not safer than the prescriptive code.

a fire condition (i.e., thermomechanical analysis of the structure). The heat transfer analysis defines the temperature inside structural elements, and the structural analysis demonstrates the behaviour of structure such as the deflection, load bearing, the level of stress, and strain in structural members. It is then possible to verify whether the member temperature, the deflection of an element, and the fire-induced stress are within the acceptable values (which is called acceptance criterion in the US). This ensures that structural failure or compartmentation failure does not occur, and fire protection products are used within their tested limits.

Different methodologies have been developed to quantify the thermal environment for structural design such as Method of Babrauskas [4], [5], Method of Law [6], Japanese Model [7], Swedish Model developed by Pettersson, Magnusson and Thelandersson [8], Method of Delichatsios et al. [9], EC 1-1-2 parametric fire [3]. All these methodologies demand a lengthy and difficult calculation to generate the temperature-time curves required for the thermal analysis of structure (except Magnusson and Thelandersson method they provide a series of curves). A description of these methods can be found in [10], [11]. The following sections focus on an overview of the most common methodologies (fire model) to quantify the thermal actions for the structural fire safety design. These methodologies for predicting the fire temperature (temperature-time), are presented below in chronological order they were developed. The emphasis will be on the more recently developed fire methodology (Travelling Fires) because it is more applicable to the performance-based design of very large compartments. Travelling fires replies to the desire for a simplified and comprehensive way / tool that can express the thermal environment in large compartment (where other methods and softwares may be overly complicated and really black-boxish to what is being done in the calculation).

The assumption and limitation of the methods are also discussed hereafter.

1.2 Fire Methodology for Small Compartments

In a small compartment after the ignition, the fire grows in size. The fire then reaches maximum intensity when all combustible materials in the room burn (fully developed fire). The decay phase starts when the rate of gaseous fuel decreases as a result of fuel consumption. During the fully developed fire stage, the structural elements reach the maximum temperature at which they can lose the load-bearing capacity.

The standard fire [12]–[14] and EC 1-1-2 parametric fire are most commonly being used to define the thermal action of the fully developed fire, where the whole compartment is involved in the fire (fully developed).

The standard fire curve assumes a fully developed fire with a homogeneous temperature inside the compartment. The temperature-time curve increases indefinitely according to a logarithmic relationship. Figure 1.2 shows the ISO 834 standard fire (ISO standard fire) temperature-time curve defined by Eq. (1.1) (°C).

$$T = 20 + 345 (\log (8t + 1)) \tag{1.1}$$

The ISO standard fire curve was developed from the tests undertaken early in the 20th century for the purpose of fire rating and fire testing [15]. The recent historical review shows that the standard fire curve does not have the scientific background to represent a real fire condition [16]. Major shortcomings of the standard fire curve are the lack of cooling phase and no consideration for the fuel load density, compartment geometry, and ventilation in a compartment. A real fire in large compartments has both heating and cooling phases. A scenario for structural fire safety design should address both phases to capture both types of deformations occurring in a room (which are especially important for the post-fire aspect and firefighter safety). The standard fire does not capture this scenario. The cooling phase is essential to assess the behaviour of certain structural elements [16], [17] or passive fire protection [18]. The maximum compartment temperature is also sensitive to the amount of fuel load density, building characteristics, and ventilation condition [11]. ISO standard curve does not address the real fire, but it is being used due to its simplicity and tradition. .

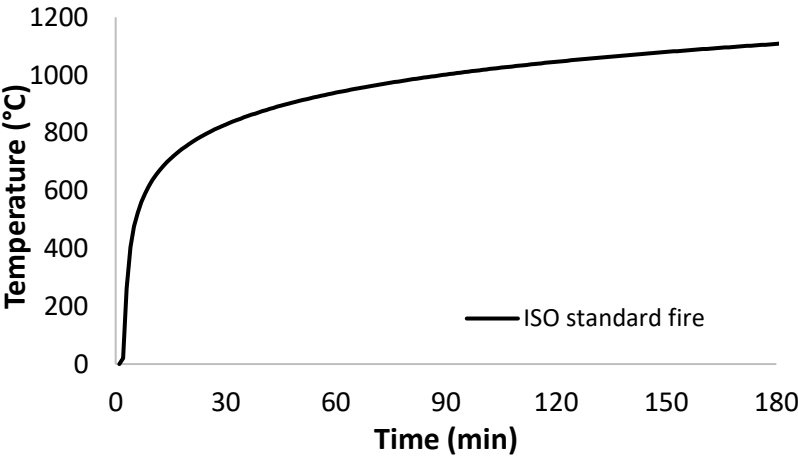


Figure 1.2 The ISO standard fire curve.

EC 1-1-2 presents the parametric temperature-time curve to calculate the gas temperature of the fully developed fire. The model considers the fuel load, ventilation size and thermal properties of the boundary condition. The gas temperature is expressed as:

$$T_g = 1325 [1 - 0.324 \exp(-0.2t^*) - 0.204 \exp(-1.7t^*) - 0.472 \exp(-19t^*)] \quad (1.2)$$

where t^* a nonphysical time parameter, related to physical time [4]. Figure 1.3 shows an illustrative example of the parametric fire temperature-time curves for different ventilation conditions in an arbitrary compartment.

The equation seems to have been derived based on the work of Pettersson [19]. The experiments used in the work of Pettersson were highly instrumented with thermocouples, which was also recording the radiation received from the compartment walls. This means that the cooling phase of the parametric fire is not representing really the gas temperature. As such the cooling phase of the parametric fire remains questionable. Comparison between a series of fire tests and parametric fire also showed that the fire duration from the parametric fire was underpredicted for all eight tests [20].

Parametric fire gives the boundary condition for structures exposed to fire in the form of temperature. As discussed by Torero [21] because the thermal boundary conditions at the exposed surface of a structural element are based on conservation of energy; thus, heat flux is an accurate boundary condition at the exposed surface of the structural element.

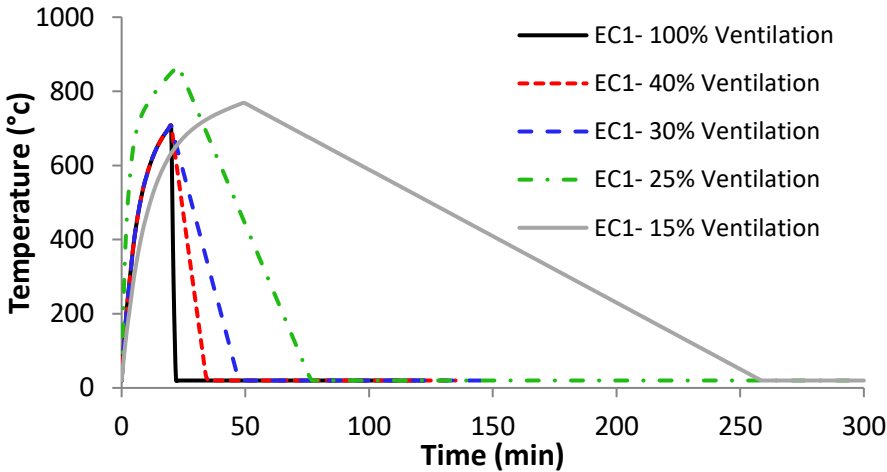


Figure 1.3 Example of temperature-time curves calculated from the parametric fire of EC 1-1-2 for an arbitrary compartment showing long-cold and short-hot fires.

Parametric fire assumes uniform temperature and uniform burning conditions for the fire. This model can be applied to a rectangular compartment with floor areas up to 500 m² and 4 m in height. Its use remains widespread even though the model cannot be used without continual reference to Eurocode. Complete details of the parametric fire are given in [3].

1.3 Fire Methodology for Very Large Compartments

This section presents the fire methodologies applicable to the performance-based design of structures with very large compartments. In very large compartments, fires have been observed to travel across the compartment floor, have a duration of many hours, and produce a non-uniform thermal environment inside the compartment, such as those observed in World Trade Center Tower 1, 2, 7 (2001), Windsor Tower Madrid (2006), Faculty of Architecture building fire at TU Delf (2008) [22], Plasco Building (2017) [23]. Such fires have been named “Travelling fires”. The definition of very large compartments is by intention generic here.

The concept of travelling fires has been reviewed and developed in the last decade [24]–[27] particularly to characterize the possible thermal environment for structural design purposes. The first proposed methodology names Large Firecell model, which divides the large compartment into a number of design areas. The large Firecell model of Clifton assumes that the fully developed fire occurs in certain design areas at any time and parametric fire provides the temperature of the design area.

Rein et al. [25] and Stern-Gottfried et. al. [27] have developed an alternative methodology to address the travelling fires in large compartments (denoted as TFM). The TFM gives the non-uniform temperature in a large compartment. The TFM provides a family of travelling fires curves in a large compartment, with each fire has a different area of burning, which takes account of variables of the real fire. This methodology considers the near field (i.e., flame region assumed to be 1200°C) and the far field (i.e., hot gases region far from the flame) effect of a fire, instead of a uniform temperature field. Fire burns locally for a specific local burning time, travels throughout the compartment and structural elements at the ceiling level, sees the impact of the far field and near field temperature. Figure 1.4 illustrates an example of temperature-time curves of travelling fires in arbitrary locations at the ceiling level, as the fire moves through an arbitrary compartment.

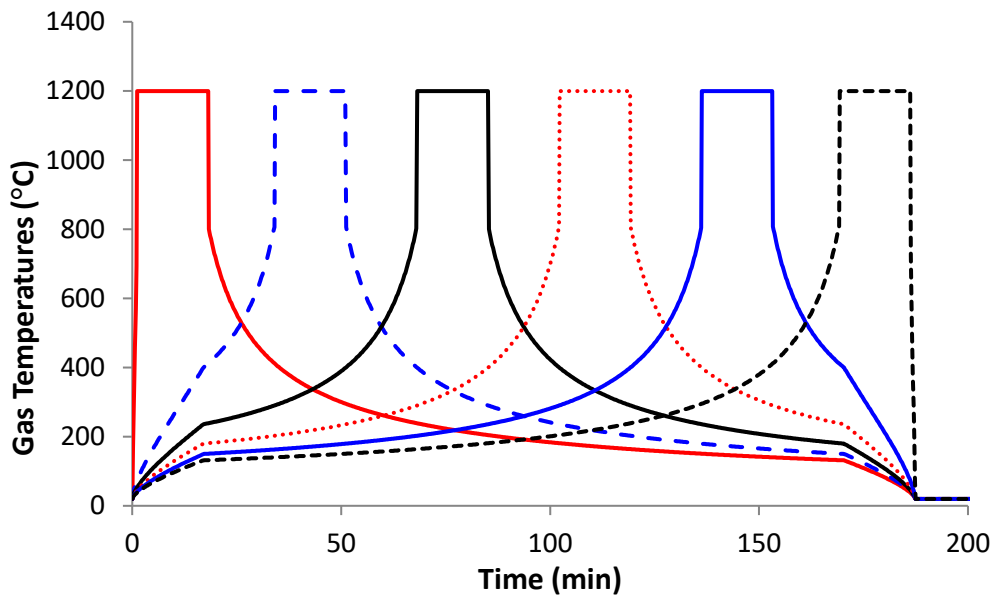


Figure 1.4 An Illustrative example of travelling fires of a 10% fire area, as the fire travels through an arbitrary compartment. Each curve gives the temperature -time in an arbitrary location at the ceiling level.

One of the newly developed methodologies improved travelling fires methodology (iTFM), based on the concept of ‘traveling fires’ in large compartments [27] has also been advanced by Rackauskaite et. al. [28]. The methodology considers a family of possible travelling fires, where each fire has a different burning area and spread rate. Thermal conditions from the family of fires allow selecting the most challenging scenario for structural design. In iTFM the concept of flapping is included, so the near-field temperature, where the flame is impinging the ceiling, ranges from 800°C – 1200 °C (1200 °C generally adopted for conservativeness). The far field temperature, where the hot gas temperature is estimated, can be calculated by Alpert’s correlations [29], which were developed from fire tests with an unconfined ceiling [30].

It is important to note that travelling fires methodology is not predictive and is intended to be used as a complementary tool by designers when undertaking structural fire engineering analyses for robustness in addition to traditional design fires (after discussion with an important consultancy the author realized that dozen of building have used travelling fire in the design process). Some works in the applications of travelling fires for structural design can be found elsewhere [31]–[33] where they have shown both travelling fires and traditional methods; that assume uniform burning and homogenous temperature conditions throughout a compartment, are important and should be considered in the design of modern, large open plan building. Other modifications to the TFM can be found in the work by [34], [35].

Some important assumptions associated with travelling fires metrology (TFM) are listed below:

1. Flame extension under the ceiling: TFM bounds the near field (i.e., the flame region) to the flapping length under the ceiling and does not consider the flame extension beyond this region. During the fire, the flame could extend a few meters under the ceiling. Therefore, the structural elements would experience more intense heating under the direct impact of the flame instead of the hot gases.
2. Steady flame spread: TFM assumes that the leading and trailing edge of fire have the same fire spread rate. As such the flame spread rate is assumed constant during the fire.
3. Uniform fuel load: like traditional methodologies TFM assumes a uniform fire load throughout the compartment. In real fire compartment conditions, the fuel load distribution inside the compartment may not be uniform because of the presence of free spaces.
4. Constant burning time: the burning time is a consequence of fuel load density (item 3) and fire spread rate (item 2) in accordance with TFM. In the fire condition, the variation of burning time would affect the duration of thermal exposure to a structural element.
5. Fuel height: the TFM assumes that the height of all burning objects is equal, whereas in a fire compartment objects with different heights could be found. This can impact the length of flame extension under the ceiling.

The assumptions noted aim to produce a representative travelling fire scenario that can be used as a reasonable estimate to produce a safe structural design.

Figure 1.5 presents the evolution of travelling fire models before the start of this thesis, with a focus on the methodology used for this work, iTFM.

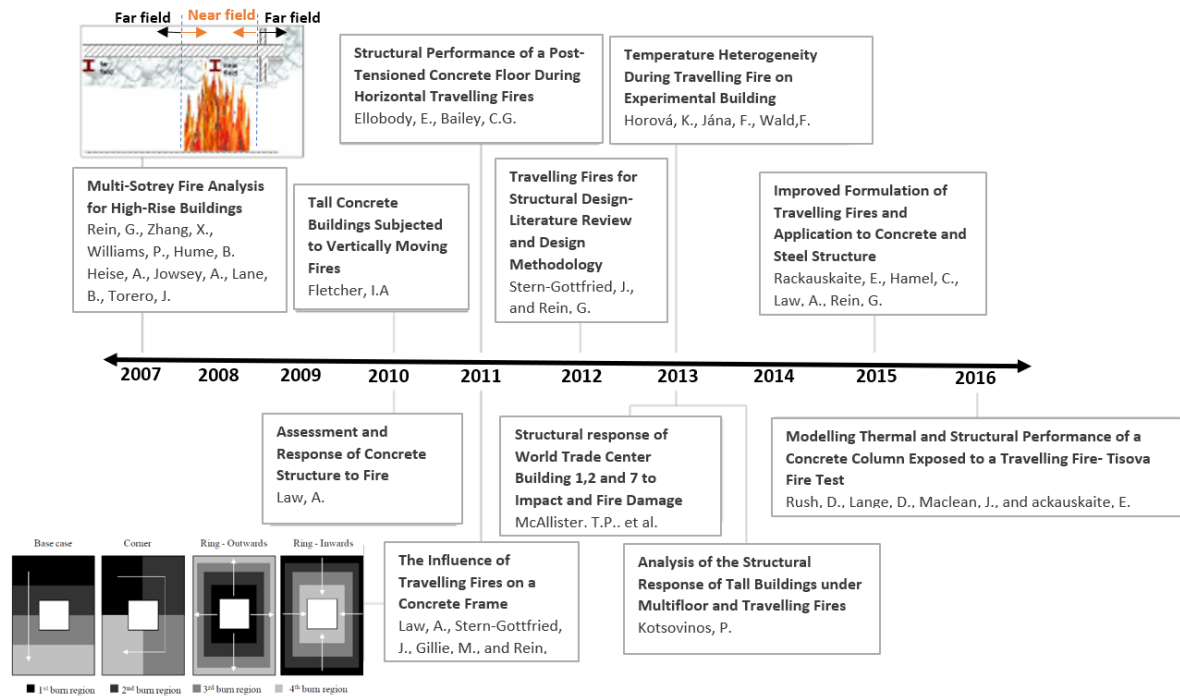


Figure 1.5. Brief background history of the Travelling Fires Methodology in literature as related to this study (post 2007 and before 2016 - Figure adapted from [33]).

1.4 Motivation

Most of the current structural fire design guidance does not account for travelling fires due to the lack of enough experimental data in a large compartment. For example, EC 1-1-2 [3], which is the required standard in Europe, highlights localized fire, parametric fire, and advanced models. Localized fires are mainly used to study the behaviour of isolated elements such as columns or beams. Parametric fire or zone models provide a homogeneous temperature throughout the compartment. Parametric fire has limitations such as: valid for rectangular compartments less than 500 m² and 4 m ceiling height. Note that large compartments tests in the order of 500 m² confirming these boundaries are not available and that the EC 1-1-2 standard limited the use of the parametric fire to 500 m². Recently the concept of travelling fire is included in few Published Documents [36], [37] and ISO standard fire [38] for the application of engineering approaches to fire safety in buildings. To address the gap for the performance-based design of very large compartments, more engineering guidance are expected to incorporate the traveling fire methodology. This work study the background data required to make the design recommendations and guidelines for travelling fires scenario for the performance-based design of large compartments.

This work aims to improve design fire methodologies and processes used for the structural fire design of open plan compartments. To this end, this project attempts to revisit some of the assumptions of the TFM, and to perform experimental studies in a large open plan compartment. The aim is to improve the assumptions or to justify the absence of some mechanism in TFM. The further development of travelling fires methodology presented here can be applied for the performance-based design of the large compartments. The experimental studies intend to support the development of design tools and to justify the incorporation of travelling fires in current design methodologies and fire safety engineering guidance.

It should be noted that this thesis is dealing with TFM and non-combustible materials and may not be taken out of context for other material types where TFM hasn't been fully explored on yet.

1.5 Outline of Thesis

In this work, the traditional method with uniform temperature (parametric fire) and travelling fires developed in this thesis (fTFM), are applied to assess the performance of structural elements in large open plan buildings. The examples of application enable readers to understand the generic behaviour of structure when exposed to uniform and non-uniform temperatures.

Chapter 2 presents the application of the parametric fire on a concrete slab in an office building of 420 m². A detailed sensitivity study to the main parameters in the parametric fire and the heat transfer calculations is conducted. This was done to assess the sensitivity of structural element response to input parameter uncertainty. The sensitivity analysis identified the most influential input parameters for the structure and the range of values for each input parameter for which the design is structurally safe. This chapter also applies a simple and structured probabilistic methodology to determine the reliability of a structural element exposed to fire when designed following Eurocode 1-1-2, while accounting for uncertainties in input parameters. The probabilistic approach is discussed in detail in this chapter. This novel study conducts for the first time a probabilistic calculation using the EC 1-1-2 parametric curve.

Chapter 3 gives the details of the further development of the travelling fires methodology. This chapter revisited the near field assumption of TFM and developed the fTFM (Travelling fires with flame extension). This chapter formulated the TFM in terms of heat flux rather than temperatures, thus allowing for a more formal heat transfer boundary condition between the gas and the surface of the structural element. This chapter analyses the impact of travelling fires with flame extension (fTFM),

without flame extension, and the EC 1-1-2 parametric fire on different types of structure: concrete beam, protected, and unprotected steel. The results showed that travelling fires with and without flame extension are more onerous thermally to the structural element than the EC 1-1-2 parametric fire.

Chapter 4 demonstrates how the fTFM methodology can be applied probabilistically to determine the reliability and probability of failure of a structural element exposed to fire in a very large compartment. A similar concrete structure to that used in Chapter 2 is used to study and define the reliability of a fire affected structure following uniform fire condition and travelling fires with flame extension. The results show that structure is being close to failure in the case of travelling fires.

Chapter 5 presents the x-TWO travelling fire experiments (consists of two experiments) that the author of this thesis led in 2019 in Poland. x-ONE in 2017, in which the author of this thesis was also involved, and x-TWO are the largest fire compartments studied to date. These three experiments are linked and provide a valuable set of data in traveling fire dynamics in a very large compartment. The recorded temperature, fire spread, and visual observations are discussed. This chapter shows that the prediction from fTFM methodology is in good agreement with the results of x-TWO experiment.

Chapter 6 is a conclusion for this thesis and presents recommended future work.

Chapter 2

Probabilistic Study of the Resistance of a Simply-supported Reinforced Concrete Slab, according to a Eurocode Parametric Fire

Summary²

This chapter presents the application of a simple probabilistic methodology to determine the reliability of a structural element exposed to fire when designed following Eurocode 1991-1-2 (EC 1-1-2). Eurocodes are being used extensively within the European Union in the design of many buildings and structures. Here, the methodology is applied to a simply-supported, reinforced concrete slab 180 mm thick, with a standard load-bearing fire resistance of 90 min. The slab is subjected to a fire in an office compartment of 420 m² floor area and 4 m height. Temperature time curves are produced using the EC 1-1-2 parametric fire curve, which assumes uniform temperature and a uniform burning condition for the fire. Heat transfer calculations identify the plausible worst-case scenarios in terms of maximum rebar temperature. It was found that a ventilation-controlled fire with the opening factor of 0.02 m^{1/2} results in a maximum rebar temperature of 448°C after 102 min of fire exposure. Sensitivity analyses to the main parameters in the EC 1-1-2 fire curves and the heat transfer calculations are performed using a one-at-a-time (OAT) method. The failure probability is then calculated for a series of input parameters using the Monte Carlo method. The results show that this slab has a 0.3% probability of failure when the compartment is designed with all layers of safety in place (detection and sprinkler systems, safe access route, and fire fighting devices are available). The unavailability of sprinkler systems results in a 1% probability of failure. When both sprinkler system and detection are not available in the building, the probability of failure is 8%. This novel study conducts for the first time

² This chapter is based on “Heidari, M., Robert, F., Lange, D., and Rein, G., 2019. Probabilistic Study of the Resistance of a Simply-Supported Reinforced Concrete Slab According to Eurocode Parametric Fire. *Fire Technology* 55, 1377–1404.”

a probabilistic calculation using the EC 1-1-2 parametric curve, helping engineers to identify the most critical design fires and the probabilistic resistance assumed in EC 1-1-2.

2.1 Introduction

Performance-based design for fire has been incorporated into legal frameworks around the world [39] and allows designers to employ a rational engineering approach to the provision of fire safety in the built environment [40].

The fundamental principles of performance-based fire engineering for structures are outlined in multiple guidance codes [41], [42]. Performance-based design codes lay down what performance requirements need to be met by a designer, leaving scope for alternative, systems, and methods to be used in a building's design, whereas prescriptive design codes simply describe how a building should be built.³ Performance-based design codes mainly discuss qualitatively, rather than quantitatively, the factors and input parameters that should be considered in the design process. Designers should define the input variables required for a design using any number of sources. This can lead to significant variability in the design fires used, and thus inconsistent levels of safety for buildings [43].

“Epistemic” and “Aleatory” uncertainties exist in any engineering problem. The former is connected to a lack of complete scientific knowledge, and limited data sources for the modelled scenario, while the latter is linked to the stochastic variability in the population [44]. These uncertainties lead to the need for assumptions and simplifications to be made in analytical and numerical models, and within methodologies used by engineers for structural fire safety design [44], [45]. A sensitivity analysis can be used to characterise the significance of uncertainties in order to determine the impact of these on the results of any analysis.

Moving from a prescriptive approach to performance-based design enables designers to apply knowledge of real structural behaviour during the fire, while accounting for uncertainties allows designers to quantify the reliability of the proposed solution, as well as the overall level of risk

³ Some countries use objective-based design which is essentially the same as performance-based design, though there is more of a reliance on the standard as a benchmark.

associated with the design, and to more confidently inform any further decision-making based on the results [46]–[48].

Reliability-based structural fire engineering has progressed in recent years. Examples in the literature include the application of the Monte Carlo method and various variable reduction techniques to determine the probability of failure and/or the reliability of both protected and unprotected elements [49], to evaluate the behaviour of steel beams under fire, taking account of uncertainties in the fire load [50], to evaluate designs carried out according to EN 1992-1-2, and to study the influence of the input variables for a slab the ISO standard fire [51]. A new set of fire resistance periods in the development of codes of practice DD9999 were developed in [52], and a risk-based methodology was defined, while the fundamental design challenges in the context of time equivalence were addressed in [53]. Other examples could be mentioned, including identifying the most critical fire scenarios for the structural response of car parks to fires [54], and the failure probability of redundant cables in a cable tunnel fire [55]. An approach such as this, based on the Monte Carlo method, can compensate for the lack of certainty in modelling inputs in the case of real fires, as there is the opportunity to vary input parameters within a defined range.

This chapter presents a method to identify the most important parameters that need to be considered in a fire safety engineering design. It presents a structured approach that could help to justify some of the assumptions and simplifications which are made in fire safety engineering by identifying parameters for which more information is needed for different applications, thus allowing engineers to exclude variations in some of the other parameters in Monte Carlo analysis; in turn, reducing the number of runs needed in Monte Carlo analysis to obtain a converged answer.

2.2 Methodology

Several fire scenarios for a uniformly burning and fully developed fire were produced based on a range of values for input parameters such as fuel load, ventilation size, the contribution of fire protection systems, boundary material properties etc. to select a “reference case” fire scenario. A set of temperature-time curves were produced in accordance with the EC 1-1-2 parametric fire method [3], which assumes a uniformly burning fire and is valid for compartments with floor areas up to 500 m² and 4 m height [3]. Heat transfer analyses were then carried out to identify the “reference case” scenario with the aim of sensitivity analyses. The analytical equation given in EC 1-1-2 [3] to calculate the fire temperature (°C) is:

$$T_g = 1325 [1 - 0.324 \exp(-0.2t^*) - 0.204 \exp(-1.7t^*) - 0.472 \exp(-19t^*)] \quad (2.1)$$

$$t^* = t \cdot \Gamma \quad (\text{h}) \quad (2.2)$$

where t is the time (h), Γ is given as:

$$\Gamma = \frac{\left(\frac{O}{b}\right)^2}{\left(\frac{0.04}{1160}\right)^2} \quad (2.3)$$

$$O = \frac{A_v (H_{eq})^{0.5}}{A_t} \quad (2.4)$$

where b is the thermal inertia of the enclosure boundary, O is the opening factor of the fire compartment [$\text{m}^{1/2}$], A_v is the total vertical opening on all walls [m^2], H_{eq} is weighted average of window heights on the wall [m], and A_t is the total area of enclosure (walls, ceiling and floor, including openings) [m^2]. The maximum temperature T_{\max} occurs at t^*_{\max} as:

$$t^*_{\max} = t_{\max} \cdot \Gamma \quad (\text{h}) \quad (2.5)$$

$$t_{\max} = \max \left[0.2 \cdot 10^{-3} \cdot \frac{q_{t,d}}{O}; t_{\text{lim}} \right] \quad (\text{h}) \quad (2.6)$$

$$q_{t,d} = q_{f,d} \cdot \frac{A_f}{A_t} \quad (2.7)$$

where $q_{t,d}$ is the design value of the fire load density related to the total surface area A_t of the enclosure (walls, ceiling and floor, including openings) [MJ/m^2], and $q_{f,d}$ is the design value of the fire load density related to the surface area A_f of the floor [MJ/m^2].

The limiting temperature t_{lim} of 25 min is taken, assuming a medium fire growth rate [3]. After t^*_{\max} the cooling phase begins and the temperature-time curve during this phase is given by:

$$T_g = T_{\max} - 625 (t^* - t^*_{\max} \cdot x) \quad \text{for } t^*_{\max} \leq 0.5 \quad (2.8)$$

$$T_g = T_{\max} - 250 (3 - t_{\max}^*) \cdot (t^* - t_{\max}^* \cdot x) \quad \text{for } 0.5 \leq t_{\max}^* \leq 2 \quad (2.9)$$

$$T_g = T_{\max} - 250 (t^* - t_{\max}^* \cdot x) \quad \text{for } 2 \leq t_{\max}^* \quad (2.10)$$

Once this fundamental part has been addressed, a detailed sensitivity analysis of the main parameters in the EC 1-1-2 parametric curves and heat transfer model were performed for a wide range of values. The heat transfer was solved using a one-dimensional finite difference method for conductive heat transfer inside the material, and boundary conditions for both convective and radiant heating were taken into account [27], [56]. As such, a range of input variables in the EC 1-1-2 parametric fire and heat transfer model was investigated (Table 2.1 and Table 2.2). A sensitivity analysis of the “reference case” scenario examined a large number of fire scenarios using a One-at-a-Time method (OAT).

Table 2.1 Parameter values for the reference case and range of input variables investigated using the EC 1-1-2 parametric approach.

Parameters	Reference Case	Range for OAT	Range for Monte Carlo / Distribution	Comment
Characteristic Fuel Load Density ($q_{f,k}$)	511 MJ/m ²	[347-1315]	Mean=411MJ/m ² , Coefficient of Variance=0.3 Gumbel	OAT values cover sparsely furnished (classroom) to densely loaded (library, business office) spaces. Reference case value is taken as the 80th percentile design value for office buildings [3]. Values for MC represent the office fire load distribution in [3].
Fire Fighting Measures Index (FFMI)	0.66	[0.148-3.37]	Probability calculated for different values of FFMI	Extreme values taken for the representative value of the different active fire fighting measures. Reference case value is taken assuming that there are sprinklers, auto detections by smoke and alarms, safe access routes, and fire fighting devices as active fire fighting measures [3].
Opening factor (O)	0.02 m ^{1/2}	[0.02-0.2]	[0.02-0.2] Uniform	Range taken to cover all possible opening factors in accordance with the limitation of [3] (i.e., 0.02<=O<=0.2). The reference

Parameters	Reference Case	Range for OAT	Range for Monte Carlo / Distribution	Comment
				case is determined by the analysis in Section 4.2. [3].
Thermal Inertia (b)	1659 W.s ^{1/2} /m ² K	[1159-2200]	[1159-2200] Uniform	Range taken to represent the extent of concrete thermal conductivities, specific heats, and densities for normal-weight concrete. The reference case value is for the lower limit of thermal conductivity for normal concrete with ambient temperature density and the specific heat [1], [11].
Coefficient in Γ (C_{Γ})	$8.41 \cdot 10^8$	[$7.58 \cdot 10^8$ - $9.25 \cdot 10^8$]	$8.41 \cdot 10^8$	Range taken to test sensitivity assuming +/-10% variation from the reference case from EC 1-1-2[3].
Coefficient in t_{\max} ($C_{t_{\max}}$)	$0.2 \cdot 10^{-3}$	[$0.018 \cdot 10^{-3}$ - $2.2 \cdot 10^{-3}$]	[$0.018 \cdot 10^{-3}$ - $2.2 \cdot 10^{-3}$] Uniform	Range taken to test the sensitivity assuming +/-10% variation of the reference case [3].
Time Limit (t_{\lim})	0.333 h	[0.333-0.416]	[0.333-0.416] Uniform	Range is from fast fire growth rate to slow fire growth rate. The reference case value is taken as the medium fire growth rate recommended for office [3].
Coefficient in Γ_{\lim} ($C_{\Gamma_{\lim}}$)	$8.41 \cdot 10^8$	[$7.58 \cdot 10^8$ - $9.25 \cdot 10^8$]	$8.41 \cdot 10^8$	Range taken to test the sensitivity assuming +/-10% variation of the reference case [3].
Coefficient in O_{\lim} ($C_{O_{\lim}}$)	$0.1 \cdot 10^{-3}$	[$0.9 \cdot 10^{-4}$ - $0.11 \cdot 10^{-3}$]	$0.1 \cdot 10^{-3}$	Range taken to test the sensitivity assuming +/-10% variation of the reference case [3].
Floor Area (A_f)	420 m ²	[387-462]	420	Range taken to test the sensitivity assuming +/-10% variation of the reference case. Reference case value is taken from the geometry of the compartment.
Total Area (A_t)	1192 m ²	[1072-1311]	1192	Range taken to test the sensitivity assuming +/-10% variation of the reference case. Reference case value is taken from the geometry of the compartment.

Table 2.2 Parameter values for the reference case and range of input variables investigated in the heat transfer model.

Parameters	Reference Case	Range for OAT	Range for Monte Carlo / Distribution	Comment
Axis distance of reinforcement (d_r)	44 mm	[20-50]	[34-54] Uniform	Range for MC taken to test the sensitivity assuming 10 mm variation of the concrete cover. Reference case value as per the design of the building [57].
Sample thickness	400 mm	[360-4400]	400	Range taken to test the sensitivity assuming +/-10% variation of the base case
Density (ρ)	2300 kg/m ³	[1900-2300]	[1900-2300] Uniform	Range taken to represent concrete densities of normal concrete [11]. Reference case value is taken as siliceous concrete density from EC 2-1-2 [1].
Thermal Conductivity (K)	1.33 W/m.K	[1-1.95]	[1-1.95] Uniform	Range taken for representative values of light and normal weight concrete thermal conductivities. The reference case value is taken as the lower limit of thermal conductivity of normal weight concrete in ambient temperature from EC 2-1-2 [1].
Specific heat (c)	900 J/kg.K	[840-1100]	[840-1100] Uniform	Range taken to represent limits of concrete specific heats for light and normal weight concrete. The reference case value is taken from EC 2-1-2 [1].
Convective Coefficient – Exposed Surface (h_c)	35 W/m ² .K	[10-100]	[10-100] Uniform	Range taken to represent limits in a fire condition. Reference case value is taken from Eurocode guidance [3], [27].
Convective Coefficient – Unexposed surface (h_b)	4 W/m ² .K	[2-10]	[2 –10] Uniform	Range taken to represent limits in a fire condition. Reference case value is taken from EC 1-1-2 [3].
Emissivity (ϵ)	0.7	[0.6-0.8]	[0.6–0.8] Uniform	Range taken to test sensitivity. Reference case value is taken from EC 1-1-2 and EC 2-1-2 [1], [3]

OAT is a sensitivity analysis method, which simply varies one input at a time, keeping others at their baseline, and calculates the variation in the output. All input parameters are examined, and results are compared to determine which of the input parameters have the highest impact on the final results. The OAT sensitivity analysis has been used in different examples, such as identifying the governing parameters of a solid ignition model and global level of confidence associated with the model predictions [58] and determining the most sensitive parameters in travelling fires methodology for structural design [27]. The OAT sensitivity analysis was useful in this study to determine which input data were important for further the Monte Carlo analysis and required more information, and which were unimportant, thus reducing the number of variables required to be considered as uncertain. In addition, it highlighted the range of possible fire scenarios for which the designed element is structurally safe.

A Monte Carlo analysis was then carried out to evaluate the reliability of the concrete slab, in terms of the failure probability P_f , given the uncertainty in key model parameters. Monte Carlo analysis is a method that performs numerical experiments using a large number of randomly generated sample sets from the input space, containing all possible values of the input variables according to their probability distributions. It is suitable when it is impossible to compute an exact result with a deterministic approach and also to understand the impact of uncertainty in forecast modelling [59].

2.3 Case Study

The methodology presented here was applied to a simply-supported reinforced concrete slab 180 mm thick with 44 mm axis-distance of the tension reinforcements to the soffit of the slab (fire exposed surface) and a concrete cover of 36 mm. The compartment was an open-plan office building, 30.25 m long by 14.25 m wide and 4 m high (Figure 2.1). The simplified calculation method in Eurocode 1992-1-2 (EC 2-1-2) [1] was used to measure the performance of the slab, as the simply-supported slab was subjected to a uniformly distributed load, and the design at ambient temperature was based on linear analysis. There are different methods to evaluate the failure modes of concrete structures for different levels of assessment in fires: maximum deflection (which is typically taken as a ratio of deflection), the maximum temperature of the tension reinforcement, the ultimate strain in the tension reinforcement, and the shear capacity [1]. The slab is exposed to fire from below, so the strength of the structural element may be assumed to be a function of the temperature of the rebar in the tension zone [40]. The critical temperature of the tension reinforcement in the slab was therefore selected as the limiting criteria.

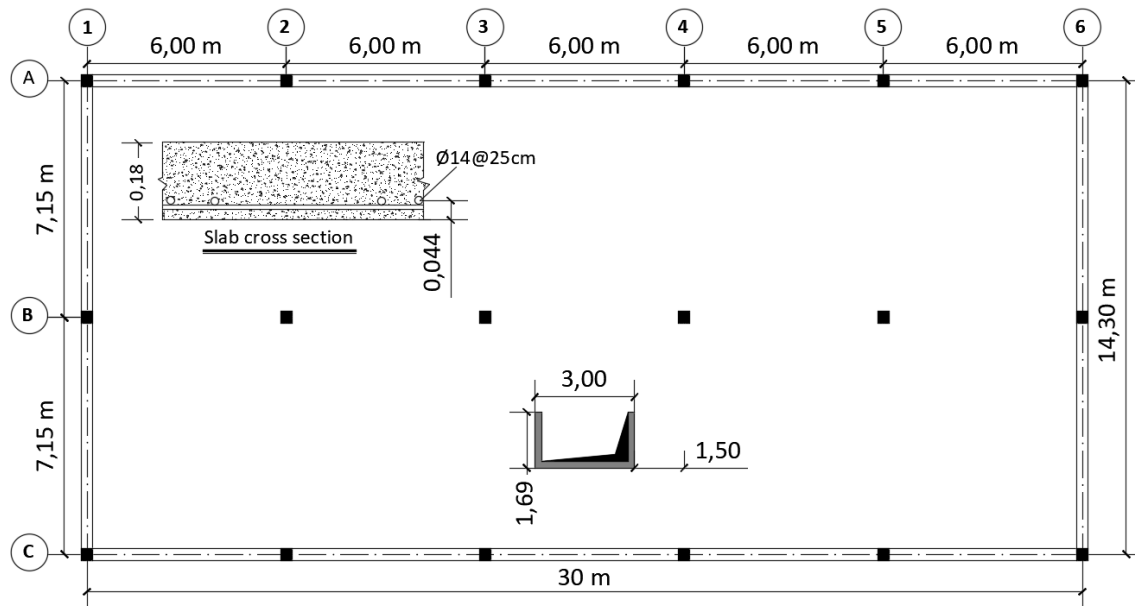


Figure 2.1 Plan and elevation of the structure and slab cross-section, dimensions in meter.

The critical temperature of the reinforcement steel was calculated assuming a reduction factor of 0.6 for the load combination (e.g. permanent and variable loads) in the fire situation [1]. The effects of actions on the structural element (e.g. internal force, moment) for the fire situation, may be deduced from those determined in normal temperature design using the reduction factor for the load combination in the fire situation [1]. A partial safety factor of 1.15 for reinforcement steel was selected in accordance with EC 2-1-1 [60]. As such, failure in the selected structural member for the fire situation, occurred when the reduction factor for the strength of reinforcement steel was 0.52. In accordance with clause 4.2 [1], for rebar (hot rolled) in concrete and for strain greater than 2% (which is the case for slabs and beams without a high reinforcement ratio), the critical temperature is 583°C. This temperature is normally considered as the limiting temperature above which steel loses strength [11] such that the failure of a typical simply supported slab could occur under the load assumed to be applied during a fire. The maximum temperature of the tension rebar was compared with the critical rebar temperature.

It was assumed that explosive spalling is unlikely to occur, as the XC1 class is considered with moisture content less than 3% and the concrete strength is below 55 MPa in accordance with EC2-1-2 [1].

A concrete density of 2300 kg/m³, the thermal conductivity of 1.33 W/m.K, specific heat of 900 J/kg.K, convective heat transfer coefficient of 35 W/m².K for the exposed surface and 4 W/m².K for the

unexposed surface of the concrete element, and emissivity of 0.7 were assumed [3], [60]. In this illustrative example, the concrete properties were assumed to be constant. It is shown elsewhere that 1D heat transfer with constant effective properties results in a 7-15% higher in-depth concrete temperature than the case of temperature-dependent concrete properties [27]. Therefore, we deemed the method in this chapter to be appropriate, because it is simple but still accurate enough. To make the reference case scenario representative of habitual practice for this type of building, it was assumed that suppression and detection systems operated in the case of a fire, and safe access routes and firefighting devices were fitted in the building. The design value of the fire load density $q_{f,d}$ related to the surface area A_f of the floor in Annex E of EC 1-1-2 is given by:

$$q_{f,d} = q_{f,k} \cdot \delta_{q1} \cdot \delta_{q2} \cdot \delta_n \cdot m \text{ (MJ/m}^2\text{)} \quad (2.11)$$

The product of i) characteristic fire load density for an office building ($q_{f,k}$) equal to 511 MJ/m² (80% fractile), ii) different active firefighting measures (δ_n) assumed to be 0.66 (Table 2.2), iii) fire activation risk due to the size of the compartment (δ_{q1}) equal to 1.53, iv) fire activation risk due to the type of occupancy (δ_{q2}) equal to 1, and v) a combustion factor of $m=0.8$, were assumed to be 0.8 in accordance with EC 1-1-2 [3]. As such the design value of the fire load density, $q_{f,d}$ is 410 MJ/m².

It should be noted that the Eurocodes are the required standards, providing a common approach for the design of buildings within the European Union and being used extensively in the design of buildings and slabs. On the other hand, each country is expected to issue a National Annex to the Eurocodes and choose those parameters which are left open in the Eurocode for national choice, known as Nationally Determined Parameters, to be used in the design of buildings in the country concerned [3]. For example, there are national annexes of EC 1-1-2 that do not use the factors in Eq. (2.11), which affects characteristic fire load density ($q_{f,k}$) [61]. A number of slabs around Europe have been designed without applying the Annex E of EC 1-1-2, therefore, for comparison, these cases were also considered.

2.4 Design Fire

The fire duration and severity in a fully developed fire depend on the amount of ventilation and the nature, distribution, and quantity of fuel, which all have a significant effect on duration and severity [11].

In a modern building, a double or triple glazed system may not break as readily as single panels of ordinary glass. Characteristics, orientation, and dimensions of the glazed external openings are architectural variables. Due to all the uncertainties associated with glass breakage and fall-out of glass [62], both fuel-controlled and ventilation-controlled design fires were examined. To cover all possibilities of ventilation, a series of parametric temperature-time curves were produced, in which the opening factor varied from 0.02 to 0.2 m^{1/2}, in accordance with the limitations imposed by EC 1-1-2 [3]. The external walls were considered to be 100% glazed and ranges of the opening factor cover all possibilities of glass breakage. The thermal inertia of the concrete and glazing were assumed to be 1659 and 1312 W.s^{1/2}/m²K respectively. The calculated average compartment temperatures for different opening factors are presented in Figure 2.2.

The results show that opening factors lying between 0.097 and 0.2 m^{1/2} produced a relatively short fuel-controlled fire. The decrease in opening factor to below 0.097 m^{1/2} resulted in a fire restricted by ventilation. Opening factors between 0.074 and 0.02 m^{1/2}, due to the façade glass breakage, resulted in a ventilation-controlled fire with peak gas temperatures between 750°C and 850°C.

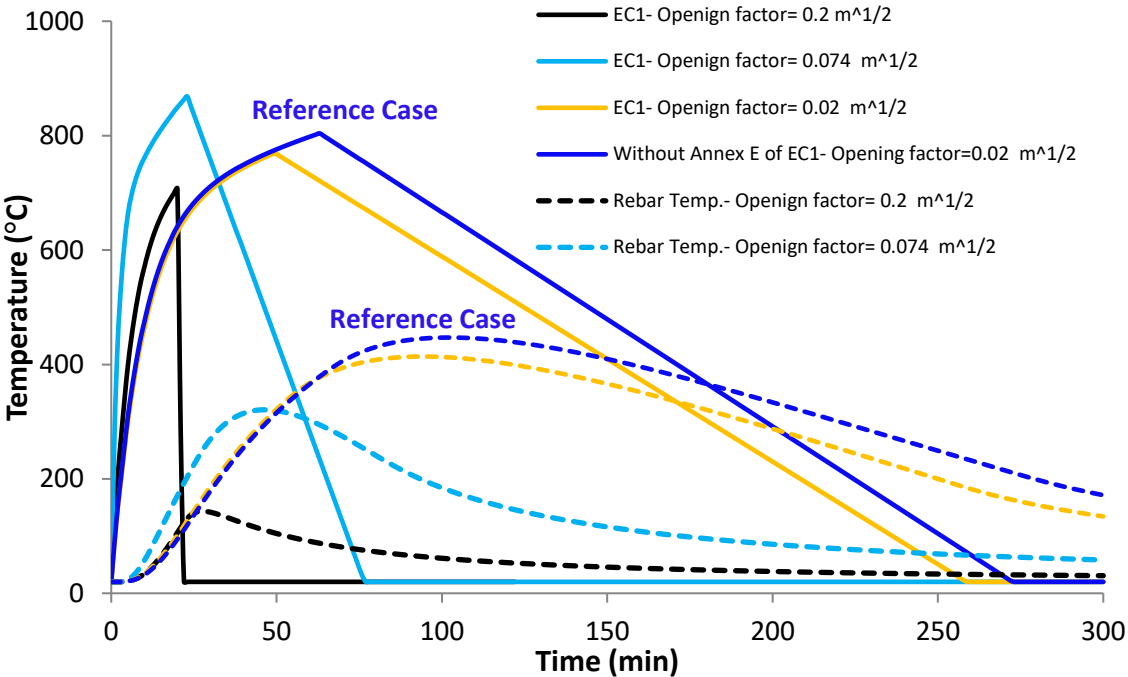


Figure 2.2 Gas temperature in a compartment for different opening factors using the EC 1-1-2 parametric approach and resulting rebar temperatures in the concrete slab. The reference case with the maximum rebar temperature is obtained from ventilation-controlled fires without using Annex E of EC 1-1-2 and was used for sensitivity analysis.

The calculated temperature fields were used as an input to a one-dimensional heat transfer model to calculate the resulting temperature in the concrete slab at the location of the rebar. The rebar was assumed to have the same temperature as the adjacent concrete, as it has a much higher thermal diffusivity than concrete.

A comparison of the rebar temperatures in Figure 2.2. clearly shows that the highest temperatures were caused by a ventilation-controlled fire, obtained from an opening factor of $0.02 \text{ m}^{1/2}$. The maximum rebar temperature was 408°C after 95 min of fire exposure. This scenario is named the “reference case” scenario and was used for further analysis.

Without considering Annex E of EC 1-1-2, Figure 2.2. shows that the maximum rebar temperature obtained from an opening factor of $0.02 \text{ m}^{1/2}$ was 448°C after 102 min of fire exposure which is 9% higher than the case in accordance with Annex E of EC 1-1-2.

2.5 Parametric Sensitivity Study using OAT

As the most challenging scenario was the one with an opening factor of $0.02 \text{ m}^{1/2}$, it was examined as the “reference case” for all the sensitivity studies performed in this section. The OAT (one-at-a-time) method was used to observe how varying one input variable affects the output results, particularly the maximum rebar temperature (RMT) and time to reach the maximum rebar temperature (t_{RMT}). In OAT sensitivity analysis, the input parameters were incremented across the ranges investigated.

The parameter values for the reference case scenario and the ranges investigated are given in (Table 2.1 and Table 2.2). The study includes all the input variables in the EC 1-1-2 parametric fire and the heat transfer models.

The following sections present the sensitivity analysis of the parameters in (Table 2.1 and Table 2.2).

2.5.1 Characteristic Fire Load Density

The amount of fuel in a building significantly alters the dynamics of fire. The available guidance provides the characteristic ranges of the fire load, which should include temporary and permanent fire loads, and the fire loads from construction elements, linings, and finishes [3]. Some national annexes of EC 1-1-2 provide different values of fire load density for an individual occupancy and recommend using the 80% or 90% fractile [61]. On the other hand, a comparison of the office fire load density in EC 1-1-2 with recent surveys shows that the fire load given in EC 1-1-2 may be unconservative

compared to the data in the survey. Results of the survey are approximately 40% higher [63] than EC 1-1-2, and therefore, the 95% fractile is a reasonable fire load density for an office building [64].

The range of fire load density was therefore selected to cover everything from sparsely furnished (classroom, 347 MJ/m²) [3] to densely loaded (business office, 1315 MJ/m²) spaces [40].

Figure 2.3 shows the variations of the maximum rebar temperature and the corresponding time, relative to the reference case, with a characteristic fire load density ranging from 347 to 1315 MJ/m².

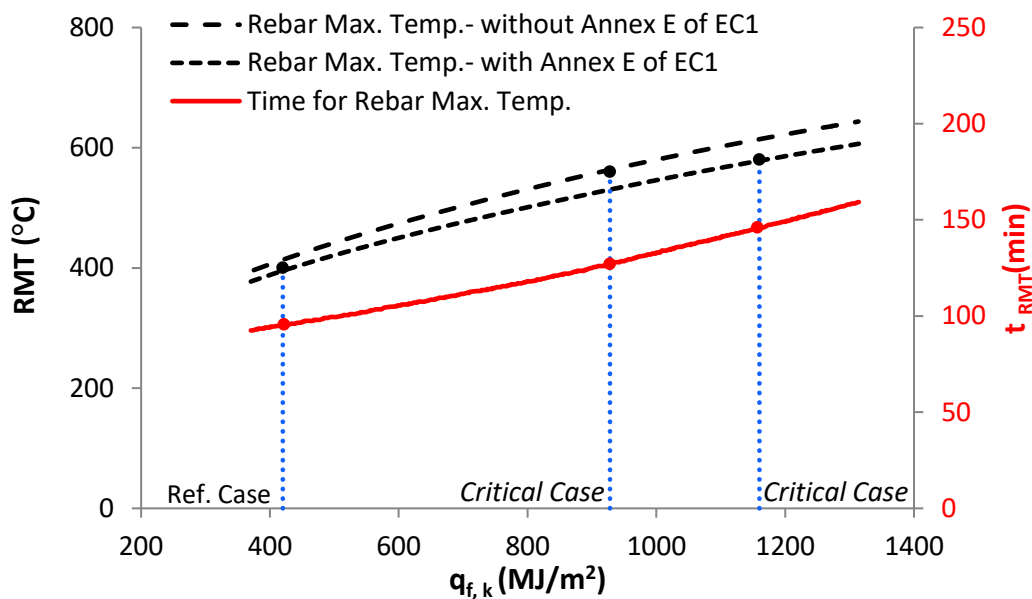


Figure 2.3 Maximum rebar temperature and corresponding times vs. characteristic fuel load density with and without factors in Annex E of EC 1-1-2.

The results show that the critical rebar temperature (critical case) occurred when the characteristic fire load density was above 1140 MJ/m² after 140 min of fire exposure, using the Annex E of EC 1-1-2. Without considering Annex E of EC 1-1-2, the critical case occurred for a characteristic fire load density of 912 MJ/m² after 120 min of fire exposure. It should be noted that, when Annex E of EC 1-1-2 was used, the characteristic fire load density ($q_{f,k}$) of 1140 MJ/m² was multiplied by the product of factors in Eq.(2.11) equal to 0.8 (obtained in Section 3), and thus the design fire load density ($q_{f,d}$) was equal to 912 MJ/m² (using Eq.(2.11)). Without using Annex E of EC 1-1-2, the characteristic fire load density and the design fire load densities were both 912 MJ/m². This shows that using the factors in Annex E of EC 1-1-2 (i.e., δ_{q1} , δ_{q2} , δ_n , m) could highly decrease the characteristic fire load density used to calculate the gas temperature. Figure 2.3 indicates that without using Annex E of EC 1-1-2 the critical temperature was reached for a lower characteristic fire load density (in this case study

20% less than using Annex E of EC 1-1-2). The fuel load densities which lead to the critical cases are representative value for densely loaded (i.e., library, business office) spaces.

2.5.2 Fire Fighting Measures Index

The presence of active fire protection systems influences the severity of the fire environment and fire duration in an enclosure. This index takes into account different active firefighting measures and ranges from 0.148 (full fire protection) to 3.37 (no active fire protections and intervention of firefighters) in accordance with Annex E of EC 1-1-2 [3]. Cases with and without the firefighting measures index were studied here and serve to illustrate the effect of this method on the resulting level of safety.

Figure 2.4 shows how rebar maximum temperatures and associated times vary with the firefighting measure index.

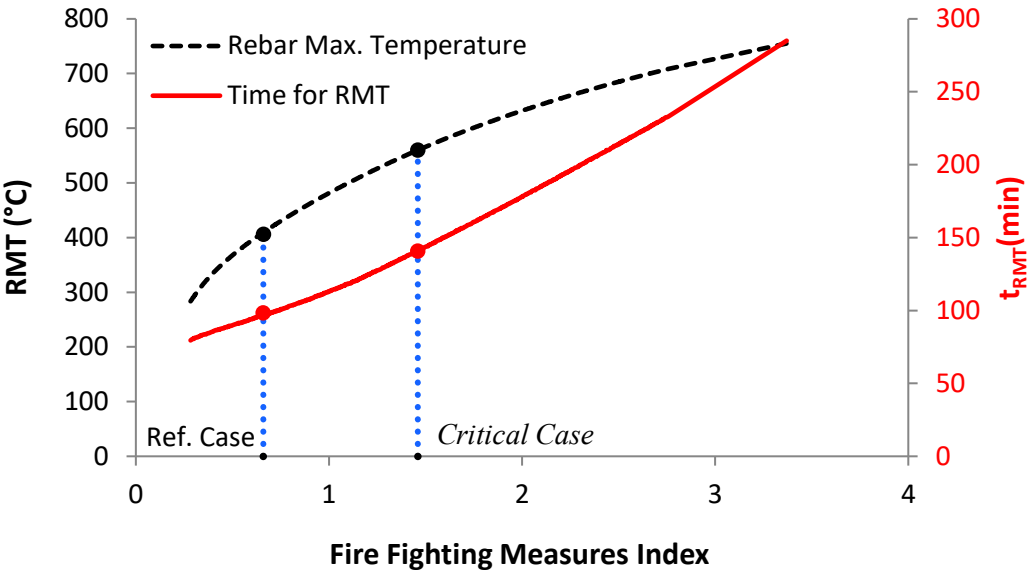


Figure 2.4 Peak rebar temperature and corresponding time vs. active fire fighting measures index in accordance to EC 1-1-2.

The results indicate that cases where the firefighting measures index has a value greater than 1.46 (i.e. the case when either sprinkler systems or detection and alarm systems are not installed [3]) resulted in a temperature greater than the rebar critical temperature (i.e. 583°C) after 150 min of fire exposure. Without using Annex E of EC 1-1-2, the maximum rebar temperature was 408°C after 95 min

of fire exposure. This demonstrates that using Annex E of EC 1-1-2 prolongs the failure time of the structural element.

2.5.3 Axis Distance of Reinforcement

Axis distance of the reinforcement is a fundamental design variable in any concrete structure and is likely to be a fixed value early in the design of a building. Typical concrete covers a range from 20 to 60mm [27]. It is worth understanding the impact of axis distances on peak rebar temperatures, as it could make a significant difference to the performance of the structure.

Figure 2.5 indicates that the peak rebar temperatures were lower than the rebar critical temperature for all axis distances. A concrete cover of 36 mm (i.e., axis distance of 46 mm) was used for the reference case; in addition, the range selected implicitly included the possible loss of 16 mm concrete cover (i.e., axis distance of 20 mm where the rebar temperature is below the critical value). For each rebar depth in Table 2.2, It was also checked that the bending strengths with different lever arms were above the applied bending moment.

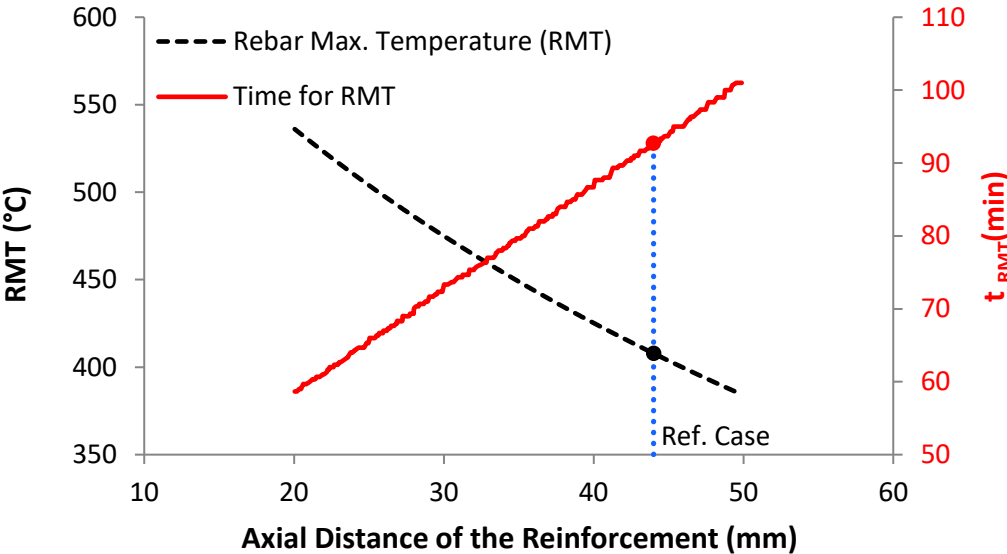


Figure 2.5 Peak rebar temperature and corresponding time vs. axis distance. No critical case is found in this range of the parameters.

2.5.4 Opening Factor

Figure 2.6 shows the variation of the maximum rebar temperature and the time taken to reach the maximum temperature with a ventilation size of 0.02 to 0.2 m^{1/2}. Figure 2.6 illustrates that the maximum rebar temperature value corresponds to the opening factor of 0.02 m^{1/2}. Notably, the sharp gradient changes in the maximum rebar temperature were due to a change in the fire environment, from fuel-controlled to ventilation-controlled. Therefore, the predicted structural element temperature from parametric fire is highly sensitive to a small variation of the size of the opening.

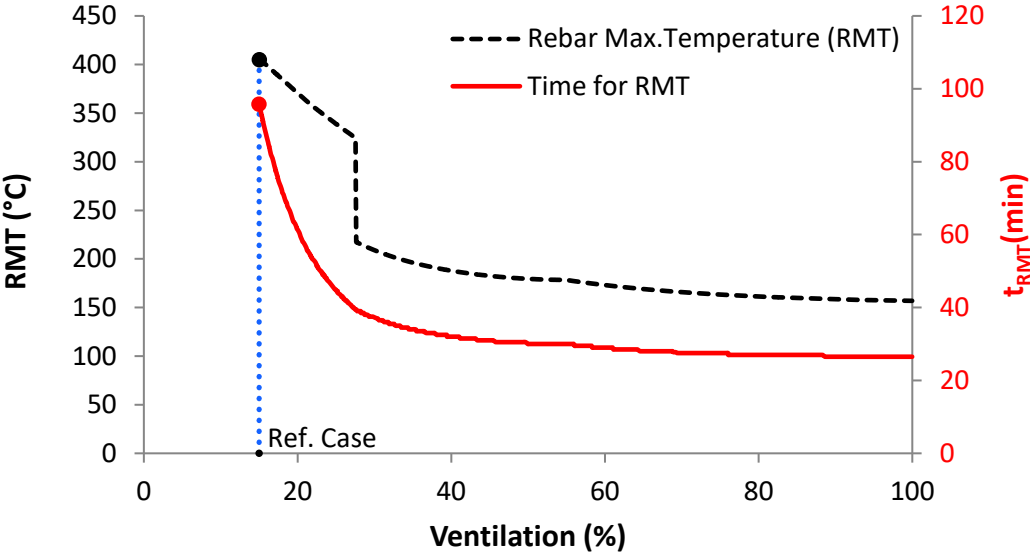


Figure 2.6 Peak rebar temperature and corresponding time vs. ventilation size. No critical case is found in this range of the parameters.

2.5.5 Concrete Density

Density varies greatly for concrete types, and guidance exists which provides typical ranges. The reference case density was taken as the density of normal weight concrete, equal to 2300 kg/m³ [1]. Figure 2.7 shows the maximum rebar temperature and the time to reach the maximum temperature against concrete densities from 1900 to 2300 kg/m³ [11]. Results show that concrete density affects the maximum rebar temperature. The results indicate that the lower the density, the higher the peak bay rebar temperatures and the shorter the time to reach the peak rebar temperature.

Figure 2.7 allows to visually determine what the implications may be for newer concrete mixes where lower densities or even higher densities may be used with the methodology presented in this paper.

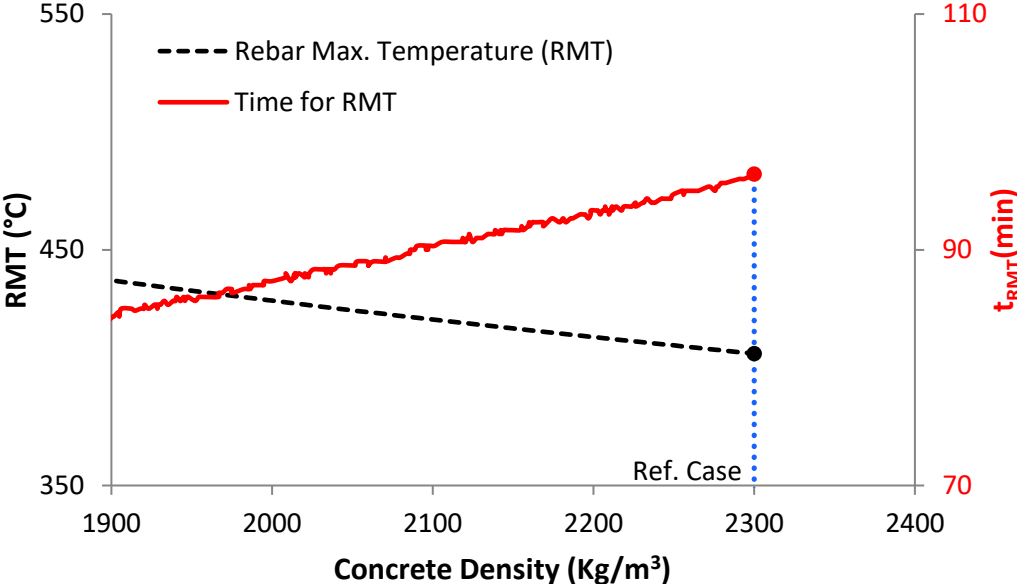


Figure 2.7: Peak rebar temperature and corresponding time vs. density of concrete. No critical case is found in this range of the parameters.

2.5.6 Other Parameters

The results from the OAT sensitivity analysis for the rest of the parameters in Table 2.1 and Table 2.2 are illustrated in Figure A 2.1 to Figure A 2.8 in Appendix A. The results demonstrate the effects of varying the input parameters on the maximum rebar temperature and the corresponding time. No critical scenario, where the slab reached the critical rebar temperature, was found in the investigated ranges of these parameters, and consequently, the range of values for which the designed slab is structurally safe (i.e., with no critical temperature) was determined. Variations in concrete thickness were not varied, and it is assumed that the effects of these variations are included in the variations in rebar depth. The results confirm that variation in the total area, sample thickness, time to reach maximum gas temperature t_{lim} , coefficients in O_{lim} and Γ_{lim} , and unexposed surface's convective coefficient do not change the maximum rebar temperature from the reference case value.

OAT analysis allowed the identification of the input parameters which have little to no impact on maximum rebar temperature, and the mean values were used for 6 input variables in further probabilistic analysis, thus reducing the number of simulations needed and their runtime.

2.6 Probabilistic Assessment of Structural Fire Safety

This section seeks to investigate the fire resistance and reliability of the reinforced slab probabilistically, using Monte Carlo simulations, accounting for the uncertainties in the fire and heat transfer models in the case of a fully developed fire.

The OAT sensitivity analysis (Section 4) identified the key input parameters which had the greatest effect on the maximum rebar temperature for the purpose of the Monte Carlo simulation. The parameter ranges found in the literature and their expected values are given in Table 2.1 and Table 2.2. Probabilistic distributions were then defined for the selected parameters. A Gumbel distribution was assumed for the fire load density in accordance with EC 1-1-2 [3], with a mean value of 411MJ/m² and a variance of 0.3. Since little is known about the probability distribution of the other input parameters [65], for the purpose of this study a uniform distribution was conservatively assumed. Consequently, any value has the same probability of being selected over the set range. This assumption is conservative since it is the shape of the tail of each distribution that is important; in this case, if the high end (or the low end if this is critical) is artificially ‘fattened’ then the likelihood of randomly sampling from the tail is increased.

In Monte Carlo simulation, a value was selected at random for each of the input variables based on the given distributions, and the maximum rebar temperature in the concrete slab was calculated as before. The results for the model were recorded and the process was repeated. The Monte Carlo analysis comprised 1500 individual runs. One way to select the number of trials in a Monte Carlo simulation is to run the model repeatedly until the mean value of the outputs converges [66]. In this case, convergence was satisfied based on a tolerance of 5 % change in the mean and standard deviation in the output. It should be noted that the probabilities of failure were small, so less than 5% change in the mean value of the outputs did not significantly affect the probabilities of failure. Therefore, it was concluded that 1500 runs were enough.

The probability of failure P_f was calculated by evaluating the ratio between the number of simulations in which the structure failed (n_f) and the number of times the simulation was performed (n), given by:

$$P_f = \frac{n_f}{n} \tag{2.12}$$

The reliability of a system (R) was defined as the probability that it will perform successfully [67], which is given by:

$$R = 1 - P_f \tag{2.13}$$

The effect of the different variables on the maximum rebar temperature was compared from the results of the OAT, which let us exclude some of the lower impact variables, and in turn, reduce the number of runs needed to obtain a converged answer. The relationship between two variables can be ranked using Spearman’s correlation coefficient [55], which shows the strength and direction of a monotonic relationship between paired data. In this study, all graphs from the OAT analysis showed a linear and monotonic relationship, with very strong strength between the input and output data.

Instead, the strength of the relationship between maximum rebar temperature and different variables (i.e., the sensitivity of the probability of failure to different input data) was obtained from the results of the OAT. The resulting percentage change in the maximum rebar temperature, against a 10% variation of each parameter from the corresponding reference case, was plotted in Figure 2.8.

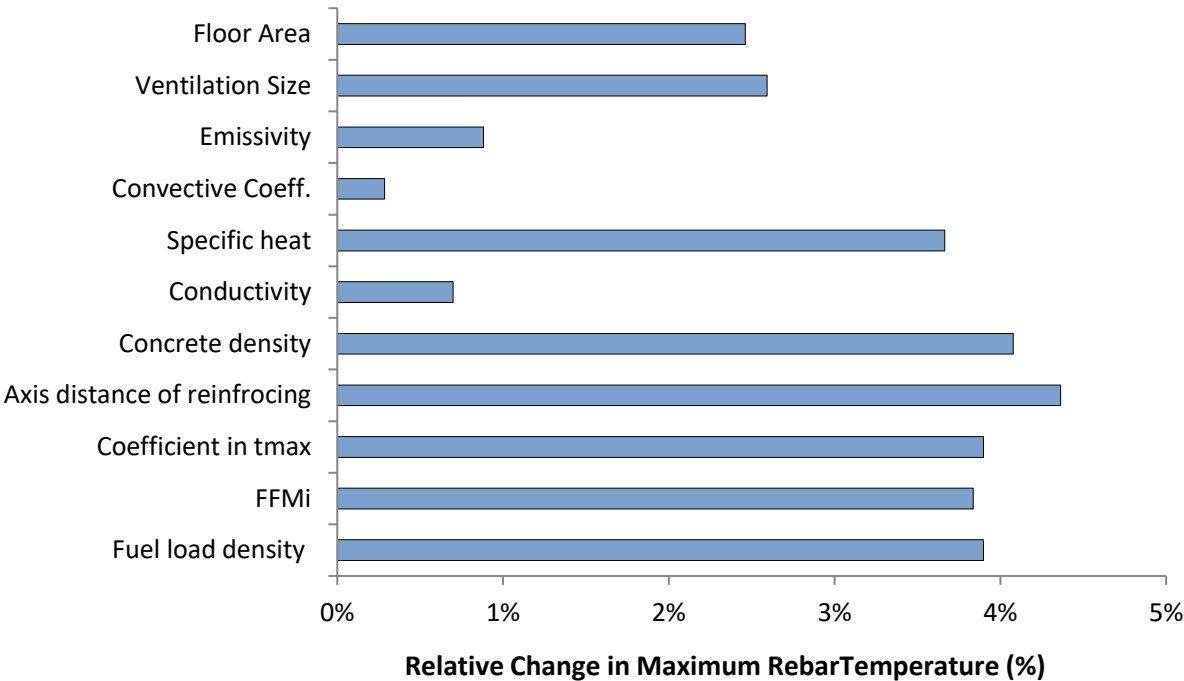


Figure 2.8 The resulting percentage change of the maximum rebar temperature to 10% variation of the reference case values of the most important input variables which were identified by the OAT sensitivity analysis.

Figure 2.8 shows that conductivity, emissivity, and convective coefficient are the lower impact variables. These parameters were excluded from the Monte Carlo simulation. The calculated reliability was thus slightly increased, and the number of simulations needed to achieve convergence of solution decreased to 750, where the probability of failure varied by less than 3.5 % in 100 iterations compare to 1500 trials (3.5% variation of probability of failure was too small). The simulation time also decreased to 2 hours for 750 runs, compared with 3.30 hours for 1500 runs, performed on a 2.1GHz Intel Core i7 processor.

The maximum rebar temperature is sensitive to the active firefighting measure index. Analyses were therefore conducted for the system with specified values for this sensitive parameter, where the probability of failure was calculated for different set up of active fire protection measures.

To examine a number of scenarios with different chains of events, an event tree approach was used. An event tree is a logical model expressing the possible outcomes of an event. The construction of event trees starts with specifying an event, and then various events following the initial event are modelled as branches of the tree. Each branch represents a specific risk scenario. The possible event sequence arising from the lack of active fire protections was structured, and the event tree is shown in Figure 2.9.

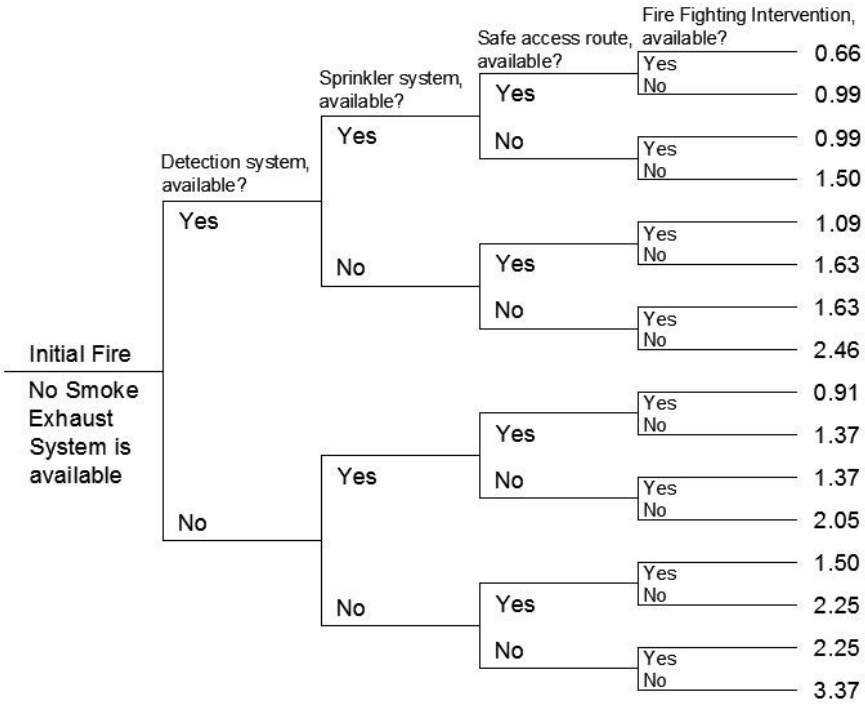


Figure 2.9 Event tree and possible scenarios for Monte Carlo sensitivity analysis. Each final scenario is an aggregation of events and was assigned a firefighting measures index in accordance with EC 1-1-2.

Each final scenario is an aggregation of events and was assigned a firefighting measures index in accordance with EC 1-1-2. Reliability analysis was performed on sub-scenarios in the event tree by varying all other parameters using Monte Carlo simulation.

For comparison, the Monte Carlo analysis was performed without considering the impact of active fire protection in Annex E of EC 1-1-2. This meant that the range for the firefighting measures index was dropped from the input variables in this specific analysis.

2.7 Results of the Monte Carlo Analysis and Discussion

Figure 2.10 shows the probability of reaching the failure criteria in a concrete slab when the active firefighting measures index ranges from 0.66 (i.e. sprinklers, automatic smoke detection and fire alarm, safe access routes, and firefighting devices) to 3.35 (no active fire protection and no intervention of fire fighters), in accordance with [3].

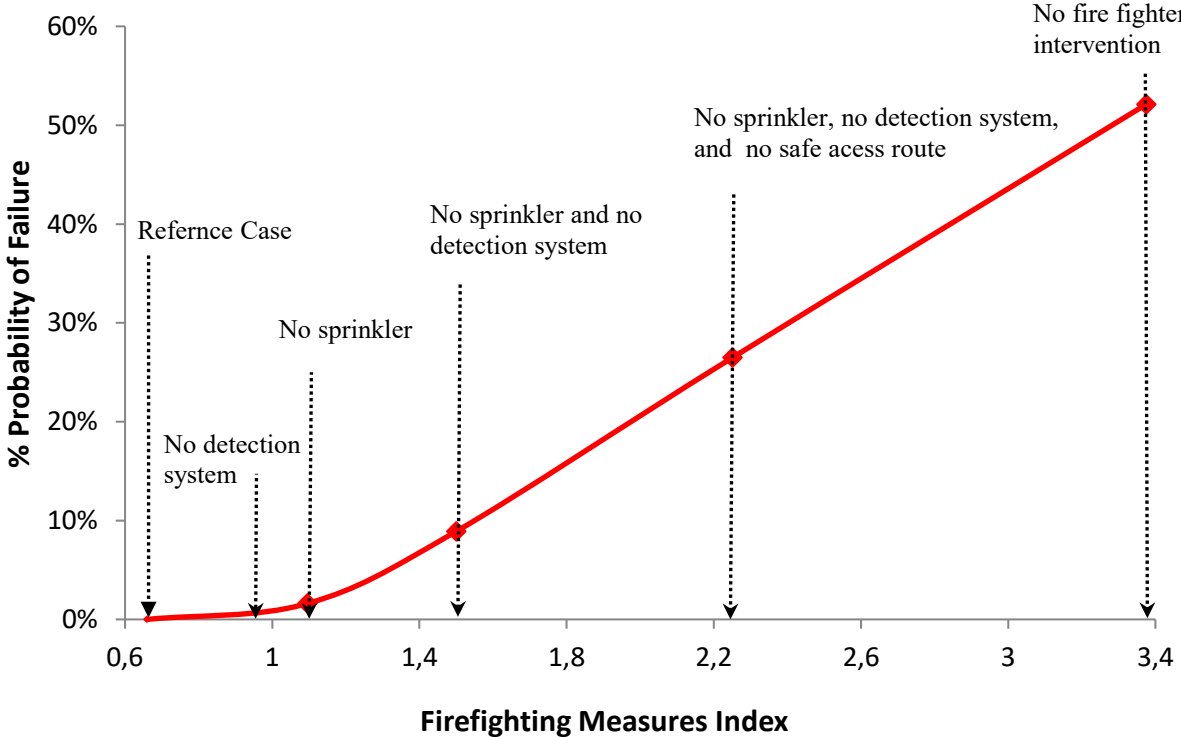


Figure 2.10 Probability of failure for a range of active firefighting measures of EC 1-1-2 from a Monte Carlo simulation based on 750 trials.

Figure 2.10 illustrates that for the reference scenario where detection and sprinkler systems, safe access route, and firefighting devices were available in the building, the probability of failure of the slab was 0.3%, therefore the reliability, R , was 99.7%, using Eq. (2.13). Unavailability of sprinkler systems, which also covers the case of “no detection system”, resulted in a 1% probability of failure. The reliability of the structure for this case was then $R = 99\%$. When both sprinkler system and detection and alarm systems were not available in the building, the probability of failure was 8%, which corresponds to 92% reliability. The higher the firefighting measure index, the higher the design fire load density and, consequently, the higher the probability of failure. The highest probability of failure corresponded to an extreme case when no active fire protection measures and no firefighting intervention were available, and therefore the randomly generated fuel load density was always multiplied by 3.37 in accordance with the methodology in EC 1-1-2 [3], which is indicated in the event tree in Figure 2.9. For this extreme case, the mean characteristic fuel load density of 411 MJ/m^2 (in Table 2.2) was multiplied by 3.37, and thus the mean value of 1385 MJ/m^2 was taken for the Monte Carlo analysis. As such a high probability of failure is expected.

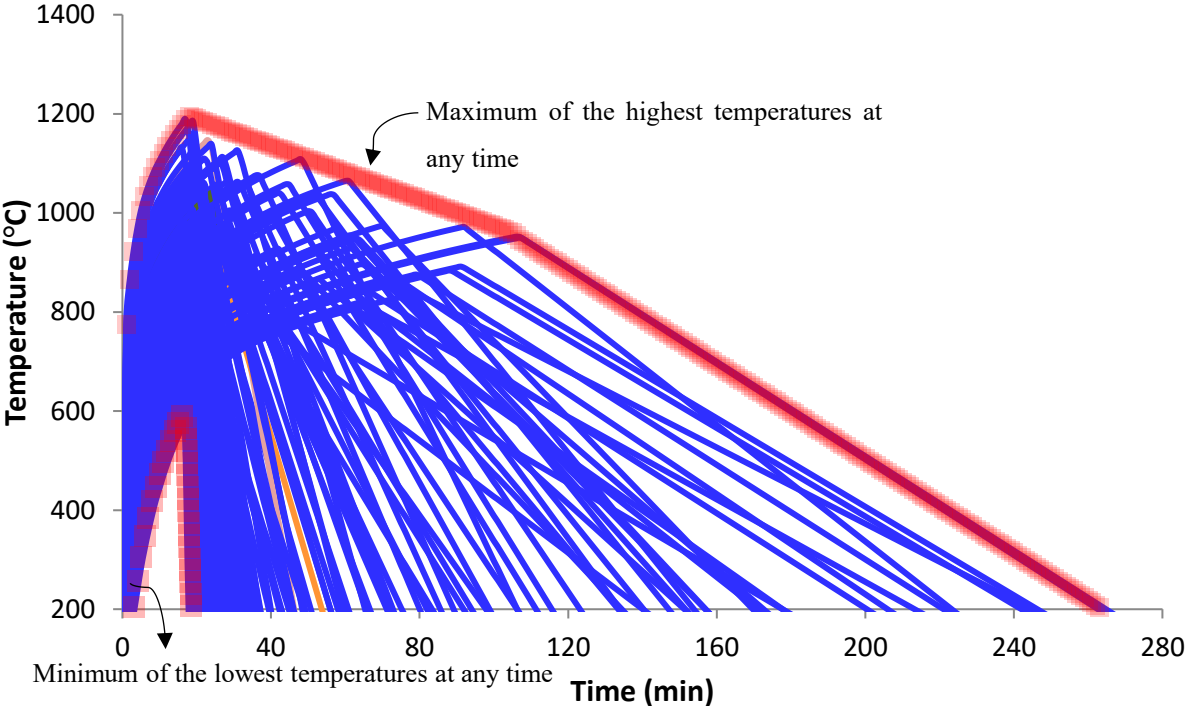


Figure 2.11 Resulting gas temperatures in the compartment from the Monte Carlo simulation using EC 1-1-2 parametric method. The red line is the converged result, and that the other lines are included to show how many scenarios are captured by the probabilistic approach. The sprinkler system is not available but there are detection system, safe access routes, and firefighting devices available in the compartment. The probability of failure is 1% in this case.

Figure 2.10 also shows that for the case without considering Annex E of EC 1-1-2 where the fire fighting measures index was taken 1, the probability of failure of the slab was 0.6%, which implies reliability of $R = 99.4\%$

For illustrative purposes, all of the possible temperature curves in the compartment, from the Monte Carlo simulation using EC 1-1-2 parametric fire, are demonstrated in Figure 2.11. The red line in Figure 2.11 is the converged result, and that the other lines are included to show how many scenarios are captured by the probabilistic approach. These gas temperatures were applied to calculate the probability of failure of the slab. In this case (Figure 2.11), the sprinkler system was not unavailable, but detection systems, safe access routes, and firefighting devices were available in the compartment.

2.8 Conclusion

The work herein applies a simple, but powerful, structured methodology to: (1) identify the most important parameters that need to be considered during fire safety engineering, and (2) to determine the reliability of a structural element exposed to fire when designed following EC 1-1-2. The methodology was applied to a simply-supported reinforced concrete slab 180 mm thick; with a standard load-bearing fire resistance of 90 min; subjected to a fire in an office building compartment of 420 m² floor area and 4 m height. Design fires were constructed in accordance with the EC 1-1-2 parametric fires, addressing both fuel-controlled and ventilation-controlled fires.

It was demonstrated that a maximum rebar temperature of 448°C was found after 102 min of fire exposure by a ventilation-controlled fire with an opening factor of 0.02 m^{1/2}, without using the Annex E of EC 1-1-2. It was found that using the Annex E of EC 1-1-2 decreased the maximum rebar temperature of the slab by 20%.

Analyses of the main input parameters in the EC 1-1-2 curves and heat transfer model were performed, in order to assess the sensitivity of the main results to parameter uncertainty, and also to define the safe and critical design fires using an OAT method. The critical design fires were found when the characteristic fire load density was above 1140 MJ/m² (densely loaded spaces) and 912 MJ/m², for cases with and without using Annex E of EC 1-1-2 respectively. It was concluded that using the factors in Annex E of EC 1-1-2 (i.e., δ_{q1} , δ_{q2} , δ_n , m) could highly affect the characteristic fire load density used to calculate the gas temperature.

The safe ranges of design fire scenarios were identified for the firefighting measures indices lower than 1.46 (i.e., sprinkler and detection systems were not available, however, safe access route and fire fighting devices were available) in the building. The axis distance of reinforcement the most sensitive parameter has a fixed value early in the design. The range selected for sensitivity analysis of axis distance of rebar implicitly included the possible loss of 24 mm concrete cover due to spalling, which does not have any impact on the resistance of the slab. The maximum gas temperature and corresponding rebar temperature from the parametric fire in EC 1-1-2 are highly sensitive to small variations of the size of the opening (i.e., ventilation), due to the change of fire environment from fuel-controlled to ventilated-controlled. The concrete density was found to have a large effect on the rebar maximum temperature. The assessment of fire safety of new products being made of low or high densities of concrete is possible using the method presented in this chapter. The OAT analysis determined that 8 out of 17 input parameters were the most sensitive in regard to changes in the maximum rebar temperature: axis distance of reinforcement, ventilation sizes, concrete density, coefficient in t_{max} , fuel load density, fire protection measures, specific heat, and floor area.

Such a structured approach could help to justify some of the assumptions and simplifications which are made in fire safety engineering, by identifying parameters for which more information is needed for different applications, thus allowing engineers to ignore some of the other parameters in Monte Carlo analysis, thus reducing the number of runs needed to have a converged answer.

It was found that the unavailability of fire protection measures, as indicated in the EC 1-1-2 method, leads to an increased probability of failure (lower reliability of structure). It was noticed that the probability of failure of the concrete slab was 0.3% (i.e., 99.7% structural element reliability) where detection and sprinkler systems, safe access route, and fire fighting devices were available in the building. Unavailability of either sprinkler systems or detection systems resulted in a 1% probability of failure of the slab (i.e., 99% reliability), and unavailability of sprinkler and detection systems resulted in an 8% probability of failure of the slab (i.e., 92% reliability). The probability of failure of the slab was equal to 0.6% (i.e., 99.4% reliability) without considering Annex E of EC 1-1-2.

The methodology presented in this chapter quantifies the reliability of a structural element in terms of collapse probabilities, using the Monte Carlo method. This methodology could be applied to define the reliability of a fire affected structure. In that case, more performance criteria and detailed structural analysis should be used to assess the failure modes of structures.

This novel study which conducted for the first time the OAT analysis and the Monte Carlo simulation of a slab exposed to the EC 1-1-2 parametric fire was considered by the International Organization for Standardization (ISO) for inclusion in an ISO technical report [68].

Chapter 3

Flame Extension and the Near Field under the Ceiling for Travelling Fires Inside Large Compartments

Summary⁴

Structures need to be designed to maintain their stability in the event of a fire. The travelling fires methodology (TFM) defines the thermal boundary condition for the structural design of large compartments of fires that do not flashover, considering near field and far field regions. TFM assumes a near field temperature of 1200 °C, where the flame is impinging on the ceiling without any extension, and gives the temperature of the hot gasses in the far field from Alpert's correlations. This chapter revisits the near field assumptions of the TFM and for the first time includes horizontal flame extension under the ceiling, which affects the heating exposure of the structural members thus their load-bearing capacity. It also formulates the thermal boundary condition in terms of heat flux rather than in terms of temperature as it is used in TFM, which allows for a more formal treatment of heat transfer. The Hasemi, Wakamatsu, and Lattimer models of heat flux from flame are applied for the near field. The methodology is applied to an open-plan generic office compartment of 960 m² floor area and 3.60 m high with concrete, and with protected and unprotected steel structural members. The near field length with flame extension (fTFM) is found to be between 1.5 and 6.5 times longer than without flame extension. The duration of the exposure to peak heat flux depends on the flame length, which is 53 min for fTFM compared to 17 min for TFM, in the case of a slow 5% floor area fire. The peak heat flux ranges from 112 to 236 kW/m² for the majority of fire sizes using the Wakamatsu model, and from 80 to 120 kW/m² for the Hasemi and Lattimer models, compared to 215 to 228 kW/m² for TFM. The results show that for all cases, TFM results in higher structural temperatures compared to different fTFM models (600°C for concrete rebar and 800°C for protected steel beam), except for the

⁴ This chapter is based on "Heidari, M., Kotsovinos, P., and Rein, G., 2020. Flame extension and the near field under the ceiling for travelling fires inside large compartments, *Fire and Materials*, vol. 44, no. 3, pp. 423–436."

Wakamatsu model that for small fires sizes leads to approximately 20% higher temperatures than TFM. These findings mitigate the uncertainty around the TFM near field model and confirm that it is conservative for the calculation of the thermal load on structures. This study contributes to the creation of design tools for better structural fire engineering.

3.1 Introduction

TFM considers the near field and far field regions of fire [27], [28]. The near field characterizes the region, where the flame is impinging on the ceiling without any extension. Far field is the hot gas region beyond the near field. As the fire travels throughout the compartment, the structural elements at the ceiling level experience thermal exposure from the far field and near field regions.

The assumptions in the travelling fires methodology produce a simple and reasonable representation of travelling fires scenarios that can be used conservatively for structural design. The methodology does not intend to represent all processes related to fire dynamics in large compartments, which further research is still required. This chapter revisits the near field assumption of TFM and includes the flame extension under the ceiling. It thus considers the full extension of the near field region, which affects the heating exposure to the structural members. This new concept is labelled in this thesis as traveling fire with flame extension (fTFM).

TFM has traditionally been expressed in terms of gas temperatures; rather than heat fluxes [27], [28]. This is to provide a simple thermal boundary condition that can be readily used by structural engineers, following the standard of the ISO834 [13] and EC 1-1-2 [3] parametric design fires that are traditionally adopted in design. These traditional design fires assume uniform temperature and uniform burning conditions [3], which are not valid for large compartments [26]. In addition, the standard fire can only be used for comparative design purposes or benchmarking in some countries where objective-based codes are used. The use of temperature is generally appropriate for heat transfer within the gas phase [11], [21]. However, in order to consider the flame extension under the ceiling, the boundary conditions are best to be expressed in terms of incoming heat fluxes. Available methodologies describing flame extension under the ceiling utilize heat flux in their expressions. Heat flux is an appropriate boundary condition that can be used to determine the structural element temperature and thus structural behaviour. This is discussed by Torero et al. [21] since the thermal boundary conditions at the exposed surface of a structural element are based on conservation of energy.

In this chapter, a methodology to calculate the horizontal flame length under the ceiling is investigated, thus allowing to determine the heat flux along the length of flame under the ceiling; in turn, improving the near field assumption of TFM to obtain a better boundary condition for a surface exposed to a travelling fire. Comparison for a generic open-plan office compartment is presented. The thermal response of a concrete slab and protected and unprotected steel beams subjected to travelling fires with flame extension (fTFM) is studied based on three different heat flux calculation methodologies, along with iTFM and the EC 1-1-2 parametric fire curve.

3.2 Flame Extension in Compartment Fires

When the flame height exceeds the ceiling height, a part of the flame deflects horizontally and becomes a part of a shallow layer under the ceiling that carries heat and smoke to the area far from the fire location (i.e., ceiling jet). The flame length below the ceiling controls the heat transfer to the ceiling from the flame. Studies on the flame extension under a non-combustible ceiling [11], [69] suggest that the ratio of the horizontal part of the flame to the cut-off height due to the presence of a ceiling could range from 0.88 to 12, depending on the configuration involved. A considerable flame extension can occur when the fire is large in comparison to the ceiling height as discussed by Drysdale [11].

Hasemi et al. [70] studied the behavior of flame under an unconfined ceiling during a set of experiments and found that the flame length under the ceiling data could be correlated with non-dimensional heat release rate, given by:

$$L_H = 2.9H \cdot (Q^*)^{0.33} - H \quad (3.1)$$

$$Q^* = \frac{Q}{1.11 \cdot 10^6 \cdot H^{\frac{5}{2}}} \quad (3.2)$$

where L_H [m] is the horizontal flame length along the ceiling away from the symmetrical flame axis, H [m] is the ceiling height above the fire source, Q is the heat release rate [W], and Q^* is the non-dimensional heat release rate. These equations, which are adopted in EC 1-1-2 (Annex C) applied in this chapter. Other methods are also available to calculate the horizontal part of flame under the ceiling, depending on the configuration [71].

Hasemi et al. [70] also carried out experiments to measure the incident heat flux from a localized fire to an unconfined flat ceiling located above the different sizes of propane burners (0.3 m, 0.5 m, and 1 m in diameter) (Figure 3.1(a)). Their study considers heat release rates and ceiling heights and measured the incident heat flux to the ceiling from fire and fire plume impinging on the ceiling. They measured heat flux at different locations r from the flame centreline axis, using heat flux gauges. The peak heat flux of 100 kW/m^2 was measured at the stagnation point (the symmetrical flame axis) as illustrated in Figure 3.1 (b).

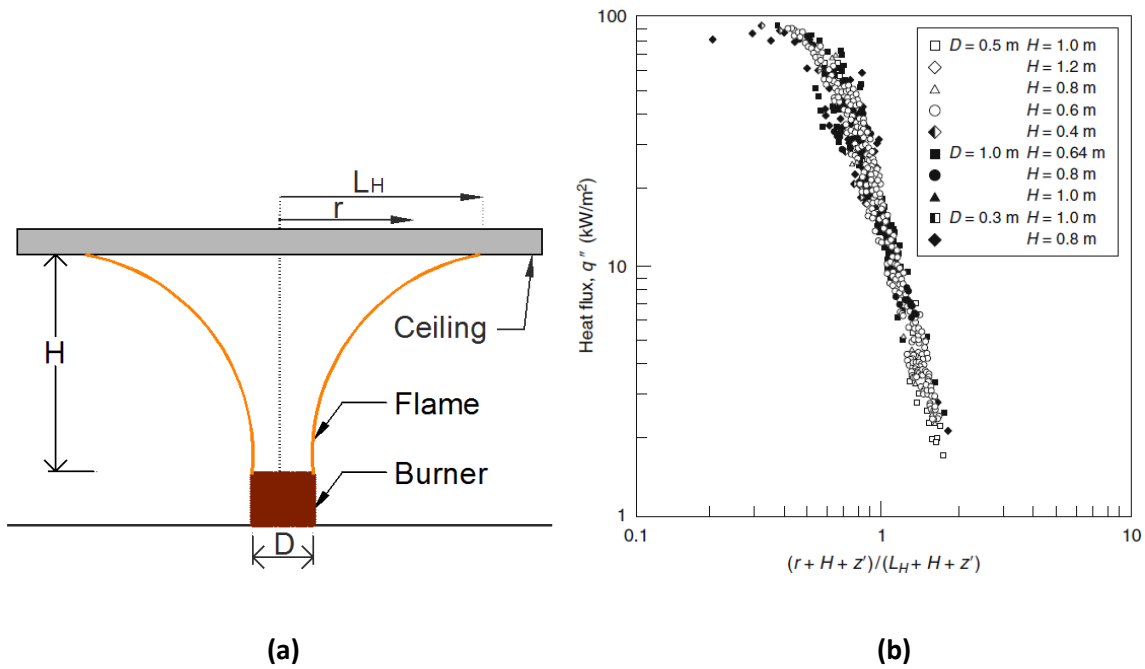


Figure 3.1 (a) Sketch of a flame impinging on the ceiling and extending horizontally. (b) Measured heat fluxes under an unconfined ceiling from an impinging buoyant diffusion flame reported by Hasemi et al. [70] L_H is the flame extension under the ceiling, given by Eq. (3.1). y is the normalized distance of the studied point from the virtual fire source (see Eq. (3.3))

Further experiments [72] with heat release rates of up to 61 MW and fire surface area of 150 m^2 using wood and polystyrene, showed a good prediction of the Hasemi model in the area above the fire zone and presented the following expressions to determine the received heat flux to the ceiling from localized fires flame when the flame is impinging on the ceiling:

$$q_c'' = \begin{cases} 100 & \text{for } y \leq 0.3 \\ 136.3 - 121y & \text{for } 0.3 < y \leq 1 \\ 15y^{-3.7} & \text{for } y > 1 \end{cases} \quad (3.3)$$

$$y = \frac{(r + H + z')}{(L_H + H + z')} \quad (3.4)$$

$$z' = 2.4D \cdot (Q_D^{*\frac{2}{5}} - Q_D^{*\frac{2}{3}}) \quad \text{for } Q_D^* < 1 \quad (3.5)$$

$$z' = 2.4D \cdot (1 - Q_D^{*\frac{2}{5}}) \quad \text{for } Q_D^* \geq 1 \quad (3.6)$$

$$Q_D^* = \frac{Q}{1.11 \cdot 10^6 \cdot D^{\frac{5}{2}}} \quad (3.7)$$

where q_c'' [kW/m²] is the incident heat flux at the ceiling, r [m] is the horizontal distance [m] between the centerline axis of the fire and a point along the ceiling where the thermal flux is calculated, y is the normalized distance of the studied point along the ceiling from the virtual fire source, H [m] is the ceiling height above fire source, z' [m] is the virtual origin of the fire, Q_D^* is the non-dimensional heat release rate, and D [m] is the diameter of the fire (see Figure 3.1 (a)). These expressions were adopted by EC 1-1-2 [3] to calculate the horizontal flame extension under the ceiling, and thus the heat flux received by the fire exposed unit surface area at the level of the ceiling.

Wakamatsu et al. [71] also studied the same problem and presents a correlation for the incident heat flux to the ceiling as a function of y , the normalized distance of the studied point from the virtual fire source, given by:

$$q_c'' = 518.8e^{-3.7y} \quad (3.8)$$

The heat flux measurements in the Myllymaki [73] experiments from fires impinging on I-beam mounted to a ceiling, using heptane pool fires and different ceiling heights, show a good agreement between the Wakamatsu equation and the tests data. Lattimer [71] reviewed a number of studies on thermal conditions produced by fires impinging on the ceiling. He discussed the methods to determine the heat flux boundary condition for structural members at the level of the ceiling. Based on the data from Hasemi [70] and Myllymaki [73] experiments, Lattimer [71] presents the following equations to calculate the incident heat flux to an unconfined ceiling.

$$q_c'' = 120 \quad \text{for } y \leq 0.5 \quad (3.9)$$

$$q_c'' = 682e^{-3.4y} \quad \text{for } y > 0.5 \quad (3.10)$$

The model by Lattimer [71] sets the peak heat flux to 120 kW/m² at y less than or equal 0.5, unlike the Wakamatsu et al. [71] model that does not have a peak heat flux as plotted in Figure 3.2.. The curve from Wakamatsu equation and the data from Hasemi et al. [70] are illustrated in Figure 3.2. for comparison. It can be seen that the Wakamatsu equation and the test data are almost in the same range when y is greater than 0.45, but the Wakamatsu equation overestimates the heat flux for smaller values of y .

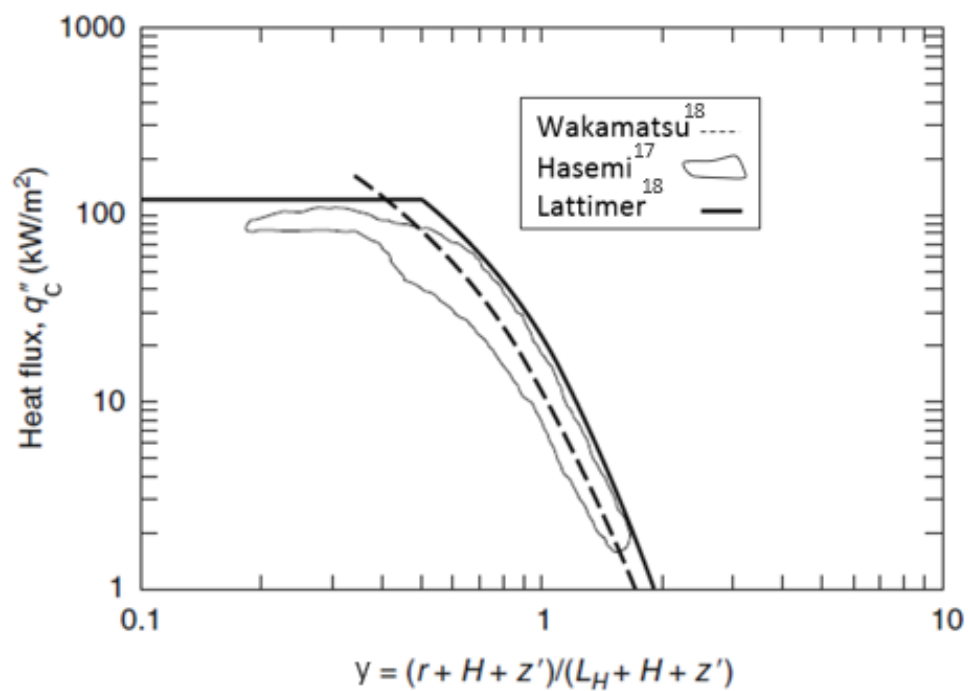


Figure 3.2 From [71], a comparison of the data from Hasemi et al. [70] (outlined area), the dashed line represents the Wakamatsu and the continuous line represents the bounding fit to the data from Hasemi and Wakamatsu.

For comparative purposes and given that the flame extension has not been studied for travelling fires, all three models available in the literature, Hasemi, Wakamatsu, and Lattimer, will be applied in this study. All models will be combined individually with iTFM to consider flame extension (fTFM) and determine the heat flux boundary condition under the ceiling to the structural elements. It should be noted that the calculated heat flux here does not apply to columns.

3.3 Travelling Fires with Flame Extension

3.3.1 Background to TFM

TFM [27], [28] produces a temporally and spatially non-uniform temperature distribution. The methodology can consider a range of possible flame lengths, L_f [m], which is equivalent as fire diameter (D) in 1D compartment, by assuming different fire spread rates, s [m/s]. These spread rates control the time required for the leading edge of the fire to travel while the trailing edge of the fire is governed by the time required for the fuel to burn out (t_b). The flame length, L_f , is therefore defined as:

$$L_{f \min/\max} = s_{\min/\max} \cdot t_b \quad (3.11)$$

$$t_b = \frac{q_f}{Q''} \quad (3.12)$$

Fire spread rates between 0.1 and 19 mm/s have been determined from various experiments conducted to date on wood crib fires [28]. The range of possible fire sizes is from $\frac{L_{f \min}}{L}$ to $\frac{L_{f \max}}{L}$ where L [m] is the length of the compartment. t_b [s] is the local burning time, which is a function of the fuel load density, q_f [J/m²], and the heat release rate per unit area Q'' [W/m²].

Total fire duration t_t [s], and location of the leading edge of the fire, relative to the end of the compartment where the fire started x' [m], can be calculated as follow:

$$t_t = t_b \cdot \left(\frac{L}{L_f} + 1 \right) \quad (3.13)$$

$$x' = s \cdot t \quad (3.14)$$

TFM assumes that the fire travels throughout the compartment and structural elements at the ceiling level see the impact of the far field and near field temperature. The far field temperature, where the hot gas temperature is estimated, is calculated by Alpert's correlations [30], which were developed based on set fire tests with an unconfined ceiling, with heat release rate ranging from 600 kW to 98 MW (Figure 3.3). TFM uses Alpert's correlation for the reason of simplicity since the difference between Alpert's correlation and other available methods for far field temperature are negligible and

considering the additional complexity, the computational time required, and uncertainty in the parameters associated with other methods [28]. The far field temperature T_{ff} [°C], is obtained by the following expressions:

$$T_{ff} = T_{\infty} + \frac{5.38}{H} \cdot \left[\frac{L \cdot L_t^* \cdot W \cdot Q'' \cdot 10^{-3}}{(x + 0.5L \cdot L_t^* - x'_t)} \right]^{\frac{2}{3}} \quad (3.15)$$

$$\text{For } x' \leq L \rightarrow x'_t = s \cdot t; L_t^* = \min \left[\frac{L_f}{L}, \frac{s \cdot t}{L} \right] \quad (3.16)$$

$$\text{For } x' > L \rightarrow x'_t = L; L_t^* = 1 + \frac{L_f - s \cdot t}{L} \quad (3.17)$$

where T_{∞} [°C] is the ambient temperature, W [m] is the width of the compartment, x [m] is the location of interest in the compartment from the ignition point, x'_t [m] is the location of the leading edge of the fire at time step t [s], and L_t^* is the varying dimensionless fire size which depends on the location of the leading edge of the fire.

TFM assumes the near field temperature to be $T_{nf} = 1200^{\circ}\text{C}$. The phenomenon of flame flapping can be incorporated, which considers a non-vertical flame resulting from ventilation and turbulence. This flapping phenomenon includes the cooler smoke with the fluctuating flame, calculated by Alpert's correlation, into near field temperature and decreases the near field temperatures for small fire sizes. A flapping angle of $\theta = \pm 6.5^{\circ}$ is typically assumed in iTFM. The equation used to calculate the reduced near field temperature due to flapping is a combination of near field temperature and Alpert's correlation [28]. The flapping effect is incorporated in travelling fires with flame extension.

3.3.2 TFM with Flame Extension (fTFM)

TFM bounds the near field (i.e., the flame region) to the flapping length under the ceiling and does not consider the flame extension beyond this region. In reality, the fire could extend a few meters under the ceiling. Therefore, the structural elements would experience more intense heating under the direct impact of the flame instead of the hot gases. This chapter includes the flame extension into TFM and extends the formulation of the near field region of the TFM, which allows for a better resolution of the near field.

The flame extension equation (Eq. (3.1)) is a function of the non-dimensional heat release rate, and subsequently is a function of the heat release rate. Considering this, the non-dimensional heat release rate can be calculated as follows, using the heat release rate from TFM:

$$Q^* = \frac{L \cdot L_t^* \cdot W \cdot Q''}{1.11 \cdot 10^6 \cdot H^{\frac{5}{2}}} \quad (3.18)$$

where Q'' [W/m²] is the heat release rate per unit area. Eqs. (3.16) and (3.17) are used to define varying fire size and location of the leading edge based on whether the fire is still increasing in size or at its maximum size (Eq. (3.16)), or has reached the far end of the compartment and is decaying (Eq. (3.17)). Combination of flame extension equation under the ceiling (Eq. (3.1) and Eq. (3.18)) results in the flame extension under the ceiling for travelling fire at time t during the fire:

$$L_H(t) = 2.9 H \cdot Q^{*0.33} - H \quad (3.19)$$

It should be noted that TFM is used to find the gas temperature distribution at all locations in the compartment when the fire is spreading in one direction and covering the complete width of the compartment. Therefore, Eq. (3.19) defines the flame extension under the ceiling in the direction that the fire is moving. This allows one to calculate the heat flux from the extended flame under the ceiling to the structural elements, using available methods to calculate the heat flux. The methodologies in Section 3.2; Hasemi, Wakamatsu, and Lattimer, are used to define the distribution of received heat flux to the ceiling from the fire, over the near field region. Figure 3.3 shows an illustrative example of the final heat flux-temperature curve using iTFM with flame extension under the ceiling, which is explained further below. Figure 3.3 illustrates the near field with flame extension, which has a length twice the flame extension length under the ceiling. The far field temperature beyond the flame region under the ceiling is calculated using Alpert's correlation, as in TFM. The far field temperature is then converted to the received heat flux to a cold surface to be consistent with the definition of heat flux of Hasemi, Wakamatsu, and Lattimer models. This heat flux conversion is a novel contribution of this work and is discussed in detail in Section 3.3.3.

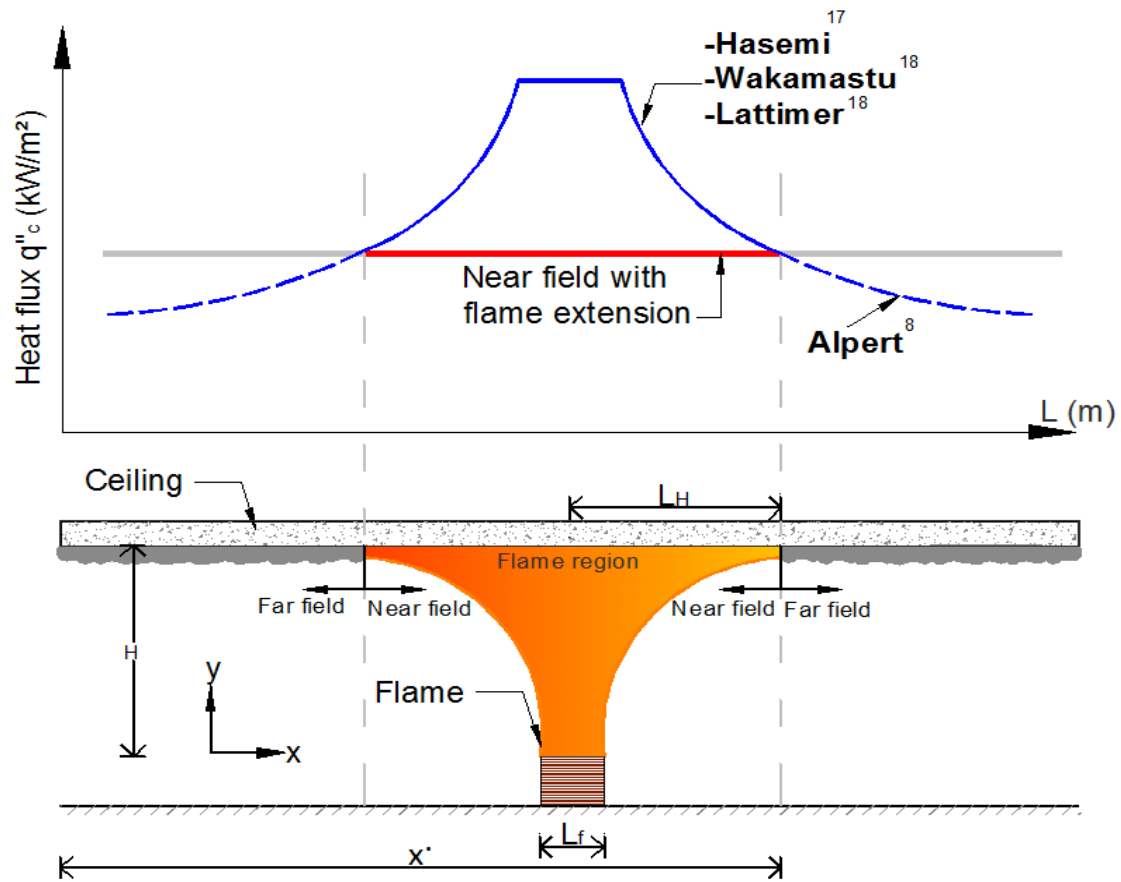


Figure 3.3 Schematic of TFM with flame extension under the ceiling. For the near field region with flame extension, the heat flux is calculated from Hasemi, Wakamatsu and Lattimer models. For the far field, the heat flux to a cold surface were calculated from TFM far field temperature. L is the length of the compartment.

The received heat flux to the ceiling in the near field region, as illustrated in Figure 3.3, at a location x and time t of interest could be then expressed as below for the three different models.

1. Hasemi:

$$q''_c(x, t) = \begin{cases} 100 & \text{for } y_t \leq 0.3 \\ 136.3 - 121y_t & \text{for } 0.3 < y_t \leq 1 \\ 15y_t^{-3.7} & \text{for } y_t > 1 \end{cases} \quad (3.20)$$

2. Wakamatsu:

$$q_c''(x, t) = 518.8e^{-3.7y_t} \quad (3.21)$$

3. Lattimer:

$$q_c''(x, t) = 120 \quad \text{for } y_t \leq 0.5 \quad (3.22)$$

$$q_c''(x, t) = 682e^{-3.4y_t} \quad \text{for } y_t > 0.5$$

The horizontal distance between the centerline vertical axis of the travelling fire and a point along the ceiling at each time step, r_t [m], and the fire size, L_f [m], in accordance with iTFM are given by:

$$r_t = |x + 0.5 L \cdot L_t^* - x_t| \quad (3.23)$$

$$L_f = 0.5 L \cdot L_t^* \quad (3.24)$$

A point of studied with distance x from the ignition point is considered in the flame region (near field) when $r_t < L_H(t)$, therefore Eqs. (3.20) to (3.22) could be applied to calculate the received heat flux to the point of studied.

The normalized distance of the point of interest from the virtual fire source, y_t , the virtual source location, z'_t (m), and Q_L^* is the non-dimensional heat release rate at time t during the fire can be calculated as follow:

$$y_t = \frac{(r_t + H + z')}{(L_H(t) + H + z')} \quad (3.25)$$

$$z'_t = 2.4 L_f \cdot (Q_L^{*\frac{2}{5}} - Q_L^{*\frac{2}{3}}) \quad \text{for } Q_L^* < 1 \quad (3.26)$$

$$z'_t = 2.4 L_f \cdot (1 - Q_L^{*\frac{2}{5}}) \quad \text{for } Q_L^* \geq 1 \quad (3.27)$$

$$Q_L^* = \frac{L \cdot L_t^* \cdot W \cdot Q''}{1.11 \cdot 10^6 \cdot L_f^2} \quad (3.28)$$

It is important to It should be noted that the nomenclature of “iTFM+Hasemi (iTFM+Ha)”, “iTFM+Wakamatsu (iTFM+Wa)” and “iTFM+Lattimer (iTFM+La)” is adopted for the different models with flame extensions included and determined in accordance with equations 20, 21, and 22 respectively.

For clarity, Figure 3.4 (a) shows an illustrative example of the received heat flux to a structural member at the ceiling level for an arbitrary location in a compartment, using the methodology presented in this chapter. The heat flux calculated from iTFM is also plotted. The combination of near field, calculated by Hasemi model, and far field from iTFM provide the total heat flux boundary condition (Figure 3.4 (b)).

It should be noted that the maximum heat flux between those calculated from Hasemi model and iTFM were selected for the near field with extension flame, assuming the peak heat flux is always below 100 kW/m² (the peak heat flux prediction of Hasemi model). This is because the heat flux from a flame cannot be lower than the heat flux from the hot gas.

In the same way, the heat flux-time curve could be generated using Wakamatsu (Eq. (3.21)) and Lattimer (Eq. (3.22)) models, assuming that the peak heat flux with Lattimer model is 120 kW/m² while there is no peak heat flux limit for the Wakamatsu model.

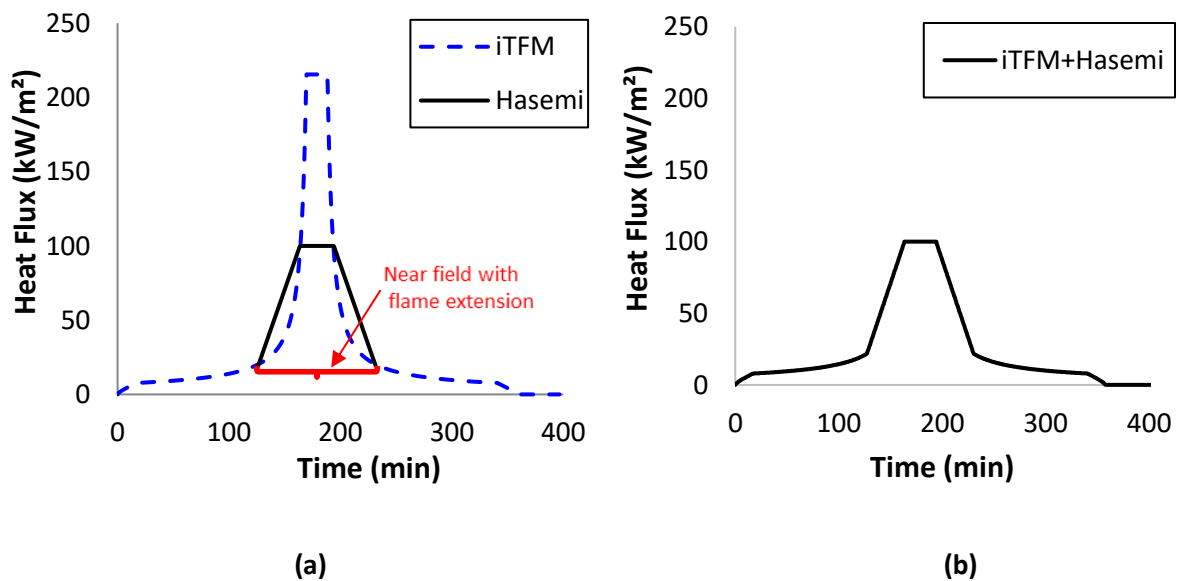


Figure 3.4 illustrative example of, (a) the heat flux at the ceiling level for an arbitrary location in a compartment using iTFM compared to the methodology with flame extension, (b) the final heat flux boundary condition in accordance with fTFM, combining the far field from iTFM and the near field from Hasemi.

3.3.3 Heat Flux Boundary Condition

As discussed in Section 3.1 and shown by Torero et al. [21], heat flux is a thermally accurate way to define the boundary condition at the exposed surface of the structural element as temperature may not always be appropriate [21]. In this section, the heat flux concepts are reviewed to extract the relevant parameters needed to convert the gas temperature from TFM to heat flux. The standard definitions and principles of the heat transfer phenomena are not described here and can be found in Incropera et al. [56].

The net heat flux boundary condition consists of heat transfer by convection (q''_{con}) and radiation (q''_{rad}) from fire to the solid surface:

$$q''_{net} = q''_{rad} + q''_{con} = \varepsilon_s \cdot \varepsilon_f \cdot \sigma \cdot \Phi \cdot [(T_g + 273)^4 - (T_s + 273)^4] + h(T_g - T_s) \quad (3.29)$$

where ε_s and ε_f are the surface and fire emissivity, σ is the Stephan Boltzmann constant ($= 5.67 \cdot 10^{-8}$ W/m²K⁴), Φ is the view factor, T_s and T_g are the surface and the gas temperature respectively, and h [W/m²] is the convective coefficient. Hasemi et al. [70] used a water-cooled heat flux gauge during the experiments to measure the maximum received heat flux. These gauges are cooled so that their surface temperature (T_s) remains low at T_∞ in the range (20–80°C). Cooling the gauge surfaces maximizes heat transfer to the surface. Gauges are coated with high emissivity coating paint ($\varepsilon \approx 0.95$) to maximize the absorbed radiation. As such, the flux gauges measure the maximum received heat flux (q''_c). The net heat flux to a surface can be also expressed in terms of q''_c by the following equation as [3], [71]:

$$q''_{net} = q''_c - \varepsilon_s \cdot \varepsilon_f \cdot \sigma \cdot \Phi \cdot [(T_s + 273)^4 - (T_\infty + 273)^4] - h \cdot (T_s - T_\infty) \quad (3.30)$$

where q''_c was measured in experiments of Hasemi [70] and Myllymaki [73]. By comparing Eq. (3.29) and Eq. (3.30), the gauge heat flux can be express as:

$$q_c'' = \varepsilon_s \cdot \varepsilon_f \cdot \sigma \cdot \Phi \cdot [(T_g + 273)^4 - (T_\infty + 273)^4] - h \cdot (T_g - T_\infty) \quad (3.31)$$

The heat Eq. (3.31) is used in this chapter to formulate the heat flux at the exposed surface of a structure in the far field (i.e. thermal boundary condition), assuming the worst case that the solid surface remains at ambient during heating (this relies on the fact that heating rate of the gases and solid occur at different time scales as per the EC 1-1-2 parametric fire [3]. Eq. (3.31) converts the far field temperature from iTFM to the heat flux consistent with the work of Hasemi [70], Wakamatsu [71], and Myllymaki [73]. Therefore, in fTFM both near and far field are expressed consistently.

3.4 Comparison for a Generic Structure

A generic steel-framed composite structure with a concrete slab and steel beams (composite floor on decking) is considered in order to study the impact of TFM with flame extension (fTFM) on the thermal response of structural members. The results are compared with the thermal analysis of the same structural elements, using the TFM and the EC 1-1-2 parametric fire (which assumes a uniform temperature inside the compartment). The structural response to thermal exposures has not been assessed in this work.

The compartment is an open-plan office building, which was a similar compartment as used before in iTFM methodology [28], with a floor area of 960 m², 40 m long by 24 m wide, and 3.6 m high (Figure 3.5). Staircases or any division are excluded from the definition of the compartment area and layout as described by [26], [27]. The building consists of a concrete slab 180 mm deep with 38 mm concrete cover and steel beams of section UB457x191 UB 133⁵ with 7 mm high-density perlite. Different flooring systems were used for this case study to provide a more comprehensive analysis where the impact of the fTFM, iTFM and parametric fire are studied. This allowed to The concrete slab has also the same thickness as the one used in Chapter 2, so the analysis in this chapter is linked more coherently to Chapter 2.

The fuel load density (q_f'') and heat release rate per unit area (Q'') are taken as 511 MJ/m² and 500 KW/m² respectively [3]. The risk-based factors of EC 1-1-2 have not been applied here and risks are

⁵ UB is the Universal Beams sizes as in the UK. UB457x191 UB 133 has a mass per meter of 133.3 kg/m², depth of 480.6 mm, width of 196.7 mm, thickness of web 15.3 mm, thickness of flange 26.3 mm.

assumed to be explicitly considered by the designer. The fire starts at the left side and travels along the compartment (see Figure 3.5).

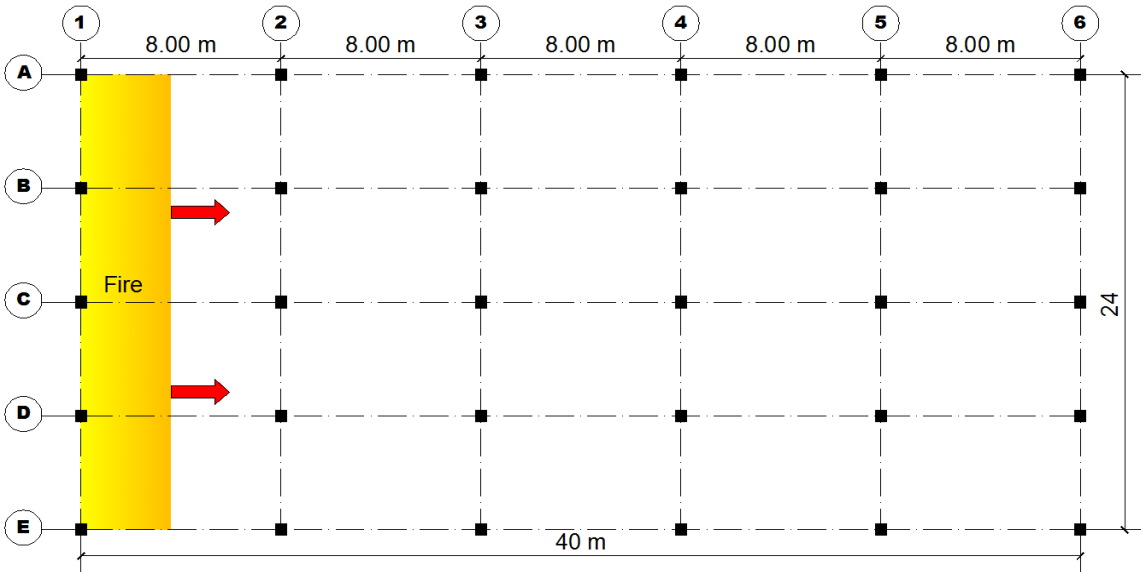


Figure 3.5 Plan of the structure. A-E and 1-8 are structural gridlines. The fire spans the full width of the compartment (gridlines A to E) and starts from the left-hand side of the compartment travelling at a constant spread rate to the right part of the compartment.

The thermal properties of concrete are taken as; specific heat of 1000 J/Kg K, the density of 2300 Kg/m³, thermal conductivity 1.33 W/m K [1], [40] with the convective heat transfer of 35 W/m² and 4 W/m² for exposed surface and backside respectively [1], [40]. The thermal properties of steel are taken as, the specific heat of 600 J/Kg K, the density of 7850 Kg/m³, with a convective coefficient of 35 W/m² [2], [40]. The thermal properties of insulation are taken as high-density perlite with 7 mm thickness; the specific heat of 1200 J/Kg K, the density of 550 Kg/m³, thermal conductivity of 0.12 W/m K [40]. Temperature-dependent thermal properties of passive protection could result in somehow higher accuracy of the steel temperature, although for the purposes of this study and sake of simplicity, constant values were applied. The net heat flux, q''_{net} , are calculated from Eq. (3.30). Heat transfer calculations are carried out as in Incropera et al. and Buchanan [40], [56], with heat flux being used as the boundary condition. In-depth concrete temperature is calculated by applying the finite-difference method for the heat conduction Eq.(3.32) [56]. The thermal conductivity of steel is higher than concrete, therefore the steel rebar temperature is assumed to be the same as adjacent concrete. It has been shown that 1D heat transfer with constant effective properties results in conservative in-depth concrete temperature [27]. The lumped mass heat transfer method [40], [56] is used for thermal analysis of the protected beam (Eq. (3.33)) and unprotected steel beam (Eq. (3.34)), as given by:

$$q''_{\text{net}} \cdot t + K \cdot \frac{T_1^t - T_0^t}{\Delta x} = \rho_c \cdot c_c \cdot \frac{\Delta x}{2} \cdot \frac{T_1^{t+1} - T_0^t}{\Delta t} \quad (3.32)$$

$$q''_{\text{net}} \cdot F \cdot \Delta t = \rho_s \cdot c_s \cdot V \cdot \Delta T_m \quad (3.33)$$

$$q''_{\text{net}} \cdot F \cdot \Delta t = \rho_s \cdot c_s \cdot V \cdot \Delta T_m + \rho_i \cdot c_i \cdot d \cdot F \cdot \frac{\Delta T_m}{2} \quad (3.34)$$

The net heat flux, q''_{net} , are calculated from Eq. (3.30).

3.4.1 Heat Flux and Flame Extension Length

A family of fires is investigated based on typical fire spread rates observed in compartment fires (0.1 to 19.3 mm/s) [28] to generate the heat flux fields across the compartment. The corresponding fire sizes were between 0.3% and 55% of the compartment area, using Eq. (3.11) (i.e., fire length between 0.11 m and 22 m). The family of fire sizes accounts for a plausible range of fuel load densities, heat release rates, fire spreads in large compartments. This allows finding the most challenging and appropriate scenarios for structural design.

The fire is assumed to be at floor level (H becomes the compartment height) and starts at the left-hand side of the compartment, spans the full width, and travel over time to the right-hand side of the compartment (Figure 3.5). Previous studies have examined the sensitivity analysis of the input parameters and demonstrated that flame spread rate is important [27], [28]. It has been shown that different fire paths and shapes do not necessarily have a significant impact on the thermomechanical response of the structure [22].

The flame extension under the ceiling for different fire sizes is calculated at each time step, in accordance with the methodology described in this chapter. Figure 3.6 demonstrates the relation between fire sizes and the maximum near field length with flame extension under the ceiling ($2L_H$, see Figure 3.3) normalized by the fire length. The normalized near field increases sharply to 6.5 for fire sizes less than 7% floor area and then decreases to 1 for 100% fire size. Figure 3.7 shows how the near field length with and without flame extension varies with the size of the fire. For example, for a 5% fire size, the near field with flame extension (fTFM) is 12.8 m while the near field calculated from TFM is 2 m. The near field length with and without flame extension (fTFM and iTFM) for a 25% fire size is 26.8 m and 10 m respectively. For the 50% fire size, the near field lengths are 36 m and 20 m using the presented methodology (fTFM) and TFM without flame extension.

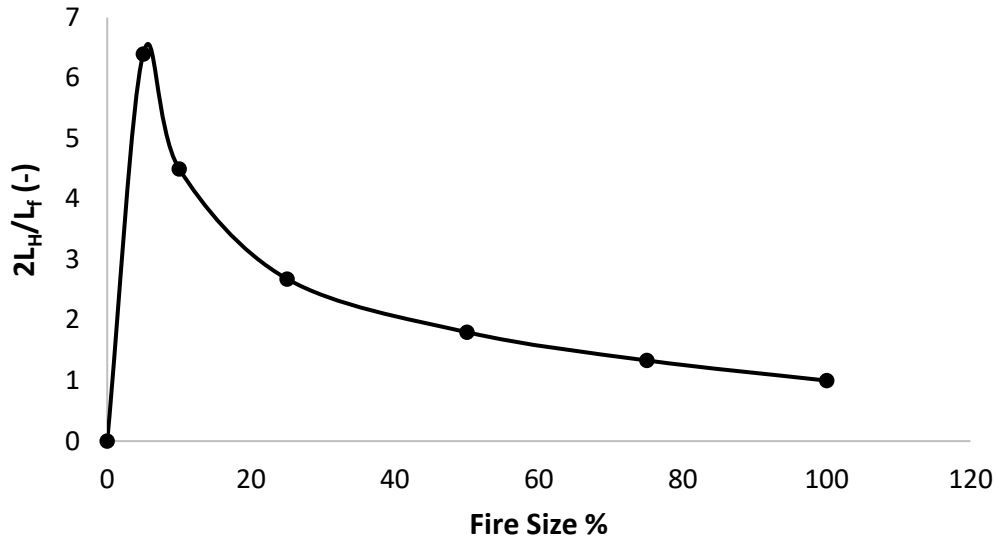


Figure 3.6 Ratio of flame extension length under the ceiling ($2L_H$) over the near field length of iTFM (L_f) vs. fire size. The smaller the size of the fire, the greater the ratio.

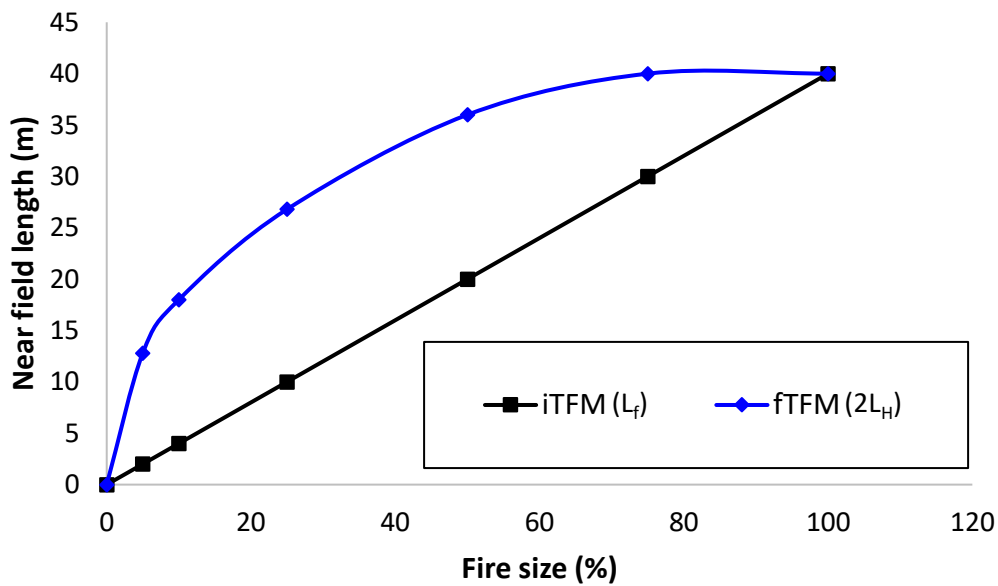


Figure 3.7 The near field with flame extension (fTFM) and iTFM for different fire sizes. The near field length with flame extension is considerably greater than the TFM near field.

Figure 3.7 illustrates that more structural elements at the ceiling could be affected by the impact of near field when the flame extension is included in TFM (by fTFM). This exposes more structural elements for a longer period to the direct heat of hot flame rather than the colder hot gases of far field at any moment in time. This change in the thermal exposure could impact the resulting structural

behavior, although this is not addressed in this chapter. However, due to the flexibility of the travelling fires methodology with the family of travelling fires, a broader range of fire sizes would include all potential phenomena. For this case study, a family of travelling fires is generated and investigated with sizes ranging from 5% to 55% of the floor area, in accordance with the methodology presented in this chapter (fTFM). The calculated heat fluxes from the TFM are also used for comparison.

Figure 3.8 illustrates the received heat flux curves from a 5% floor area travelling fire with flame extension (fTFM) and no flame extension (TFM), generated in the middle of the case study compartment. The results show how the flame extension affects the near field and far field duration.

The total burning duration is 358 min. TFM has a far field duration of 341 min and a near field duration of 17 min, with a peak heat flux of 216 kW/m². TFM with flame extension results in a total far field duration of 249 min and the near field duration of 109 min, where the Hasemi, and Lattimer result in peak heat fluxes of 100, 120 respectively. The peak heat flux from Wakamatsu is overly high and equal to 454 kW/m²(this value of heat flux is not realistic for a localized fire in an ordinary building such as commercial, office, etc. The maximum heat flux measured in the test for a localized fire beneath an unconfined ceiling and I-beam was 130 kW/m² [73].)

The peak heat flux using the flame extension and the Wakamatsu model (iTfM+Wa) is larger than the one calculated with TFM. Flame extension with the Lattimer model (iTfM+La) and the Hasemi model (iTfM+Ha) result in a lower peak heat flux than TFM. The time that the structural element is heated by the peak heat flux varies between different models, where iTfM+La has the largest duration of 52 min, iTfM+Ha and TFM had 28 min and 17 min respectively.

It should be noted that as discussed by Lattimer [71], the Wakamatsu model does not limit the peak heat flux. Therefore, for small fire sizes, very high peak heat fluxes are experienced that may not be realistic/representative. Despite this shortcoming, they are included in this work to study the relative performance from the different models.

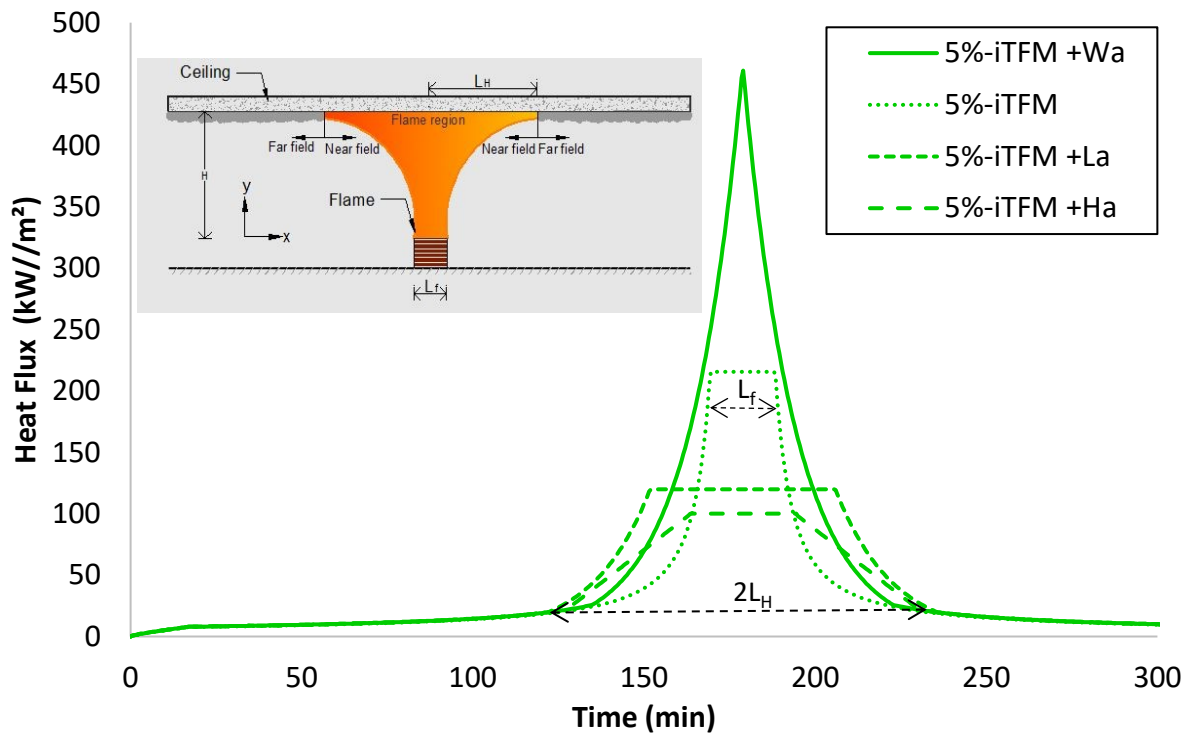


Figure 3.8 A comparison of TFM with and without flame extension for a 5% floor area travelling fire. Hasemi, Wakamatsu and Lattimer models were used for near field when the flame extension was included.

Figure 3.9 to Figure 3.11 show the heat flux-time curves and the near field durations from a family of travelling fires with and without flame extension, for a point in the middle of the compartment at the ceiling level. Eqs. (3.21), (3.22), and (3.23) are applied to determine the near field heat flux, in accordance with the presented methodology. The results illustrate that the lower the fire size, the longer the near field duration when the flame extension is included.

Figure 3.12 shows the variation of peak heat flux obtained from TFM, TFM+Ha, TFM+Wa, and TFM+La for fire sizes of 5% to 50% floor area. The peak heat fluxes decrease or remain constant when the fire size increases, except for TFM without flame extension. This is due to the shorter flame extension under the ceiling and the larger normalized distance of the studied point from the virtual fire source y_t , for the larger fire sizes. On the contrary, the smaller the fire size, the lower peak heat flux calculated from TFM, as shown in Figure 3.12. This due to the impact of flapping angle in small fire sizes of TFM.

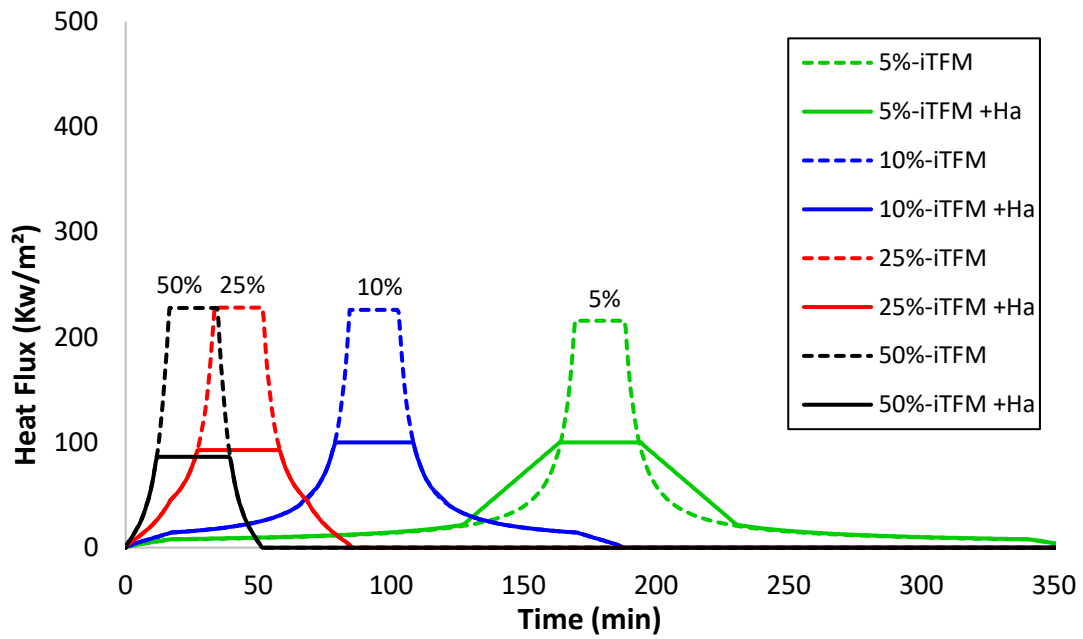


Figure 3.9 Heat flux received at the ceiling level in the middle of the compartment for a family of traveling fire sizes, using TFM and iTFM+Hasemi (iTFM+Ha). The peak heat flux in iTFM+ Hasemi is set to 100 kW/m², in accordance with Hasemi model. The impact of extended near field is more important for small fire sizes.

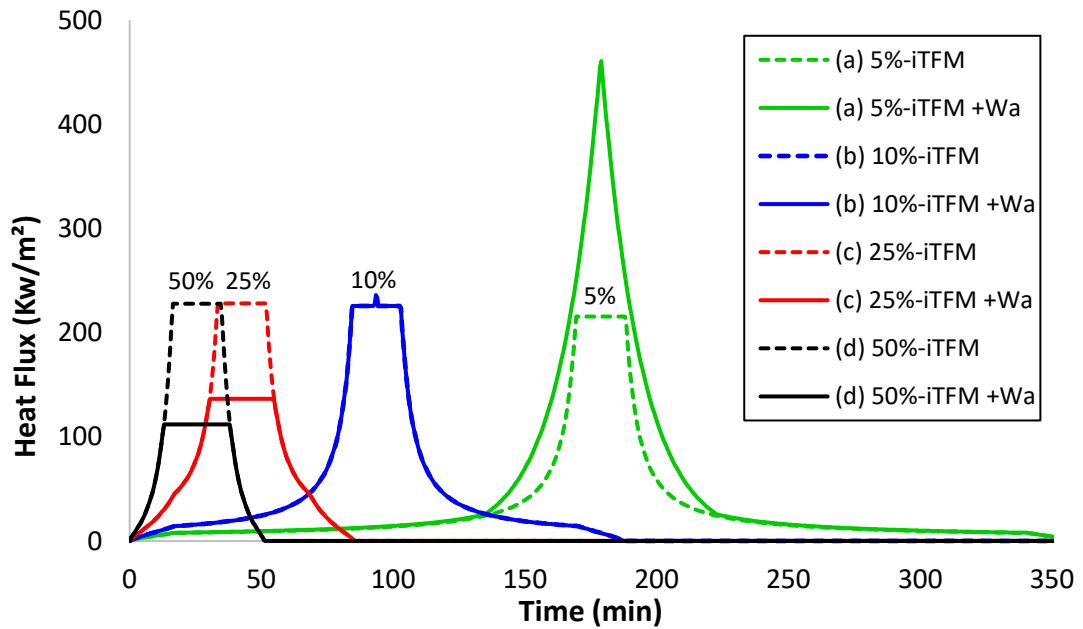


Figure 3.10 Heat flux received at the level of the ceiling in the middle of the compartment for a family of traveling fire sizes using iTFM and iTFM+Wakamatsu. The impact of extended near field is more obvious for small fire sizes.

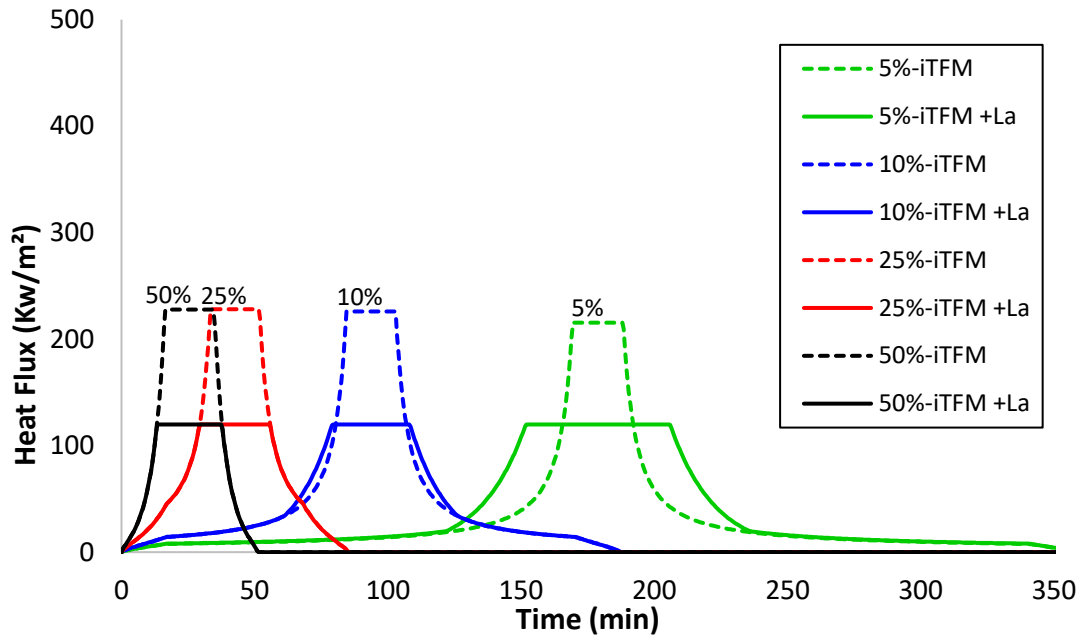


Figure 3.11 Heat flux received at the level of the ceiling in the middle of the compartment for a family of traveling fire sizes using iTFM and iTFM+Lattimer. The peak heat flux in iTFM+ Lattimer is set to 120 kW/m², in accordance with Lattimer model. The impact of extended near field is more obvious for small fire sizes.

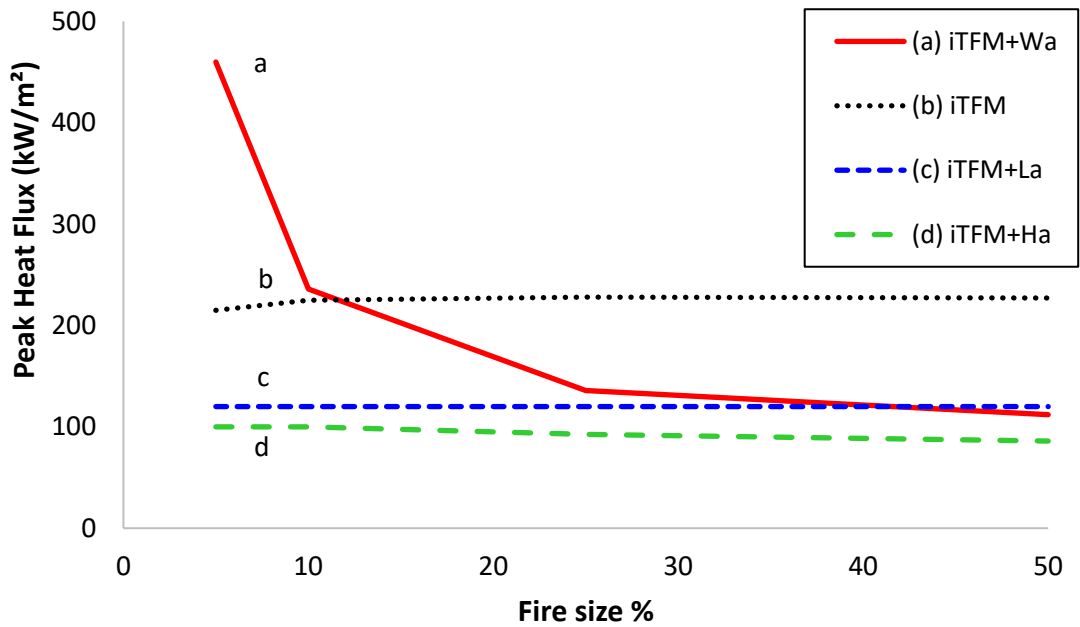


Figure 3.12 Peak heat flux versus the fire size for TFM with and without flame extension.

3.4.2 Thermal Analysis

Structural fire performance can be evaluated using different performance/failure criteria such as maximum temperature, maximum deflection, the ultimate strain, shear capacity, composite action, and continuity within the structure [1], [2], [60] depending on the method and objectives of the analysis. Thermal criteria may not always be adequate to conservatively estimate structural fire performance for complex structures [68], [74].

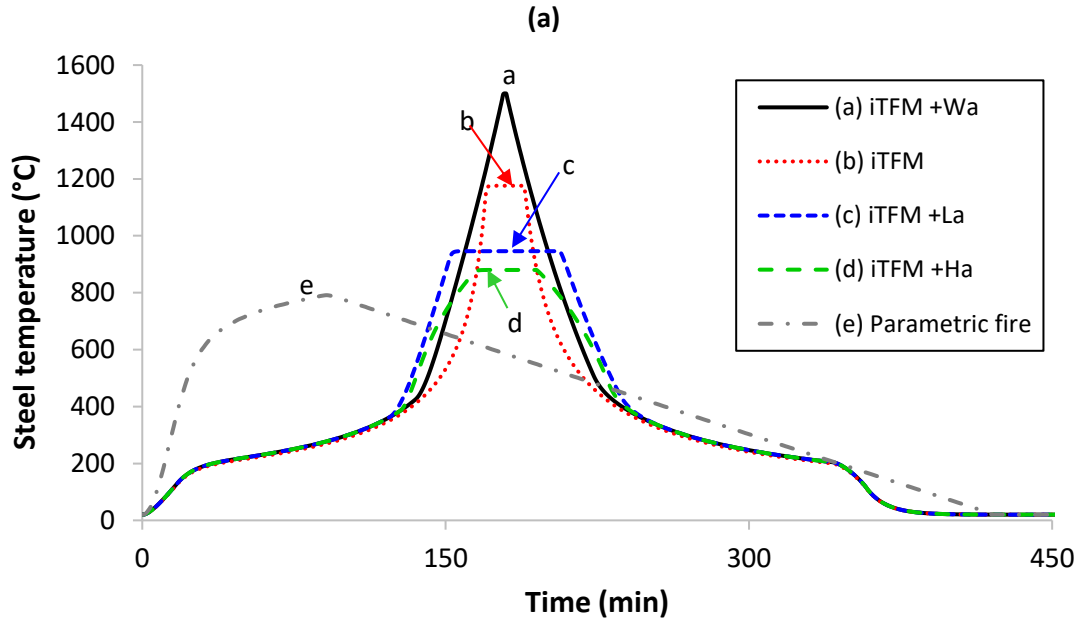
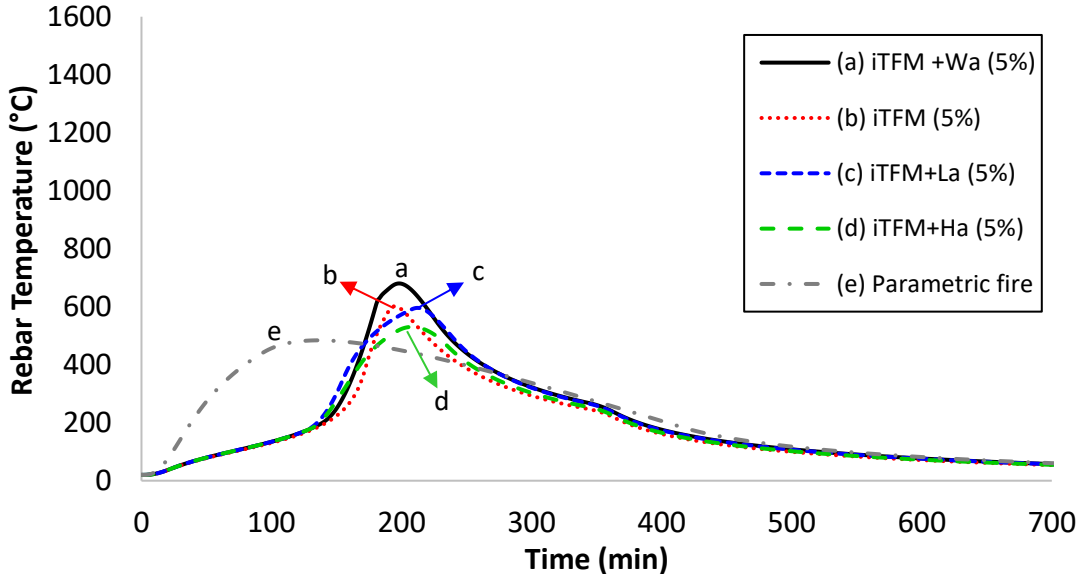
The peak rebar temperature is used as a simple performance criterion to revisit the near field assumption of TFM. The simplified calculation method using the rebar temperature is following the principles described EC 2-1-2 [1], as the simply supported slab was subjected to a uniformly distributed load and the design at ambient temperature has been based on linear analysis. This allows determining how travelling fires with flame extension and a heat flux boundary condition could affect the temperature distribution in the structural element. This is illustrated through a comparative study, where TFM and the EC 1-1-2 parametric fire are also applied. The results of the thermal analysis can be used to identify the worst-case fire scenario and the critical structural members inside the compartment.

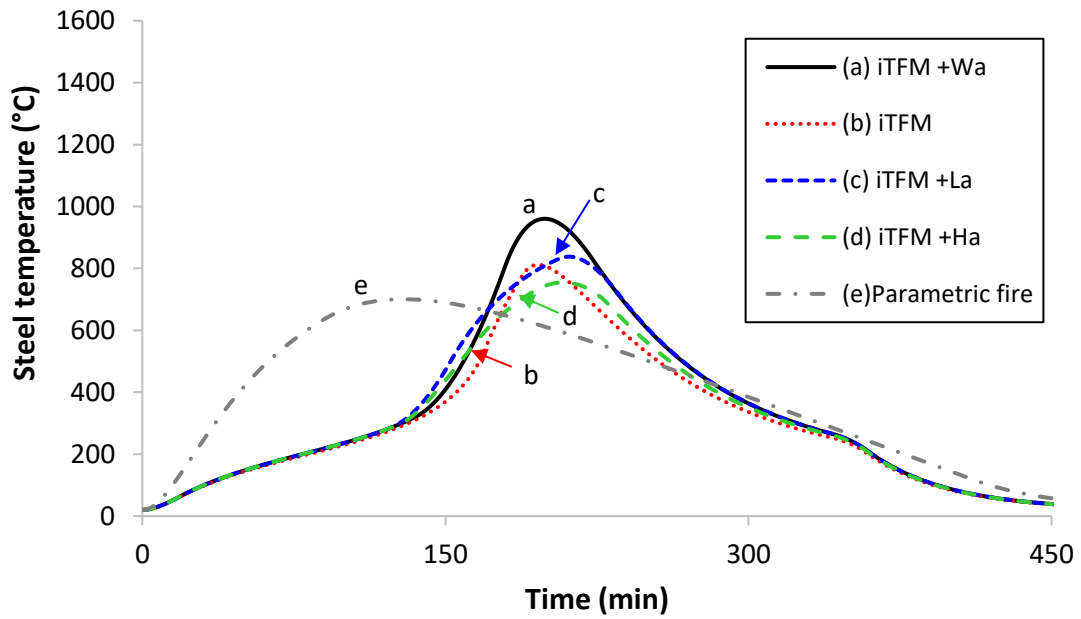
The temperature distributions within the steel beams and concrete slab in the middle of the compartment are determined. A family of travelling fires (TFM) ranging from 2.5% to 55%, showed that the 10% fire size results in the highest temperature in the structure at locations further than half of the compartment length from the fire origin [28]. Besides, the impact of flame extension and variation of heat flux was more evident for the 5% fire size, as discussed in the previous section. Therefore, for the purpose of this study, both 5% and 10 % of floor area fire size are examined. Future studies could investigate the impact of all family of travelling fires with flame extension and heat flux boundary condition at all locations in the compartment, using FEM and considering other performance criteria.

Figure 3.13 and Figure 3.14 show the resulting temperatures of the steel and concrete members at all times during a fire. Figure 3.13 shows the temperature for (a) concrete rebar, (b) unprotected and (c) protected steel for a 5% fire size. Figure 3.14 shows the same for a 10% fire size.

Figure 3.13 and Figure 3.14 show that the protected steel beam temperatures and concrete rebar temperatures follow a similar trend. As expected, the unprotected steel beam temperature quickly reaches the near field temperature due to the high conductivity and the low thermal inertia of steel.

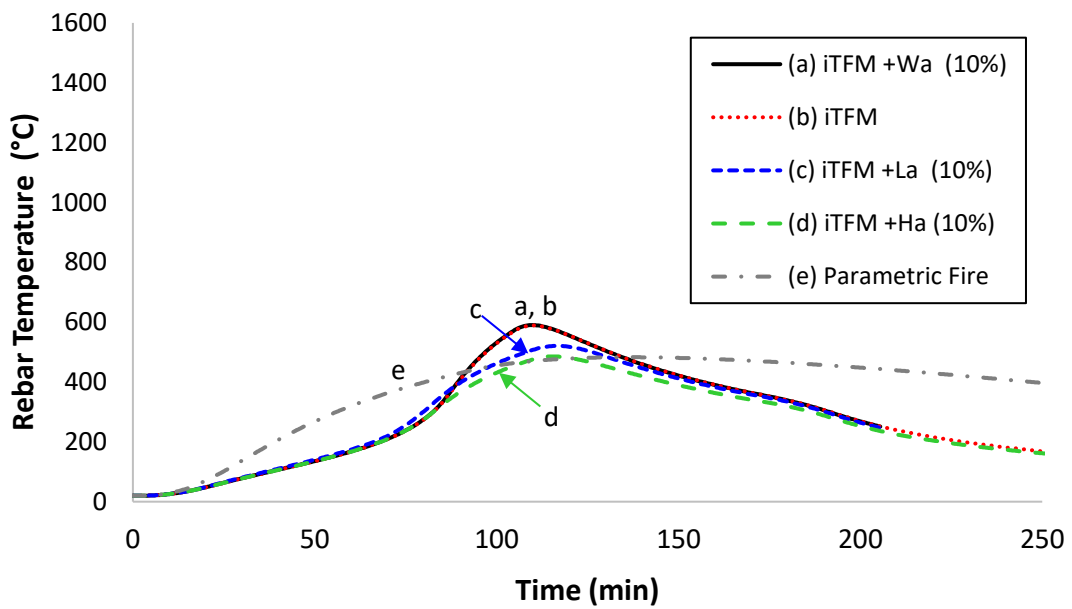
The maximum temperatures obtained for steel and concrete beams are for the 5% fire size. iTFM+Wa results in higher slab and beam temperatures than TFM, for the 5% fire size, and an equal temperature to TFM for the 10% fire size. This is due to the longer near field duration and the greater peak heat flux predicted by iTFM+Wa in comparison with TFM. It should be however noted that as discussed in the previous section, the Wakamatsu model does not have any peak heat flux like the Lattimer and Hasemi models and therefore the results may be unrealistic and overly conservative. This comparative study illustrates that the effect of TFM with flame extension is more important for smaller fire sizes.



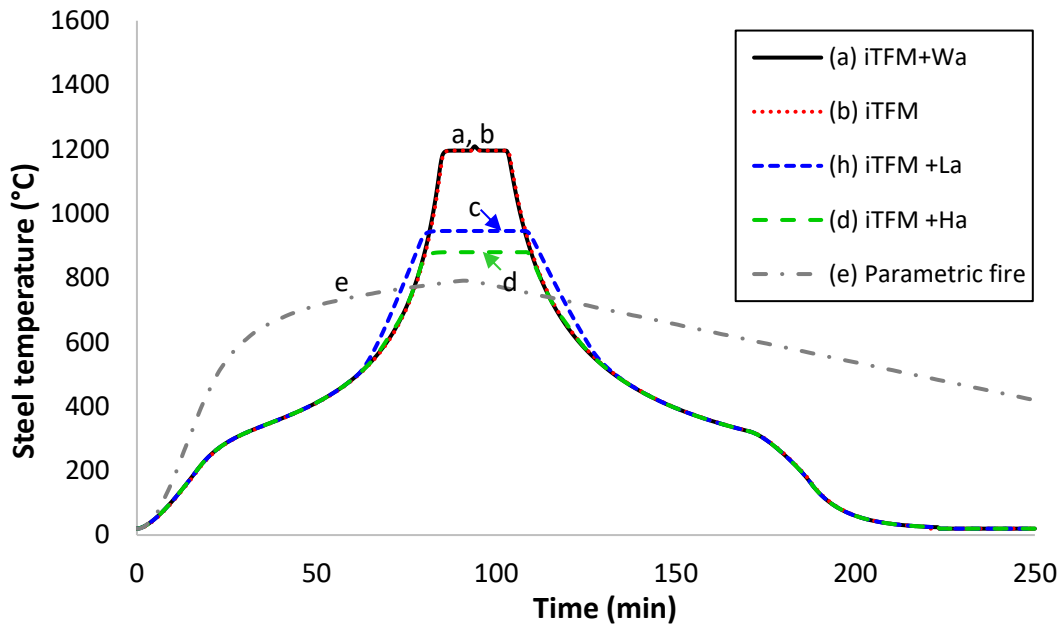


(c)

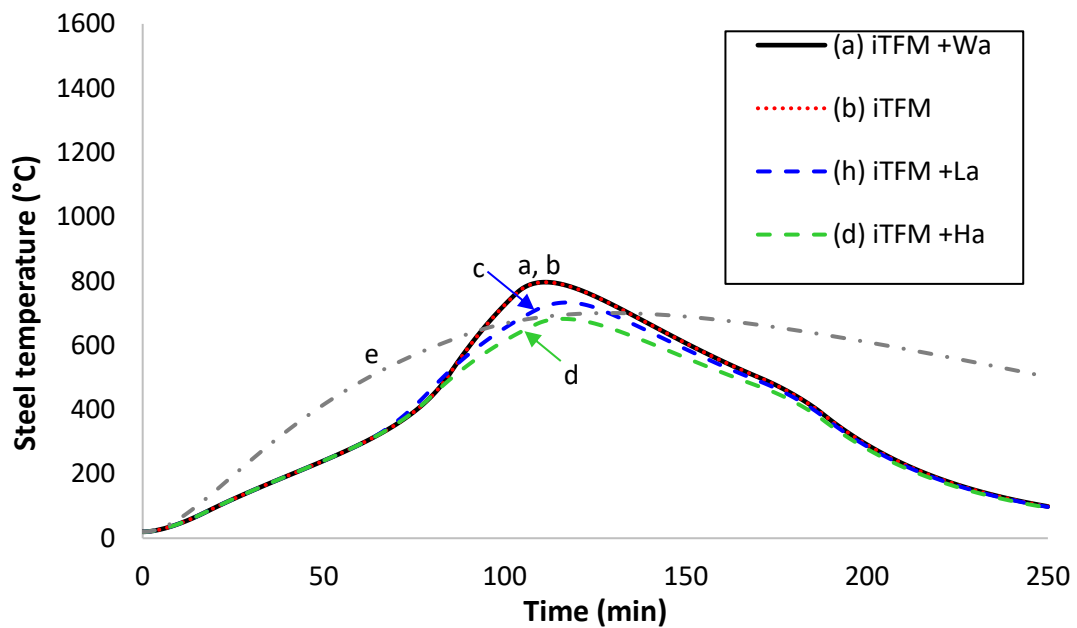
Figure 3.13 Comparison of beam temperature curves using parametric fire with 25% ventilation, 5% floor area iTFM without and with and flame extension, for (a) concrete rebar, (b) unprotected and (c) protected steel (R60) beams in the middle of the compartment.



(a)



(b)



(c)

Figure 3.14 Comparison of temperature curves using iTFM with and without flame extension with different models, for (a) concrete rebar, (b) unprotected and (c) protected steel (R60) beams in the middle of the compartment, for a fire size of 10% floor area.

In the case of the 5% fire size, the iTFM+La has a peak heat flux of 120 kW/m² in comparison with TFM with 215 kW/m² (see Figure 3.11). However, the resulting peak temperatures of the protected

steel beam and concrete slab temperatures are similar despite the large differences in heat flux for thermal analysis.

The structural element temperatures using iTFM, fTFM, and EC 1-1-2 parametric temperature-time curves are compared in Figure 3.13 and Figure 3.14. The comparison shows that both TFM with and without flame extension result in peak temperature of structural elements up to 420°C higher than the parametric fire (for 10% fire size).

The results presented in this chapter can be explored through a more detailed structural analysis (for example, whole frame behavior) considering different performance criteria, as a travelling fire with flame extension may lead to different structural behavior than that indicated by examining TFM [28] for same fire size or that suggested by the peak temperature of single elements results given here. Further study includes the impact of the family of fire sizes across the compartment.

The peak heat flux from Lattimer correlation is 120 kW/m² and from Hasemi correlation adopted in EC 1-1-2 is 100 kW/m², which limits the maximum near field prediction of TFM+Ha and TFM+La. Further sensitivity analysis is needed on the peak heat flux at the ceiling level. It should be noted that the presented methodology could be updated when more experimental data are available. The study shows that the TFM near field model can be used conservatively to assess thermal response for structural design purposes provided that a suitable range of fire sizes is selected. Future experiments in large compartments are needed to further improve the near field model.

3.5 Conclusion

The travelling fires methodology (TFM) characterizes the thermal boundary condition where fire travels across the compartment floor plate leading to fire durations of several hours and a non-uniform thermal environment inside the compartment. TFM is a design tool based on several assumptions and therefore this chapter revisits its near field assumptions.

This work for the first time considers the flame extension under the ceiling for the near field region of travelling fires, which affects the heating exposure to the structural members. This thesis also for the first time formulates the TFM in terms of heat flux rather than temperatures, thus allowing for a more formal heat transfer boundary condition between the gas and the surface of the structural element. The Hasemi, Wakamatsu, and Lattimer models are used to determine the heat flux received at the level of the ceiling. The presented methodology is applied to an office compartment of

960 m² floor area and 3.60 m high with concrete and protected and unprotected steel structural members. The analyses compare the thermal response of the concrete slab and steel structural beams when subjected to iTFM, the travelling fires models with flame extension and the EC 1-1-2 parametric fire curve, which assumes uniform temperature and a uniform burning condition.

Travelling fires with flame extension, lead to an increase in the length of the near field. For a 5% fire size, the near field with flame extension is 12.8 m where the near field length from iTFM is 2 m. The near field length with and without flame extension for a 25% fire size is 26.8 m and 10 m respectively. The analysis illustrated that the smaller the fire size, the larger impact of flame extension on the near field length.

The peak heat flux of small fire sizes, using the flame extension and the Wakamatsu model is larger the one calculated with TFM. Flame extension with the Lattimer model and the Hasemi model result in a lower peak heat flux than TFM. The time that the structural element is heated by the peak heat flux varies between different models and fire sizes. For a 5% floor area fire TFM+ Lattimer has the largest duration of 52 min, TFM+Hasemi and TFM had 28 min and 17 min respectively. The study shows that the near field duration depends on the length of flame under the ceiling, rather than the local burning time of TFM. The smaller the fire size, the longer the near field duration. This could affect the resulting temperature of the structural elements and structural behavior. Although outside the scope of this chapter, formulating the thermal boundary condition in terms of heat flux would allow determining the thermal behavior of any structural material, including timber structures.

The study shows that for all cases, TFM results in higher structural temperatures except for the Wakamatsu model, which leads to approximately 20% higher temperatures than TFM. However, the analysis has shown that the time to structural failure can be earlier when the flame extension is considered for small fire sizes.

The comparison for the generic arrangement studied in this work, with the EC 1-1-2 parametric curve illustrates that the peak temperatures resulting from the parametric fire are 484°C at the concrete rebar, 700°C for the protected steel beam, and 791°C for unprotected steel beam. For a 10% floor area travelling fire with flame extension and different models, the resulted peak temperature varies between 485°C and 590°C at the concrete rebar, 680°C and 800°C in the protected steel beam, and 880°C and 1200°C in the unprotected steel beam. Regardless of the near field model, TFM results in higher temperatures in the structure than parametric fire. Therefore, it is concluded that the EC 1-

1-2 parametric fire is less conservative, and the design of the structural elements is controlled by the TFM scenario.

Analysis of different floor systems in this chapter provided a comprehensive understanding of their behaviour when exposed to different fire models (iTFM, fTFM, and parametric fire). The benefit to the design consequences using this newer methods (fTFM) is the cost of more or less protection on the structure versus a safe and bespoke design of large and complex buildings that delivers values.

Chapter 4

Probabilistic Thermal Analysis of a Concrete Compartment Subjected to Travelling Fires with Flame Extension and Parametric Fires⁶

4.1 Introduction

Many prescriptive regulations for fire resistance worldwide define the period for which a structural element maintains its ability to carry the load when subjected to the ISO standard fire in a furnace. This method is simple in application and does not account for the frame behaviour of the building and realistic fire conditions. However, this prescriptive approach is not always the safest solution and can impose an unnecessarily onerous solution especially for modern complex buildings [75]. To address this, a performance-based probabilistic approach is an alternative approach to informing the standards required for fire safety in unique and complex buildings without following the prescriptive code limitations to the design.

Probabilistic approach and Monte Carlo Method have been applied in the research field of fire and steel/concrete structures where some recent works can be found in [76]–[81]. A Monte Carlo probabilistic method and travelling fires methodologies [27], [28], [34] as outlined in the literature, have been applied to facilitate the innovation in the design of large open buildings [53], [82]. The Monte Carlo probabilistic approach and travelling fires methodology has also been applied in real design projects [83]–[85] to assess the performance of steel and concrete framed buildings with open-plan offices. These studies showed that probabilistic risk assessment provides an alternative method to the code guidance to assess the structural performance in the case of fire. They concluded such an approach can deliver more safety, and a higher quality construction.

⁶ This chapter is being prepared for publication.

This chapter assesses the probabilistic structural fire safety design of large open plan buildings, using the recently developed fTFM methodology (travelling fires with flame extension) in Chapter 3 [86] and traditional fire methods. For this proposed method, a probabilistic approach using Monte Carlo method was applied to an open plan concrete office building [57]. This office building is the same as the one outlined in Chapter 2, where the probabilistic approach the parametric fire were applied to define the probability of slab failure. The results obtained here can therefore be compared to those outlined in Chapter 2.

The aim of the Monte Carlo-based probabilistic method in this chapter was to consider the uncertainties of input data (such as fire load, heat release rate, spread rate, etc.) used in the fTFM methodology and the traditional fire models. This approach accounts for the most severe and plausible fire scenarios and provides a robust solution to the performance of a structure under fire providing the highest level of safety.

4.2 Methodology

Thermal exposure to the structural element was calculated based on travelling fires behaviour with flame extension (fTFM) and a traditional parametric fire model [3]. Studies on the behaviour of a structure under thermal exposure from travelling fires (iTFM) and a parametric fire showed both fire models are important for representative structural fire analysis [87], [88]. Therefore, this chapter considers both fire models (fTFM and parametric fire) to calculate the probability of the failure of this building.

Parametric fire curves (see Figure 4.1), which represent a post-flashover fire with a uniform temperature inside the compartment, were generated in accordance with EC 1-1-2 (valid for 500 m² compartment area with smaller than and less than 4 m height) [3]. Travelling fires curves (see Figure 4.1) with non-uniform temperature were generated using fTFM methodology with Lattimer model for the near field heat flux as discussed in Chapter 3 [86]. It should be noted that fTFM allows the usage of either Hasemi, Lattimer, or Wakamatsu models to calculate the received heat flux (gauge heat flux) to the ceiling in the near field region. Comparison of the experimental data with the Hasemi, Lattimer, and Wakamatsu models showed that the Lattimer model is the most appropriate model to obtain the heat flux of the localized fire impinging on the ceiling, in the absence of other experimental evidence being available and further analysis. This is because based on the comparison presented in Chapter 3, the fTFM with Hasemi model underpredicts (by 20 kW/m²) the results obtained using the Lattimer

model. fTFM with the Wakamatsu model predicts unrealistic heat fluxes (about 500 kW/m²) for small fire sizes as illustrated in Chapter 3 [86].

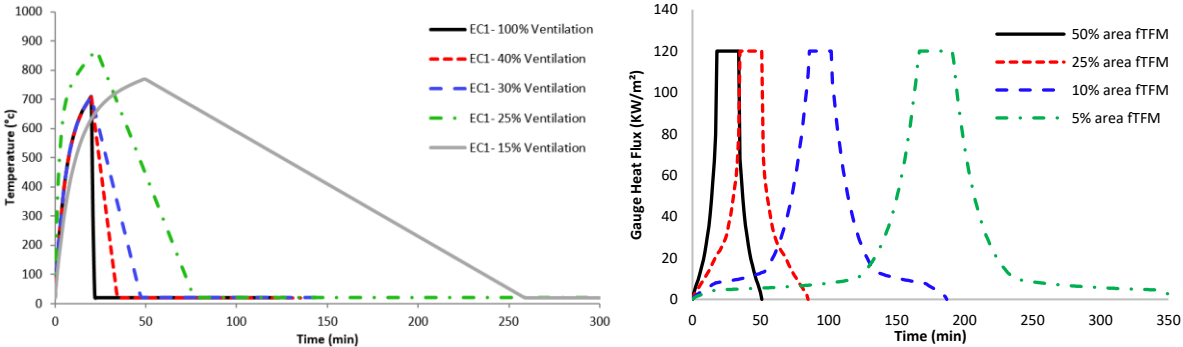


Figure 4.1 Illustrative example of the parametric fire curves of EC 1-1-2 for different ventilation conditions (right) (see Chapter 2) and family of travelling fires (fTFM) for different areas of the compartment in fire (left) (see Chapter 3) .

As mentioned in Chapter 2 the Monte Carlo method can compensate for the lack of certainty in modelling inputs in the case of real fires, as there is the opportunity to vary input parameters within a defined range. This technique has been used to determine the probability of failure and/or the reliability of the building. Monte Carlo based probabilistic approach was used in this chapter to produce the cumulative distribution function of the outcome. The cumulative distribution function curve shows the probability that the variable takes a value less than or equal to x (at any point of interest). The Monte Carlo simulation produced a large number of fire scenarios (750 scenarios) generating random input parameters for the parametric fire, travelling fires, and heat transfer models. This approach accounts for uncertainties that prevail in the real world and cannot be addressed with the deterministic approach as discussed in Chapter 2 and [52], [89].

For this purpose, the most important input parameters in the fire models (fTFM and parametric fire) and the heat transfer model were listed in Table 4.1. Details of the parametric fire model and heat transfer model are presented in Chapter 2, fTFM model is presented in Chapter 3. The previous sensitivity analysis study of a concrete slab exposed to parametric fire in Chapter 2 highlighted the important parameters for Monte Carlo analysis of parametric fire and the heat transfer model. The random input data for the parametric fire were fuel load density, ventilation size, specific heat, the floor area, and for the heat transfer model were the concrete density and the axis distance of the reinforcement. The uncertain input parameters for the Monte Carlo analysis of travelling fires, in accordance with the literature [27], were fuel load density, heat release rate, and the fire spread rate.

Variation of the fuel load density and heat release rate results in the variation of the local burning time of the traveling fire. As such, the Monte Carlo simulation of traveling fire accounts for different families of fires with different spread rates and local burning time. Input parameters, the range of input variables investigated, and their probability distribution are presented in Table 4.1.

Table 4.1 Range of input variables used in fTFM, parametric fire, and heat transfer model for the Monte Carlo simulation.

Parameters		Model	Range and Probability Distribution	Comment
Fuel Density (q_f)	Load	Parametric fire, Travelling fires	100-1100 MJ/m ² Gumbel	Values represent fire load from sparsely furnished (i.e., classroom) to densely loaded (i.e., library, business office). For the Gumbel distribution of the range: Mean=411MJ/m ² , Coefficient of Variance=0.3 [3].
Heat release rate (Q'')		Travelling fires	200 - 800 kW/m ² Uniform	Range taken for representative values of real fuels in non-industrial buildings [27].
Opening factor (O)	factor	Parametric fire	0.02-0.2 m ^{1/2} Uniform	Range taken to cover all possible opening factors in accordance with the limitation of [3] (i.e. 0.02<=O<=0.2).
Fire spread rate (s)		Travelling fires	0.1-19.3 mm/s Uniform	Fire tests and real building fire investigation reports where the fires have been observed to travel [28].
Thermal Inertia (b)	Inertia	Parametric fire	1159-2200 W.s ^{1/2} /m ² K Uniform	Range taken to represent the extent of concrete thermal conductivities, specific heats, and densities for normal-weight concrete [1], [11].
Floor Area (A_f)		Parametric fire, Travelling fires	387-462 m ² Uniform	Range taken to test the sensitivity assuming +/- 10% variation of the geometry of the compartment. The area of the compartment is 420 m ² .
Axis distance of reinforcement		Heat transfer	34-54 mm Uniform	Range taken to test the sensitivity assuming 10 mm variation of the concrete cover. The concrete cover as per the design of the building is 44mm [57].
Density (ρ)		Heat transfer, Parametric fire	1900-2300 kg/m ³ Uniform	Range taken to represent concrete densities of normal concrete [11].

Monte Carlo probabilistic analysis generated input parameters randomly from the investigated range, considering the assigned probability distribution in Table 4.1. For the fuel load density, a Gamble distribution was selected in accordance with EC 1-1-2. For the other parameters in Table 4.1, a uniform

distribution was conservatively assumed due to lack of information, as discussed in Chapter 2. The uniform distribution gives the same chance to any number in the set range to be selected randomly. Then the likelihood of sampling from the tail values is increased.

The randomly generated inputs were used in fire models (fTFM in Chapter 3 and parametric fire in Chapter 2) to establish the design fire curves, and ultimately calculate the rebar temperature in the slab using the heat transfer analysis. The rebar was assumed to have the same temperature as the adjacent concrete, as it has a much higher thermal diffusivity than concrete.

The results of each simulation were recorded. 750 runs were simulated for each of the models (fTFM and parametric fire). It was examined that increasing the number of simulations above 750 does not have any impact on the results of the study.

4.3 Case Study

The methodology outlined above was applied to probabilistically investigate the fire resistance and reliability of an open-plan office building without any interior vertical compartmentations. The aim is to present an illustrative example and a structured framework for probabilistic study using fTFM. It should be mentioned that fire resistance is interpreted as “required furnace resistance” in this work. This is discussed in more details in Section 4.4. The results were compared with the probabilistic study of the same building presented using parametric fire in Chapter 2. The building has a floor area of approximately 420 m² and a total gross area of 3 360 m². The building has 7 floors each has a height of 4 m. The building is 30 m long by 14 m wide and 28 m high. Due to the open-plan nature and the area of the compartment both parametric fire and travelling fires were studied to define the reliability of the slab. For this purpose, a 180 mm slab was selected, which is composed of reinforced continuous concrete with 44 mm axis distance of the rebar to the soffit of the slab and a concrete cover of 36 mm as explained in Chapter 2. The slab has a 90 min furnace resistance in accordance with the tabulated data in EC2 [57]. It should be noted that the failure of the slab does not equal failure of the structure, but it is a conservative approach to assume the reliability of the building is equal to the reliability of the slab. Beams and columns could be also included to have a more complete analysis, but this study aims to present an example of the probabilistic method and fTFM.

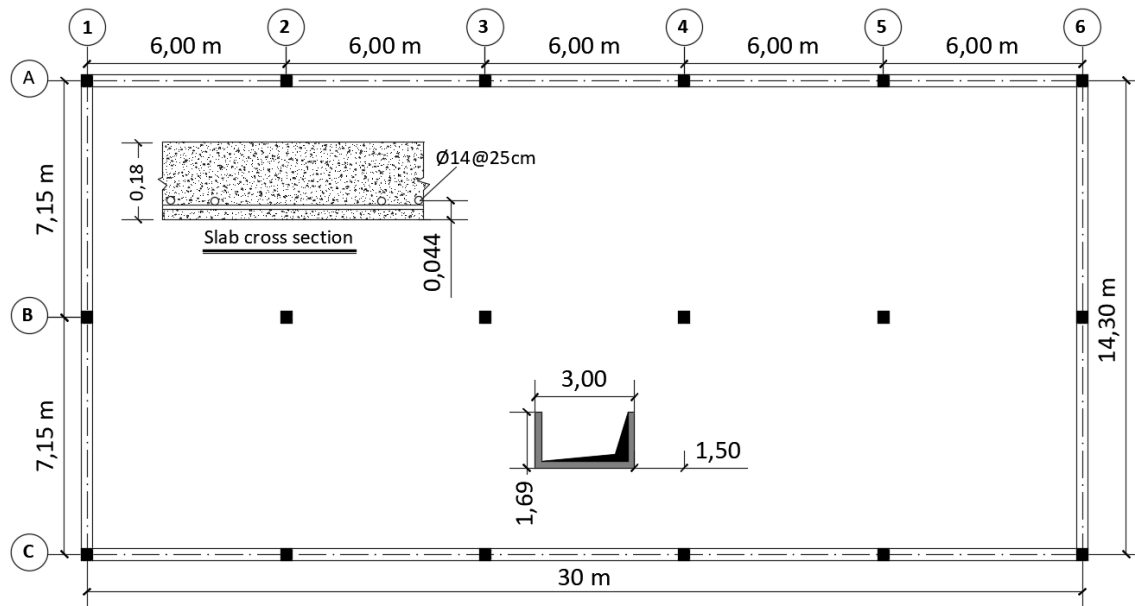


Figure 4.2 Plan of the office building and the slab cross-section as in Chapter 2, dimensions in meters.

The maximum reinforcement temperature (RMT) in the slab is assumed to be 583°C (Chapter 2) [89] set as the limiting criteria to measure the performance of this slab in accordance with EN 1992-1-2 [1]. The temperature in the slab was calculated using one-dimensional conductive heat transfer inside the material, and boundary conditions for both convective and radiant heating were taken into account [56]. To be consistent with the results in Chapter 2, thermal conductivity of 1.33 W/m K, specific heat of 900 J/kg K, convective heat transfer coefficient of 35 W/m² K for the exposed surface and 4 W/m² K for the unexposed surface of the concrete element, and emissivity of 0.7 were assumed in accordance with [3], [60]. 1D heat transfer with constant effective properties used in this chapter (the same as in Chapter 2) was assumed accurate enough to assess the performance of a concrete element as used in different studies to assess the behaviour of different structural elements under parametric fire and travelling fires [27], [33].

4.4 Probabilistic Analysis and Results

A family of fTFM curves was randomly generated using Monte Carlo method (Figure 4.3). These curves represent design fires with different fire areas with different spread rates and local burning times. Figure 4.4 illustrates the randomly generated parametric fires with a range of ventilations and fire load densities resulting in design fire curves with different duration and temperature. The figure presents the curves from the “short hot” (short duration and hot temperature) to “long cold” (longer duration compared with “short hot” fire) design fires. These randomly generated fTFM heat flux- time

curves and Parametric temperature-time curves were used to calculate the rebar temperature in the slab, as illustrated in Figure 4.3 and Figure 4.4.

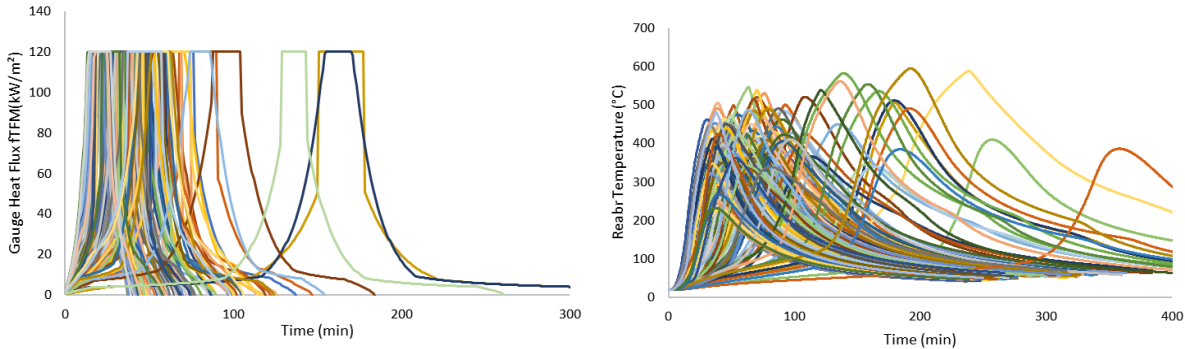


Figure 4.3 Randomly generated heat flux-time curves in the compartment from the Monte Carlo simulation using fTFM (Left) and resulting rebar temperatures (Right). The family of travelling fires represents different fire areas with different spread rates and local burning times.

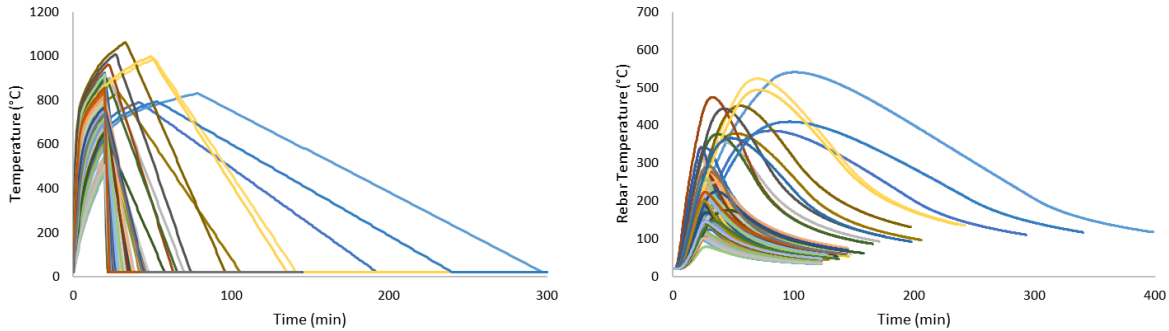
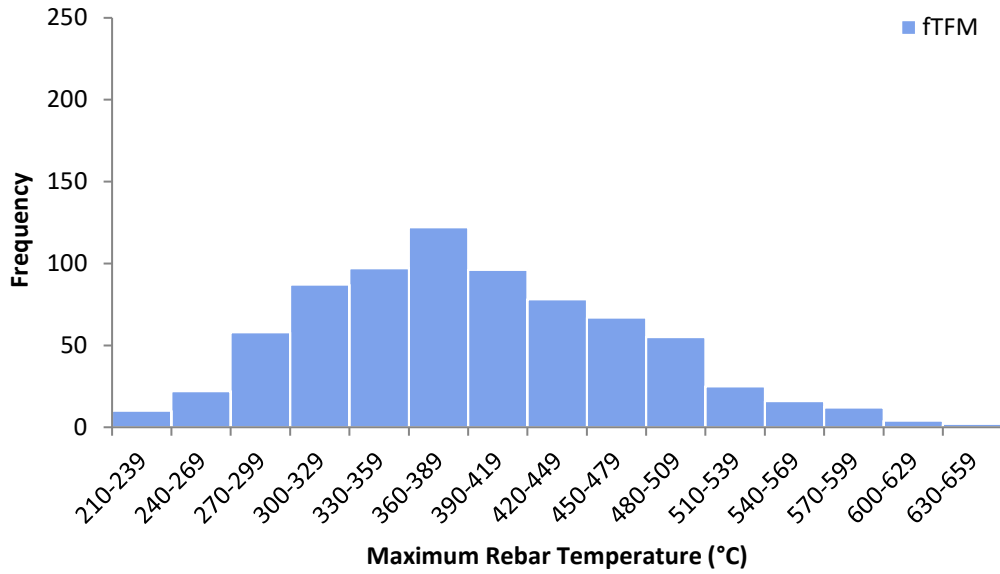
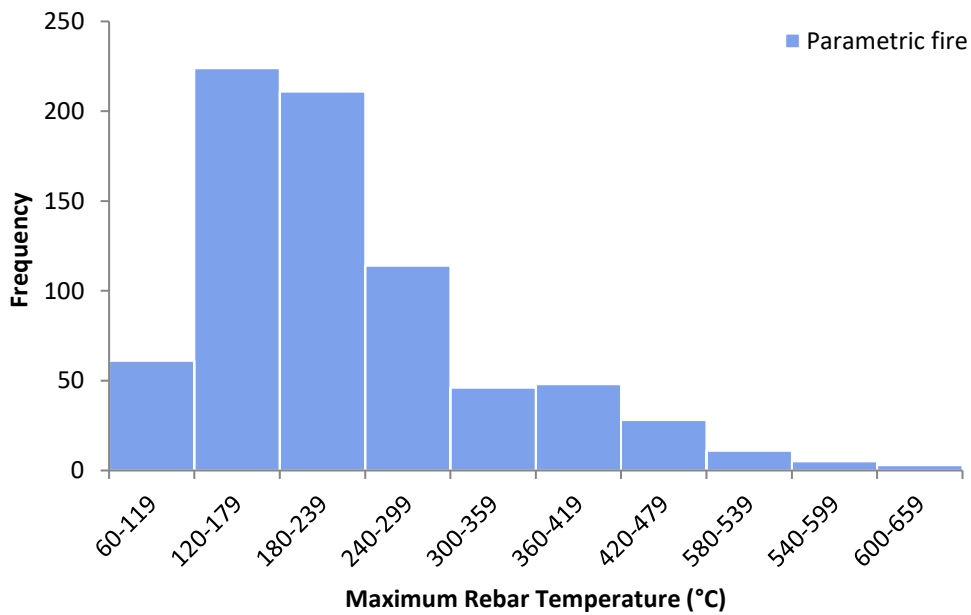


Figure 4.4 Randomly generated temperature-time curves in the compartment from the Monte Carlo simulation using EC 1-1-2 parametric method (Right) and resulting rebar temperatures (left). Parametric fires cover a range of ventilations and fire load densities.

Monte Carlo analysis of the slab provided the maximum rebar temperatures. The distribution and frequency of the maximum rebar temperatures from fTFM and parametric fire are illustrated in Figure 4.5. The figure shows that the induced maximum rebar temperature ranges from 210 to 660°C for fTFM and from 60-660°C for parametric fire. The distribution of the data shows that more maximum rebar temperatures from travelling fires fall in a higher temperature range compared with parametric fire.



(a)



(b)

Figure 4.5 Distribution and frequency of the maximum rebar temperature obtained from Monte Carlo analysis of the slab using (a) fTFM and (b) parametric fire.

Figure 4.6 presents the cumulative distribution functions (CDF) of the maximum rebar temperatures (in fractile = percentile). The figure illustrates the probability of the maximum rebar temperature reaches a value less than a selected temperature in the x-axis. In other words, the curves represent the reliability of the structural element (reliability is equal to 1 minus probability). The lower the reliability, the higher the probability of reaching the critical temperature (i.e., the structure being

closer to failure). For the critical rebar temperature of the slab, the reliabilities are 99.47% (i.e., 0.53% probability of failure) and 98.4% (i.e., 1.6% probability of failure) when subjected to parametric fire and travelling fires respectively. For a maximum rebar temperature of 230°C the reliabilities are 61% (39% probability of failure) for parametric fire and 0.4% (99.6% probability of failure) for travelling fires.

The maximum rebar temperature in the slab corresponding to specific target reliability can be compared with the critical rebar temperature, to assess the stability of the element. For example, for target reliability of 80% in Figure 4.6, the maximum rebar temperatures are 295°C for parametric fire probabilistic and 465°C for travelling fires, which are lower than the critical temperature (i.e., 583°C). As such, the structural fire design of the slab is safe for the 80% target reliability. However, the cumulative curve of the parametric fire reaches faster the higher reliabilities compare with the curve of travelling fires. In other words, the difference between two curves for reliabilities between 0% and less than 95%, show that travelling fires result in a greater rebar temperature compared with the parametric fire. This means that structure is being close to failure in the case of travelling fires.

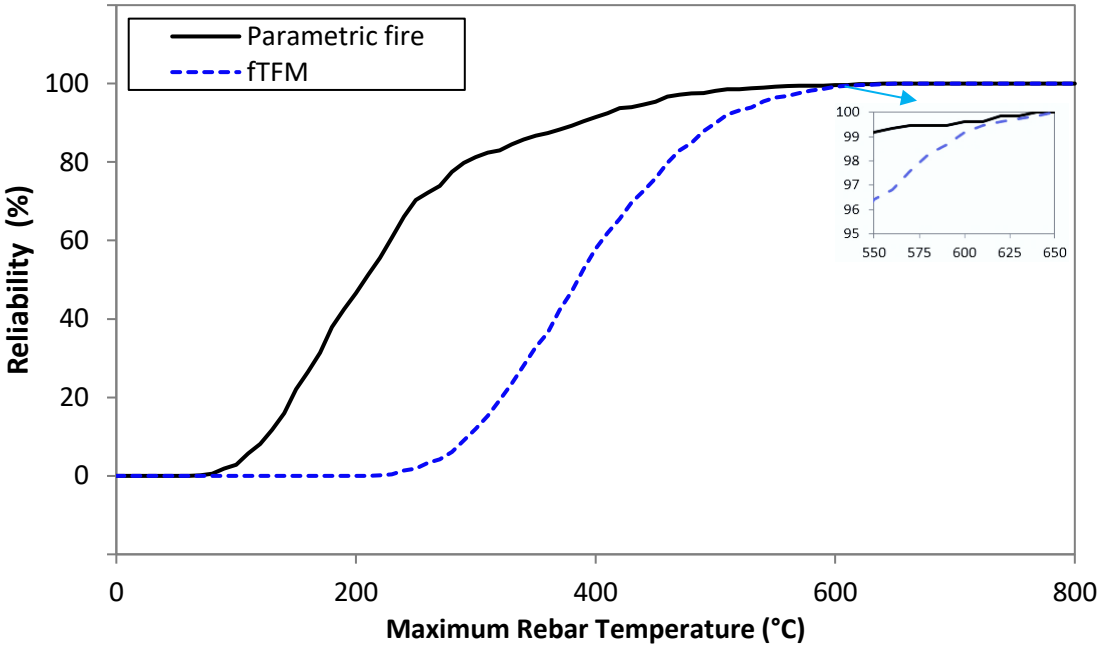


Figure 4.6 Cumulative distribution functions of the maximum rebar temperatures of a slab for parametric fire and travelling fires. This illustrates the probability of the maximum rebar temperature reaches a value less than a selected temperature on the x-axis. For the critical temperature of 583°C, the slab has the reliabilities of 99.47% for the parametric fire and 98.4% for travelling fires.

The graphical technique explained in [52] was applied to present the cumulative distributions. In this approach (i.e., graphical technique) the maximum structural element temperature obtained from each run of the fire is compared with the time taken to reach the same temperature under the standard ISO standard fire. Figure 4.7 shows an illustrative example of the graphical method of time equivalence.

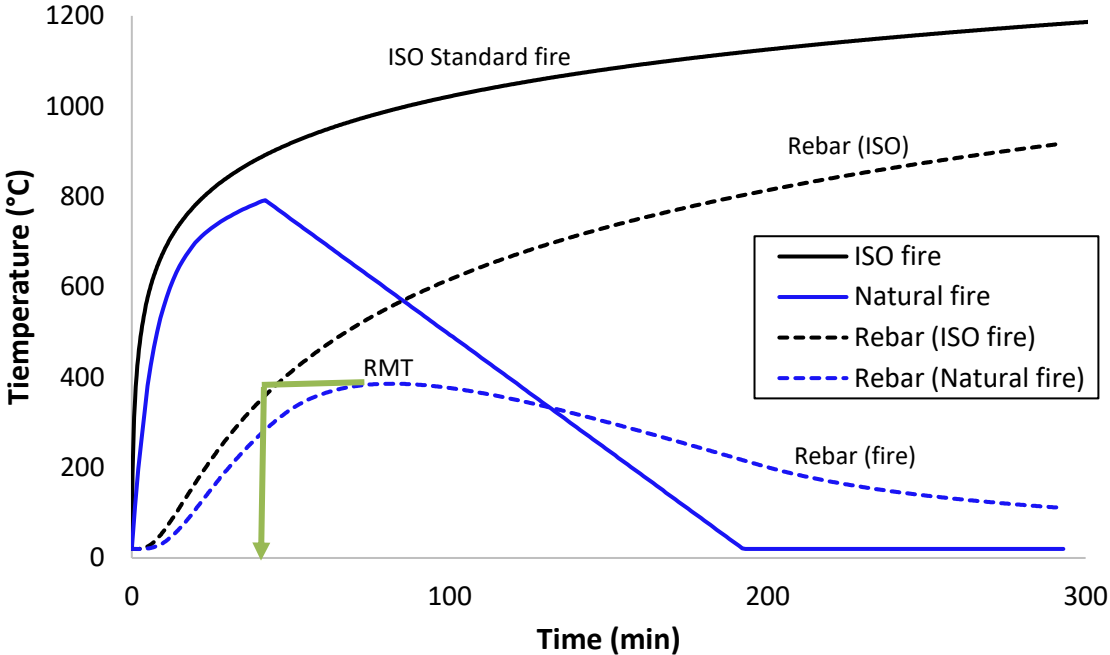


Figure 4.7 Graphical method to determine the equivalent fire severity based on ISO standard fire [52]. The maximum structural element temperature obtained from the natural fires (i.e., parametric fire) is compared with the time taken to reach the same temperature under the standard fire. RMT is the maximum rebar temperature (the figure is reproduced based on [52]).

The cumulative distributions of the equivalent fire severity for parametric fire and travelling fires are compared in Figure 4.8. The curves illustrate the structural reliability, corresponding to different furnace resistance periods for a structural member. When the required target reliability of structure is known the minimum required furnace resistance duration can be determined and vice versa using Figure 4.8. Methods are available to calculate the target reliability or acceptable level of risk [52], [53].

It can be seen in Figure 4.8 that the slab with 90 min furnace resistance (R90) [90] provides 99.47% reliability (i.e. 0.53% probability of failure) when subjected to parametric fire and 98.4% reliability (i.e. 1.6%) in case of travelling fires (FTFM). Figure 4.8 also illustrates that the parametric fire

requires a much lower furnace resistance period compared with the travelling fires for reliabilities less than 95%.

For example, a slab with 80% target reliability (resist 80% of simulated fires using Monte Carlo) requires 34 min furnace resistance to withstand possible parametric fires, and 60 min furnace resistance to resist possible travelling fires i.e., the structure being close to failure in the case of travelling fires.

The results confirm that for the furnace resistance below 30 min the reliability of the structural member is almost zero for the case of travelling fires scenario, while the slab has 73% reliability for parametric fire scenario. Figure 4.8 illustrates that the difference between the two reliability curves is significant for the fire resistances between 15 min and 60 min.

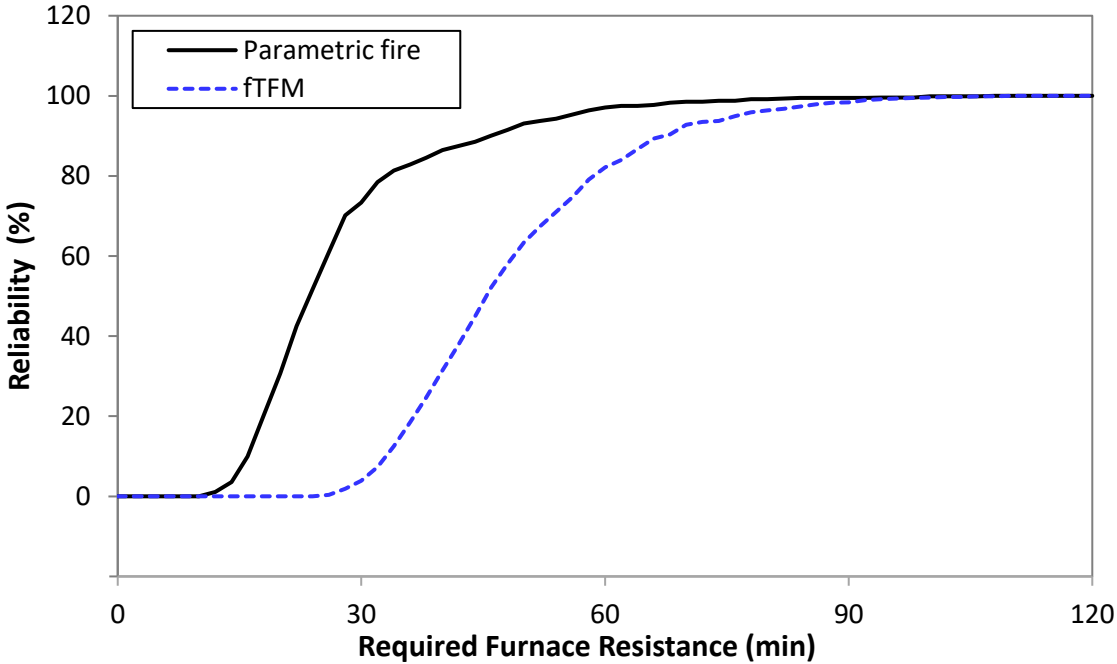


Figure 4.8 Cumulative distribution functions of the required furnace resistance for parametric fire and travelling fires. The slab with 60 min furnace resistance has a reliability of 97.47% for the parametric fire and 82.4% for travelling fires.

Figure 4.8 simply links the behaviour of structural elements under real fire to the common language of the furnace resistance period. The presented analysis is just for an element of the structure. The results can be used conservatively by assuming the reliability of the building is equal to

the reliability of the member of a structure. Meantime, the results allow defining the important fire scenarios to be considered for the structural fire design.

A summary of the furnace resistance times required for different levels of reliability are extracted from Figure 4.8 and presented in Table 4.2. The results in Table 4.2 demonstrates that the difference between the required furnace resistances of the slab studies subjected to parametric fire and travelling fires increases when the target reliability decreases.

Table 4.2 Required furnace resistance period of the slab corresponding to different reliabilities for fTFM and parametric fire as presented in Figure 4.8.

Reliability %	Required furnace resistance (min)	
	fTFM	Parametric fire
80	60	34
90	68	46
95	78	56
99	93	84

4.5 Conclusion

A Monte Carlo-based probabilistic approach was applied to define the reliability of a structure subjected to travelling fires and parametric fires. This methodology was applied for the first time to fTFM (travelling fires with flame extension) for the first time. The study in this chapter accounted for the uncertainties in the input data of fTFM such as spread rate, fuel load density, and heat release rate (thus local burning time).

For this study, a slab with R90 (90 minutes furnace resistance) was selected, with a critical rebar temperature of 583°C as the mean to assess the performance of the slab in accordance with EC 2-1-2. The results of the Monte Carlo simulation showed the reliabilities of slab were 99.47% when subjected to parametric fires (i.e., 0.53% probability of failure) and 98.4% (i.e., 1.6% probability of failure) for travelling fires. The study confirms that reliability curves allow assessing the structural performance by comparing the maximum rebar temperature corresponding to a defined reliability, with the critical rebar temperature when using fTFM methodology.

The equivalent furnace resistance for parametric fires and travelling fires were then assessed using the technique explained in [52]. In this approach, the maximum rebar temperature obtained from each run in the fire (parametric and travelling fires) is compared with the time taken to reach the same rebar temperature under the ISO standard fire. The results showed that this slab with 90 min furnace resistance (R90) provides 99.47% reliability (i.e., 0.53% probability of failure) when subjected to parametric fire and 98.4% reliability (i.e., 1.6%) in case of travelling fires (fTFM). The cumulative curve linked the reliability of the structure to the minimum required furnace resistance duration. For furnace resistance period of equal and less than 30 the reliability of slab is zero in case of travelling fires and 73% in case of parametric fire. The significant difference between the reliability curves obtained for travelling fires and parametric fire showed that the latter (fTFM) results in more severe thermal outcomes for buildings with a reliability of approximately 95% or less. This study confirms the findings in the literature [32], [88] where both travelling fires and parametric fire are emphasised as being important for the fire safety analysis of a structure.

Chapter 5

Effect of Fuel Load on Fire Dynamics in Very Large and Open-Plan Compartment: x-TWO

Summary⁷

The classic compartment fire framework has its origins in several decades of fire experiments in small compartments. In this classic approach, it is assumed that a fully developed fire will always lead to flashover. In the post-flashover stage, the temperature is assumed to be spatially uniform which forms the common assumption for structural fire design as the most onerous scenario. However, the validity of this approach for large open plan compartments has been questioned. This paper presents observations from two travelling fire experiments, x-TWO Part 1 and Part 2, conducted inside a compartment with a floor area of 380 m², the largest fire compartment studied to date. These experiments were undertaken in the same building as the previous x-ONE experiment [91]. The compartment was 10.8 m wide, 35.5 m long and 3.19 m high, well ventilated with openings representing 20% of the compartment walls. The fuel load was a continuous wood crib of load densities 355 MJ/m² in Part 1, and 250 MJ/m² in Part 2 (within typical values for office buildings). In both experiments, the fire was observed to travel with clear leading and trailing edges. Flashover was not observed, despite the complete burnout of the entire fuel load. In Part 1, the flame spread rate was not constant, instead with both the leading and trailing edges accelerating across the compartment and reached the far end 32 min after ignition. In x-TWO Part 2, the leading and the trailing edges quickly reached steady state and travelled at a nearly constant spread rate, reaching the end of the compartment 180 min after ignition. The observed distributions of temperatures were remarkably

⁷ This chapter is based on “Heidari, M., Rackauskaite, E., Bonner, M., Christensen, E., Morat, S., Mitchell, H., Kotsovinos, P., Turkowski, P., Wegrzynski, W., Tofilo, P., and Rein, G., 2020. Fire experiments inside a very large and open-plan compartment: x-TWO. Proceeding of the 11th International Conference on Structures in Fire (SiF2020), 2020.” This chapter is being prepared for publication in Special Issue of Fire Technology.

different from the conditions assumed from small compartments in structural fire engineering and could lead to different failure times and mechanisms.

5.1 Introduction

Past small compartment fire experiments (area < 100 m²) [20], [92]–[95] have provided the knowledge to formulate and validate the fully developed fire models [3], [13], [19], [96], [97] that determine the severity and thermal load of fires for structural fire design purposes. These models, including parametric fire, are challenged [11] but a convenient tool for practitioners, which typically assume a uniform and homogeneous temperature inside the compartment. However, the small compartment fire experiments and the few available large compartment fire experiments [20], [91], [98]–[103] have recorded non-uniform spatial temperatures with longer fire exposure times than those predicted by a parametric fire. Thus, the validity of models with uniform temperature assumption needs to be examined [11], particularly for large open space compartments, where travelling fires with heterogeneous temperatures [22] can be structurally the most severe fire scenario [31], [88], [104]–[107] and cause a major structural collapse [22]. These studies demonstrated that travelling fires can result in a larger strain and stress, a larger residual displacement, or the structural responses that have not ever been observed in the case of uniform temperature scenarios.

Large-scale travelling fires experiments [91], [101]–[103], [108], [109] have been conducted to identify and understand the dynamics of travelling fires and improve theoretical travelling fires models. The experiments provided a set of valuable data and confirmed the spatial and temporal temperature distributions. A review of classic literature and the description of some recent experimentation [110] showed the need for more high-resolution experimental data to provide insight into the fire dynamics of a large compartment and complex geometries. Such studies would facilitate the application of robust state-of-the-art fire safety engineering to complex geometries and modern buildings and will enhance the development of modern future cities with increased resilience to fire.

The research presented in this chapter is a part of a recent experimental campaign in a large, open-plan compartment (Area = 384 m²); this consisted of x-ONE (September 2017) [91] and x-TWO (May 2019). The author of this thesis was involved in both x-ONE and x-TWO experiments. The experiments were carried out to reveal and understand the fire dynamics in a very large compartment and measure basic fire characteristics such as temperature and spread rate. In x-ONE [91], the fire was ignited at one end of the compartment and allowed to develop naturally. The experiment captured a fast and accelerating travelling fire, gradually increasing from 3 to 167 mm/s over the uniform fuel load

of wood cribs along the length of the compartment, and lasted for 25 min. The experiment showed that flashover (defined in a classical way in [11]) does not always occur in a large compartment, but instead the fire can spread and generate a non-uniform temperature distribution across the compartment. In comparison to the EC 1-1-2 parametric fire, some structural elements experienced more onerous thermal conditions, based on analysis in [91].

One of the main objectives of the x-TWO experiments was to understand the impact of fuel load variation (the most important parameter in fire) on the temperature, fire duration, spread rate, and flame height in large compartments. The x-TWO experiments study justification to incorporate travelling fires in current design methodologies and fire safety engineering guidance. This chapter mainly focuses on the x-TWO experiment series, observations, and experimental measurements made during the experiments.

5.2 The x-TWO Building

The x-TWO experiment was carried out in a farm building⁸ located near Golaszew, 20 km west of Warsaw, Poland (the same building used for x-ONE [91]). The farm buildings tend to be very large open planned given their use so they would make ideal choices to run large scale fire experiments (it is expensive and difficult to build a compartment for large scale experiments). It is quite effective and easy to procure this type of structure. The x-TWO building was secluded and fire apparatuses on standby were easy to install, which was an advantage to use this building. The challenges in x-TWO and (x-ONE) were though controlling the safety and the risk assessment.

The building had one floor that was mostly open plan with thick external masonry walls. The beam and block concrete slab ceiling was supported by reinforced concrete columns, beams, and external masonry walls. The experiment was carried out in the open-plan section of the building which had a floor plan of approximately 384 m². The floor was 10.8 m wide, 35.5 m large, and 3.24 m high (Figure 5.1). Two doors of 2.51 m x 2.50 m were located at each end of the compartment and two doors of

⁸ Aside use of the research conducted herein (i.e. the rate of fire spread in a farm structure) could be for farm fires itself.

1.81 m x 2.50 m are in the middle of each wall in the length of the compartment. There were 29 window openings (1 m x 1 m). A sketch of the floor plan of the section of the building is shown in Figure 5.1.

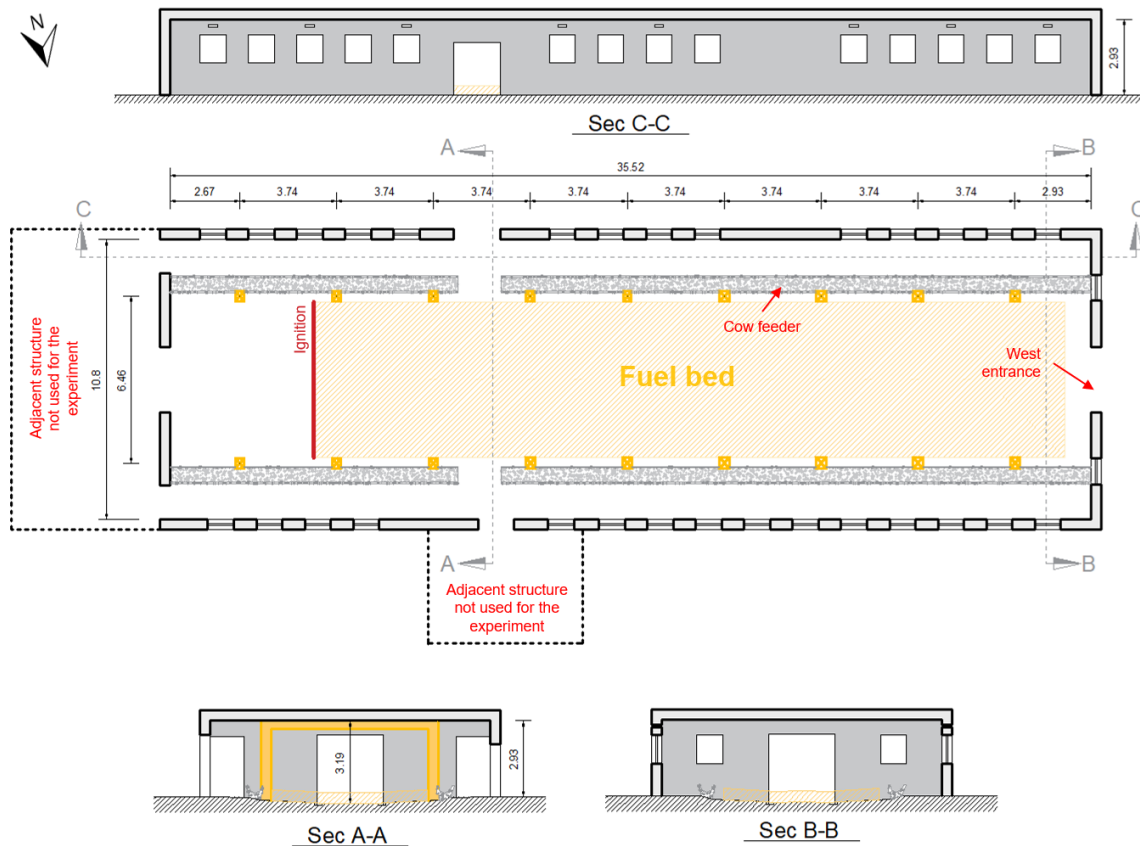


Figure 5.1. Floor plan and sections of the compartment used for x-ONE [91] and x-TWO experiments.

5.3 Fire Protection of the Structure

The structure was thermally protected to avoid significant structural damage and reduce the risk of collapse during the experiment. Ceiling, beams, and columns were protected using CONLIT 150 P slabs with a density of 165 kg/m³. CONLIT 150 System used had a fire resistance for 240 minutes. HILTI IDMS fasteners were used to bolt the Rockwool slabs to concrete elements. After the first experiment, some damaged sections of the fire protection were identified and replaced.

5.4 Ventilation

6 doors and 31 windows (1.00 m x 1.09 m) openings were available around the building (Figure 5.1 and Table 5.1). All openings were left open to represent the conditions of an open-plan

compartment with large ventilation and to minimise the likelihood of a ventilation-controlled fire. The ventilation condition was unchanged compared to x-ONE experiment [91].

Only 1 door and 1 window opening to the adjacent structure along the North elevation of the building, and all the openings to the attic were closed. The aforementioned openings were closed to eliminate any potential influence of the adjacent compartment on the fire dynamics within the main compartment, that is, to keep the fire compartment simple and only maintain ventilation openings directly to outside.

In total, 20% of the compartment walls (i.e. $A_w=56 \text{ m}^2$) are openings with an opening factor of $0.0621 \text{ m}^{1/2}$ ($A_w h^{0.5}/A_{\text{total}}$) and a weighted average opening height of 1.34 m, as stated in Annex A of EC 1-1-2 [3]. The opening factor represents the amount of compartment ventilation in a fire. The large opening factor increases the possibility of a fuel-controlled fire compartment.

Table 5.1. Opening dimensions along different elevations of the building used for the x-TWO experiment (the same as x-ONE).

Building Elevation	Door openings (m) (Number × Width × Height)	Window openings (Number × Width × Height)
East (Sec A-A in Figure 5.1)	1 × 2.54 m × 2.66 m 2 × 1.31 m × 2.34 m	None
South (Sec C-C in Figure 5.1)	1 × 1.80 m × 20.3 m	14 × 1.00 m × 1.09 m
West (Sec B-B in Figure 5.1)	1 × 2.54 m × 2.66 m	2 × 1.00 m × 1.09 m
North	1 × 1.37 m × 2.38 m (closed)	15 × 1.00 m × 1.09 m (1 opening closed)

5.5 Fuel Load

The fuel load used in x-TWO constituted of a continuous wood crib to encourage a natural spatial and temporal fire growth. The wood crib arrangement was based on the fuel design of the x-ONE experiment in September 2017 (for more details see [91]). Before the x-ONE experiment, 9 small-scale exploratory experiments were carried out to investigate different wood crib arrangements, materials to be combined with wood, and ignition methods for the optimum fuel load design. The fuel load of x-ONE was approximately 370 MJ/m^2 (19.4 kg/m^2) and covered a floor area of 174 m^2 ($6 \text{ m} \times 29 \text{ m}$). The fuel setup consisted of 11.5 layers of a continuous wood crib (4 sticks each layer), mixed with two

layers of 4 mm fibreboard to facilitate a faster flame spread and higher heat release rates than in the previously identified travelling fires experiments. This fuel load was chosen to limit the risk of damage to the structure but to still be within the range of typical fuel load densities in office buildings [3], [27], [111]. A fast and accelerating fire was observed with the total fire duration of x-ONE was 25 min.

In x-TWO, fuel load was the only parameter that was changed compared to x-ONE to understand the impact of the changes in the fire dynamics of travelling fires due to fuel load variation. The same type of wood and the same arrangement as in x-ONE was used, however, for x-TWO the fibreboard was limited to the first meter of the crib and an additional layer of 2 sticks was added to maintain an identical fuel load. It was expected that this fuel configuration would lead to a longer fire duration compared to x-ONE.

For x-TWO, the wood crib was softwood sticks with the dimensions of 3 cm x 3cm x 100 cm, average densities of 422 kg/m³ in Part 1 and 455 kg/m³ in Part 2, the heat of combustions from bomb calorimetry measurements of 18.94 MJ/kg in Part 1 and 19,62 MJ/kg in Part 2, and moisture contents of 11% in Part 1 and 14% in Part 2 (15 wood sticks were then dried in the oven at 80°C). The fuel bed area was 174 m² (6 m x 29 m) as illustrated in Figure 5.1. The fuel bed was placed 5.40 m from the East entrance and 1 m from the West entrance. The crib was lifted from the ground by placing bricks every 1 m to reduce heat losses to the concrete floor and enable air circulation below the crib (

Figure 5.2). The troughs below the wood crib were filled with concrete debris. A random sample of 50 wood sticks has been collected on the day of the experiment and weighted to obtain the average wood density.



Figure 5.2 The final wood crib arrangement used as fuel for the x-TWO experiment. Wood sticks dimensions were 3 cm × 3 cm × 1m. The image shows the completed wood crib at the moment of ignition.



Figure 5.3 The left image shows the moment of ignition. The right image shows a uniform initial linear fire forming and starting to naturally progress at the east end of the compartment.

A uniform initial linear fire along the width of the one end of wood crib (i.e., East entrance) was used to study the flame spread along the compartment. To achieve this, 6 pans (15 cm x 25 cm) each filled with 0.5 litres of methanol were located below the one end of wood cribs (i.e., East entrance). Additionally, over the first meter of the crib, two layers of 4 mm fibreboard (Barlinek underfloor board) were used to accelerate the fire spread and ensure even combustion along the width of the crib. The methanol pans were ignited simultaneously using a torch and a uniform line of fire formed as

illustrated in Figure 5.3. The summary of the fuel load of x-TWO Part 1 (x-TWO.1), x-TWO Part 2 (x-TWO.2), x-ONE and the office fuel load density of EC 1-1-2 are presented in Table 5.2.

Table 5.2. The summary of the fuel load densities in x-ONE, x-TWO, and EC 1-1-2.

Experiment/Code	x-ONE [91]	x-TWO.1	x-TWO.2	EC 1-1-2
Fuel load MJ/m ² (over the crib zone)	370	345	273	285-420
Wood crib layers	11 layers of 4 sticks 1 layer of 2 sticks	1 layer of 2 sticks 11 layers of 4 sticks 1 layer of 2 sticks	8 layers of 4 sticks 1 layer of 2 sticks	
Fiberboard layers	2 covered 6m x 29m	2 covered 6m x 1m	2 covered 6m x 1m	-
Design Consideration	- Natural fire - Save the building - Not a very slow spread - Flame impinging ceiling	Similar to x-ONE but a slower spread expected	Slower spread than x-TWO.1	-

5.6 Instrumentations and Data Collection

39 Type-K thermocouples (Ni-Cr) of 1.5 mm thickness were used to capture spatial and temporal temperature development within the compartment. 15 thermocouples were attached to 9 columns (TC). At all columns, thermocouples were attached at the height of 2.4 m above the floor with 6 columns having an additional thermocouple at the height of 1 m above the floor. 18 thermocouples were placed 5 cm below the soffits of beams (T), at mid-span and 3.5 m distance from the side walls at the height of approximately 2.9 m. 6 thermocouples (TP) were installed between blocks of mineral wool (Rockwool), in contact with the ceiling to measure the ceiling surface temperature and ensure that the structure was not exposed to severe heat, which could have led to collapse. Finally, three plate thermocouples (PT) were installed at the mid-span of the ceiling at the East end, middle, and West end of the compartment. Three Grant Squirrel SQ2020-1F8 data loggers were used in the experiments.

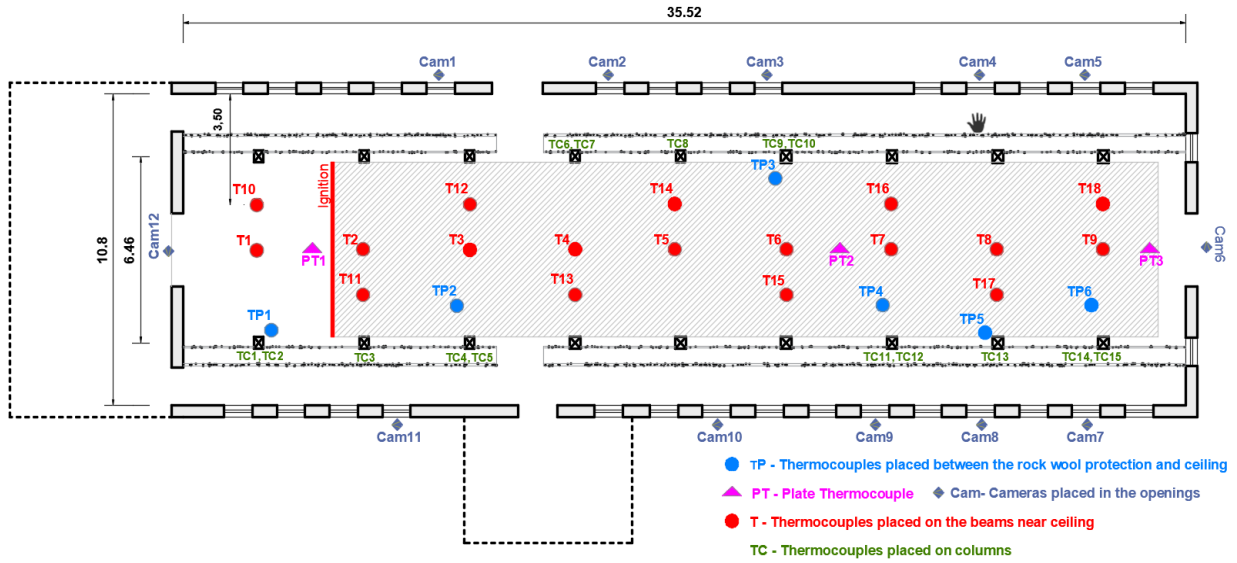


Figure 5.4 Thermocouple and camera locations in the compartment. Thermocouples (T) were placed at the soffits of beams at a height of ~2.9 m from the floor. Where there are two thermocouples (TC) at the same column, they are located at heights of 1 m and 2.4 m, while single thermocouples are located at a height of 2.4 m from the floor.

All PTs' and thermocouples' cables and data loggers were laid out in the attics to minimize the risk of direct fire exposure or damage. Several 5mm holes were drilled in the ceiling. The thermocouples were passed through the holes, so the rest of the wires remained safe above the concrete ceiling in the attics. Consequently, there was no damage to thermocouples, and all data were collected.

All thermocouples were examined before the test with a small flame to ensure that they work. The thermocouples' measurements did not show any strange jump or form (see Section 5.7.3), which confirms no potential for the thermocouples to be damaged.

Thermocouples' measurements were corrected for radiation error (radiant heat flux from the fire) using β -method. This correction assumes the thermocouple is in thermal (quasi-steady-state) equilibrium by equating the convective and radiative heat fluxes:

$$h \cdot (T_g - T_{TC}) - q''_{rf} + \varepsilon \cdot \sigma \cdot T_{TC}^4 = 0 \quad (5.1)$$

Where h is the convection coefficient, T_g is the gas temperature local to the thermocouple, T_{TC} is the recorded value at the thermocouple surface, q''_{rf} the radiative heat flux incident on the thermocouple surface, ε is the thermocouple surface emissivity, and σ is the Stefan-Boltzmann constant.

The radiative heat flux received to the thermocouple due to the fire, q''_{rf} , can be assumed to be proportional to T_{TC}^4 , hence $q''_{rf} = \beta \cdot \varepsilon \cdot \sigma \cdot T_{TC}^4$ where β is a dimensionless constant (defined as the correction coefficient) greater than 1 because the radiative heat flux due to the fire makes T_{TC} greater than T_g . Hence using these equations, T_g can be calculated as:

$$T_g = T_{TC} + \frac{\varepsilon \sigma}{h} \cdot (1 - \beta) \cdot T_{TC}^4 \quad (5.2)$$

The average heat transfer coefficient, h , is determined by evaluating the Nusselt number for flow around a sphere as described by [112], assuming a fixed local velocity of $U=12\text{ms}^{-1}$.

A parametric analysis was carried out varying β . As shown in fire experiments [11], the maximum average gas temperature measured by thermocouples in the flame is no higher than 900°C ; therefore, by setting 900°C as the maximum value of T_{TC} we can find the range of values for beta (β) through Eq. (5.3), which is $1.17 \leq \beta \leq 1.25$, which also captures the estimated error associated with thermocouple measurements (The upper value of beta corrects thermocouple temperatures from 1100°C down to 1000°C , see Figure 5.10).

13 cameras (Cam) (Vmtol GSV8560 type) recorded the test series and captured the fire size and flame spread rates. Cameras were positioned in the windows and the openings in the west and east ends, looking into the compartment. Figure 5.4 shows the location of the instrumentation used to measure the flame spread rate and the thermal exposure in the compartment. The cameras were fixed to the wall and were protected with plasterboard against thermal damage. The cameras were calibrated for image distortion as discussed in x-ONE experiment [91]. The data from all of the cameras were successfully recovered.

During the experiments, the weather conditions were recorded based on the local fire station data. In wind speed, temperature and humidity were 6.2-7.15 m/s North-West, $10\text{-}11^\circ\text{C}$, and 67-71% during x-ONE and 3-4 m/s North-East, $16\text{-}17^\circ\text{C}$, and 83-94% (a rainy day) in x-TWO.2. The impact of the wind on the fire dynamics within the compartment was out of the context of this work. For the record, in x-ONE the wind speed, temperature and humidity were 0.3-2 m/s South-West, $17.6\text{-}19.4^\circ\text{C}$, and 75-

80% respectively. In x-ONE and x-TWO the instrumentation was designed to fulfil the objective of the experiment and register the key fire characteristics such as the spatial temperature distributions at the ceiling, and vertical temperature distributions at a few selected locations.

5.7 Experimental Results

5.7.1 Observations and Fire Characteristics

After ignition, a fire developed naturally along the width of the wood cribs. The fire travelled over the surface of the fuel along the length of the compartment without rapid transition to a state of total fuel surface involvement in fire (flashover definition as identified by [11]). The experiment demonstrated that flashover does not always occur in a large compartment, but instead the fire can travel. The fire burned out after about 35 min and 180 min, in Part 1 and 2 respectively. The travelling fire and the burn out area behind the fire at different locations of the compartment and at different times are presented in Figure 5.5 (x-TWO.1) and Figure 5.6 (x-TWO.2).



Figure 5.5. Fire photos were taken from different locations (i.e., North entrance and West entrance) at four different times during the Part 1 experiment indicating fire development and progress. An accelerating travelling fire of 32 min duration was observed.



Figure 5.6. Fire photos were taken from different locations at four different times during the Part 2 experiment indicating fire development and progress. A steady-state travelling fire of 180 min was observed.

In x-TWO.1, the spread rate of the fire was observed as not constant during the whole burning time. Initially, the fire grew and spread relatively slowly (i.e., ~ 1 m in 5.5 min). Flames were observed to impinge on the ceiling at 9 min after the ignition. The leading edge spread steadily until fire reached the South entrance door (i.e., ~ 14 min), then the fire accelerated (i.e., 25 m in 8 min) to the West end of the compartment. The increase in the spread rate of fire is likely due to a combination of change of air flows within the compartment (more oxygen available to the fuel bed) as the flames approached the larger South side opening and an increase of radiation from the flames impinging on the ceiling and the smoke layer as the fire grew, thus, facilitating a faster ignition of fuel ahead of the flames and accelerated fire growth as also observed in x-ONE. It is difficult to establish which of the latter is the leading factor as the North entrance door is located only ~ 6 m from the ignition location. The leading edge of the fire reached the far end of the compartment (i.e., West entrance) at ~ 22 min.

A clear trailing edge was observed at approximately 5 min after ignition. The spread velocity of the trailing edge of the fire increased with time but slower compared to the leading edge. The fire burned out approximately 32 min after ignition. A thick smoke layer started to form in the compartment from the moment of ignition and grew quickly (see Figure 5.5). At 14 min, the flame was partially visible from the West entrance due to the build-up of the thick smoke layer. Smoke was mainly

exhausted via the windows adjacent to the location of the flame and the South and West entrances with fresh air coming in through the remaining windows and below the neutral plane of the South and West entrances. An external flaming was only observed locally due to the flame extension under the ceiling.

In x-TWO.2, the line fire along the width of the compartment grew and covered one meter of the wood cribs along the length of the compartment after 4 min. Then, the leading and the trailing edges of the fire had almost the same spread rates and travelled with a uniform accelerating rate until reached the end of the compartment after 174 min and 180 min after the ignition respectively. The fire size changed and grew slightly about 2 m in the length of wood cribs when the fire passed 1.5 m the South entrance. The reason can be the airflow to the fuel bed from the South entrance. The flame did not impinge on the ceiling. The flame height was varying between 1 m and 1.30 m above the floor during the fire. A thin layer of smoke was accumulated under the ceiling.

There was limited involvement from the fire service who watered the exterior of the building and the external flaming to prevent fire spread to the attic, which was supported by and contained timber framing. No fire damage to the building fire was observed. The mineral wool applied as protection to the ceiling, beam, and columns was not observed to fall off during the fire in x-TWO.1.

5.7.2 Fire Spread

A travelling fire is a limited burning area of the compartment floor that spread across the floor plate [24], [27], [28], [34], [35], [86]. Along a single axis of travel, the burning area is constrained by the leading edge (front of the fire) and the trailing edge (fuel burn out takes place) of the fire (Figure 5.7), both of which progress through the compartment until the total available fuel is consumed. Location and spread rates of the leading and trailing edges from the point of ignition at discrete time intervals were achieved using image data from an array of cameras positioned at all windows across the compartment (See camera's location in Figure 5.4).

Figure 5.7 and Figure 5.8 show the extracted locations of the flame, and spread rates of the flames on the floor, as well the best-fit curves for each set of data, for Part 1 and Part 2, respectively.

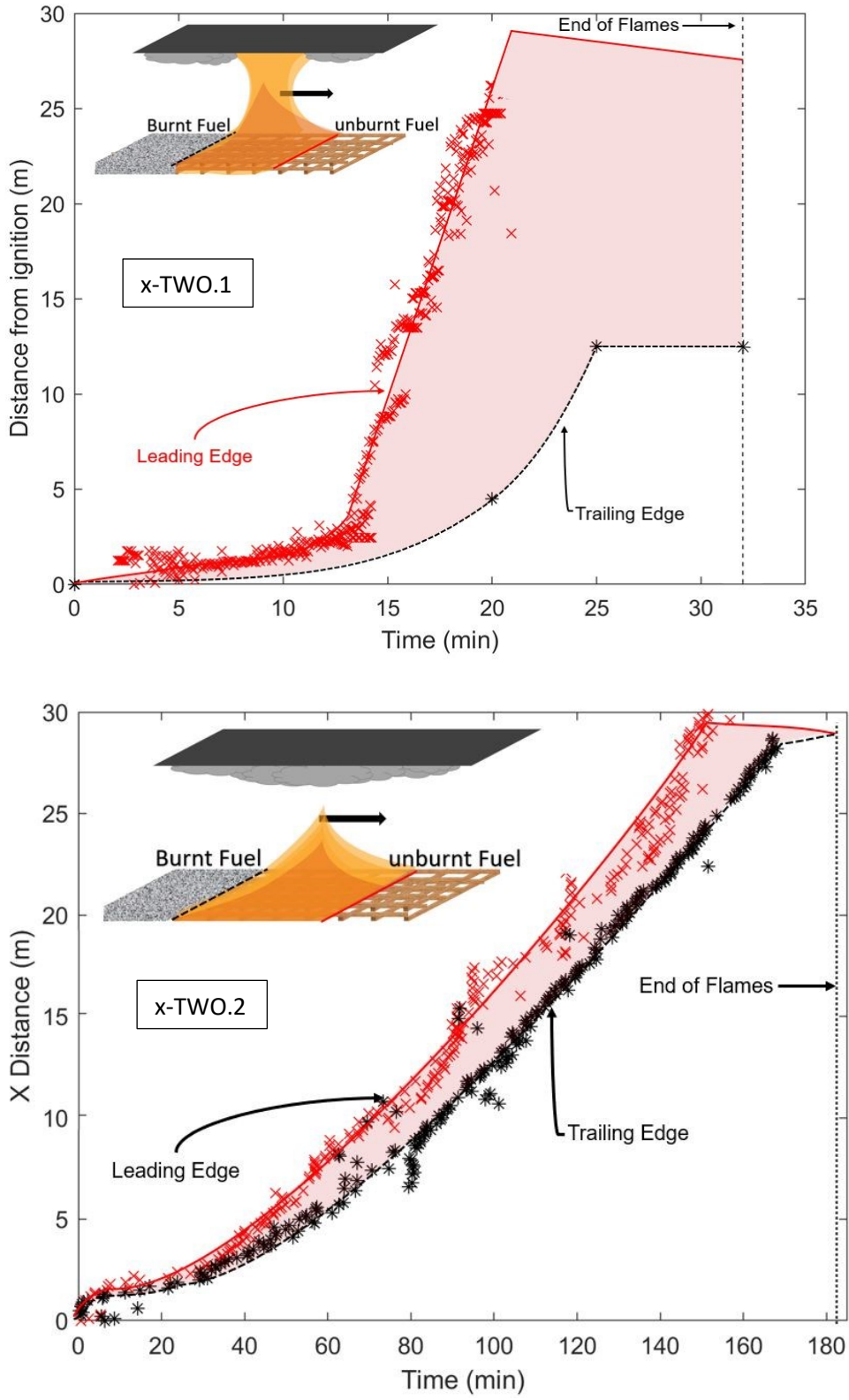


Figure 5.7 Distance of leading and trailing edges from the ignition point for x-TWO.1 (top) and x-TWO.2 (bottom). Crosses (x) indicate the location of the leading edge and asterisks (*) indicates the extracted trailing leading edge of the flame.

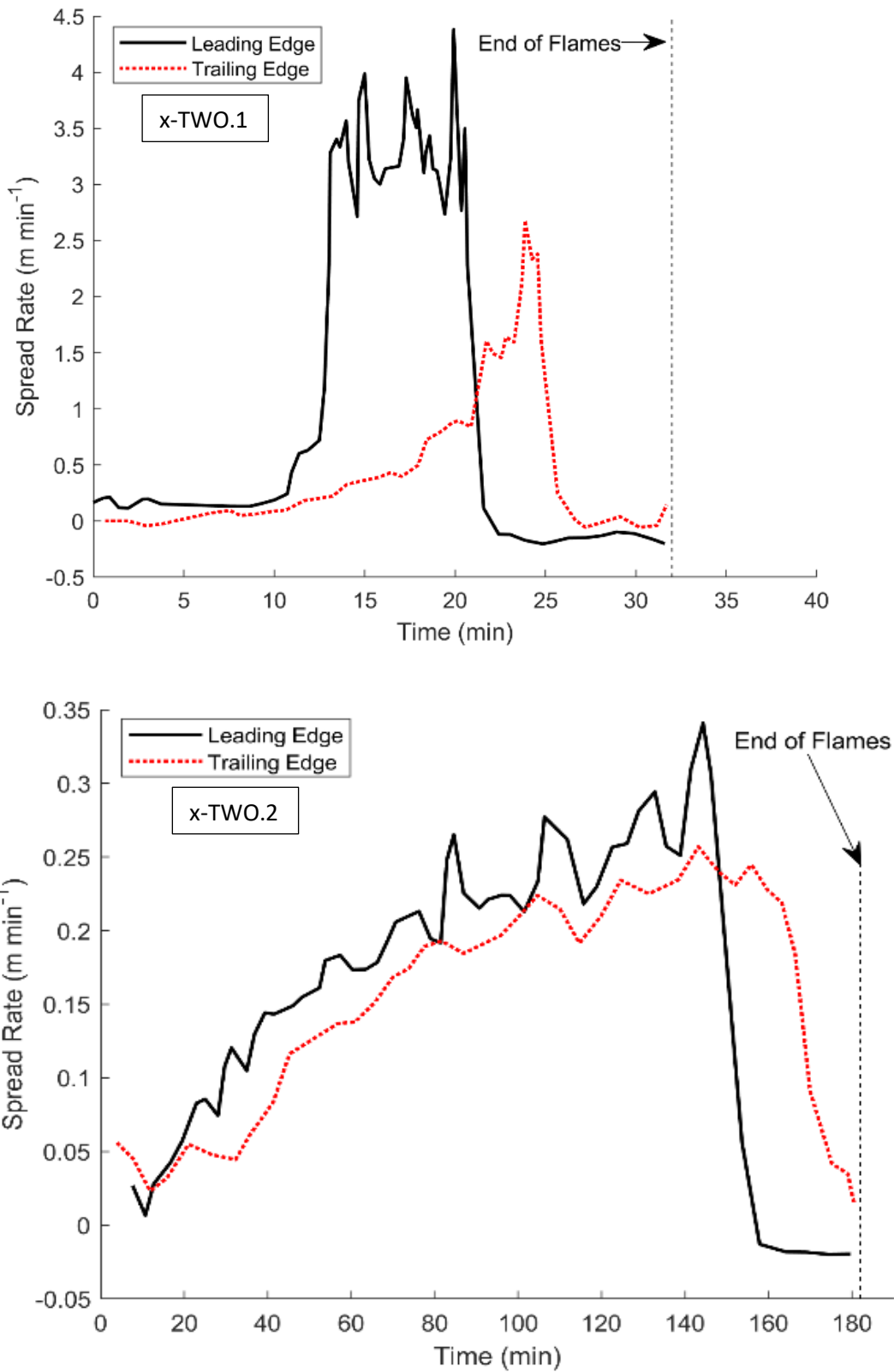


Figure 5.8 Spread rates of leading and trailing edges from the ignition point for x-TWO.1 (Top) and Part 2 (Bottom).

As discussed in the x-TWO.1 the flame spread rate increased during the experiment as illustrated in Figure 5.7 and Figure 5.8. The fire had an initial spread rate of 0.25 m/min until arriving in the South entrance at about 14 min. The flame spread rate then increased significantly to an average value of almost 3.5 m/min until reaching the end of wood crib near the West entrance. After 5 min from the ignition, a clear trailing edge of fire started to move along the compartment, with the spread rate of ~ 0.25 m/min almost the same as the leading edge. The spread rate increased from 13 min after the ignition of the fire, with a maximum value of 2.5 m/min. Therefore, different spread rates of the leading and trailing edges have resulted in a continuously growing fire during the experiment. This means that the front of the fire was travelling at a different speed compared to the trailing edge of the fire, and the fire size was not steady in size as assumed in TFM methodology. This confirms that the impact of a family of travelling fires with different near field sizes should be examined on the structure when the TFM is applied.

The visualisation for x-TWO.2 shows after a brief period until the fire reaches the South entrance after 25 min, then the leading and trailing edges had a uniform acceleration with an average spread rate of 0.22 m/min. The trailing edge spread rate was consistent ~ 0.02 meters per minute, which was less than the leading edge, where the fire size slightly increases from 40 min-140 min. The fire travelled across the compartment, finally burned out at the other end 180 min after ignition and without flashover.

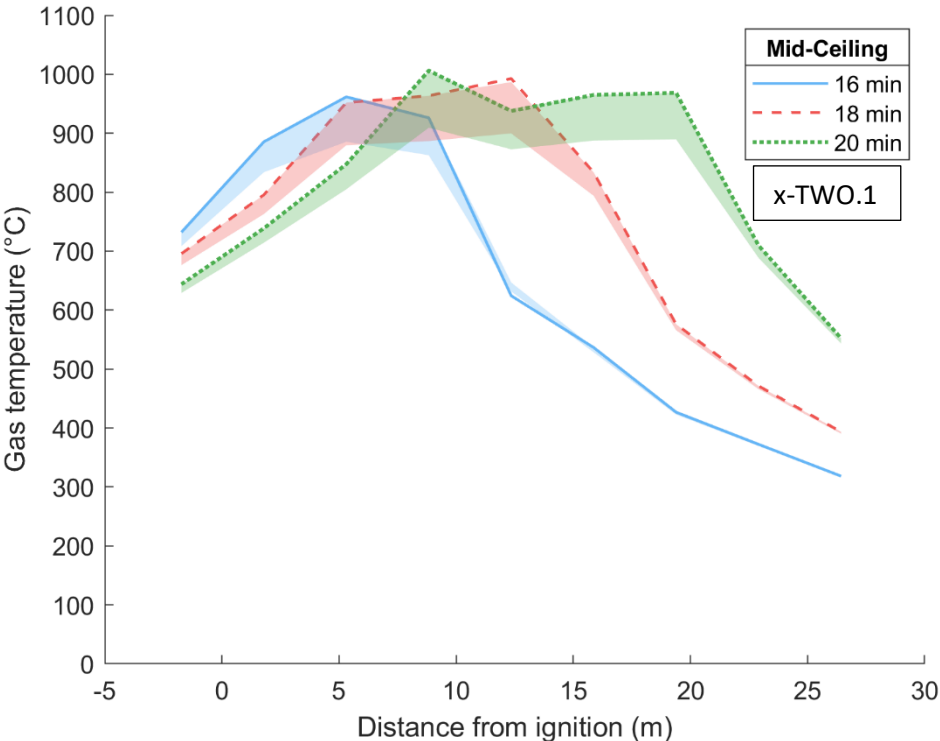
Compared to x-ONE, both x-TWO.1 and 2 lasted longer in fire duration, as x-ONE reached extinguishment 25 min after ignition, and the leading edge reaching the end of the compartment after 12 mins. Similarly, the peak rates of spread of both the leading and trailing edges of x-ONE were significantly higher than those for x-TWO.1 and 2, with maximum spread rates of 13.5 m/min and 6 m/min for the leading and trailing edges, respectively. This, considering the similarity in ventilation conditions between x-ONE and x-TWO, further shows that the spread rate of a travelling fire is a function of the fuel load density.

The experiments confirmed that for the same ventilation conditions the lower fuel load density results in smaller fire size, lower flame height, and thinner smoke layer. Therefore less radiation from the flame and smoke reached the fuel bed. Consequently, lower flame spread and longer fire duration are reached.

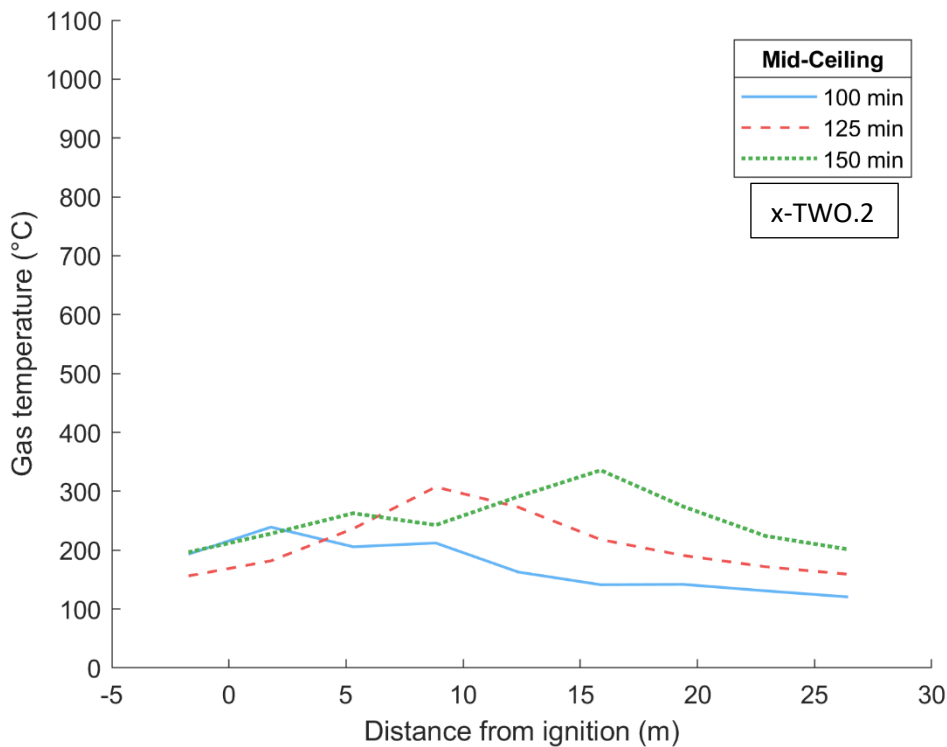
5.7.3 Gas Temperature

Temperatures throughout the compartment were measured with thermocouples recording the gas temperature as the fire travelled in the compartment. Figure 5.9 shows the special and temporal evolution of the gas phase temperature at the beam soffit level at a height of 2.90 m from the floor (near the ceiling) along the fire path for, x-TWO.1, and x-TWO.2 (at different time steps after ignition). Figure 5.10 presents the corrected gas temperatures, obtained from thermocouples, at different locations of the compartment from the ignition point for x-ONE, x-TWO.1, and x-TWO.2. The first and the last set of thermocouples were located at 2.8) m behind and 27.1 m from the ignition location towards the West entrance (See TCs location in Figure 5.4). x-ONE and x-TWO are a part of the same experimental campaign, thus the temperature results of x-ONE were presented here for comparison..

The shaded region in Figure 5.9 and Figure 5.10 describes the region of correction bounded by correction coefficients of $1.17 \leq \beta \leq 1.25$ using the radiation correction methodology (β -method). The radiation error of the Part 2 result was near zero, as the thermocouples were about 1.50 m above the flame height and measured the plume temperature.



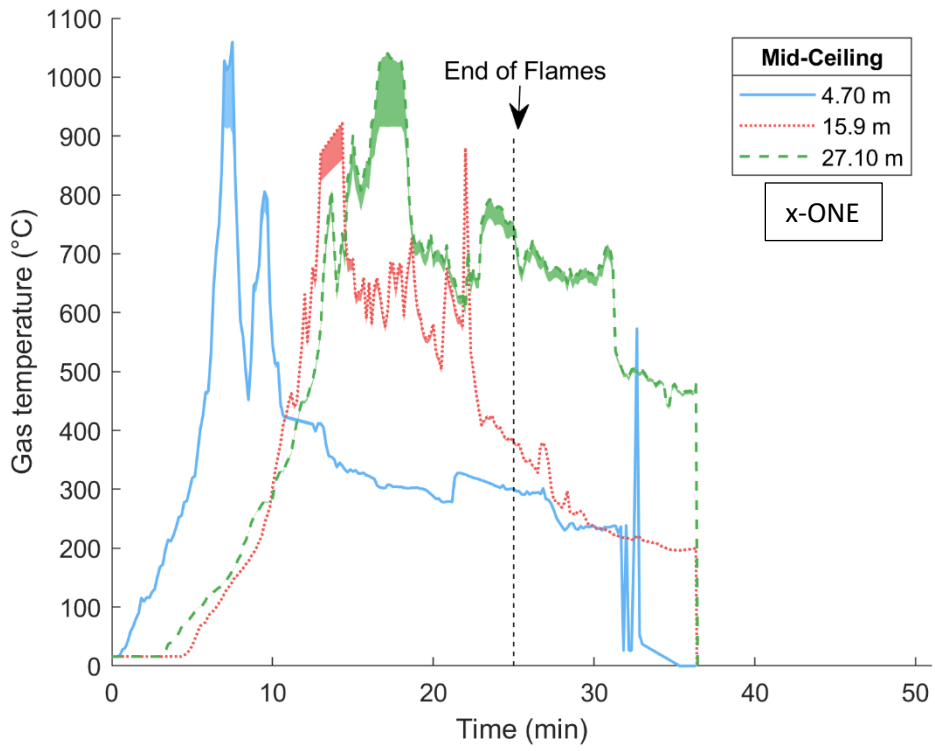
(a)



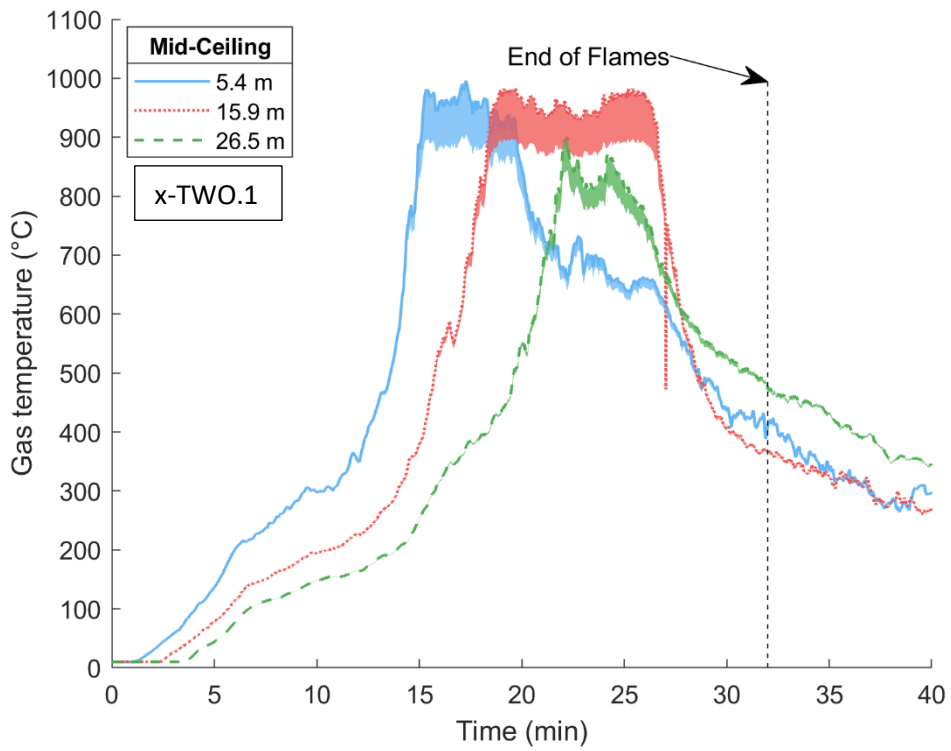
(b)

Figure 5.9 Gas temperatures from the thermocouples installed in the mid-ceiling along the length of the compartment corrected for radiation error. Near field and far field locations change at different time steps from the ignition for x-TWO.1 (a) and Part 2 (b). The shaded region describes the region of correction bounded.

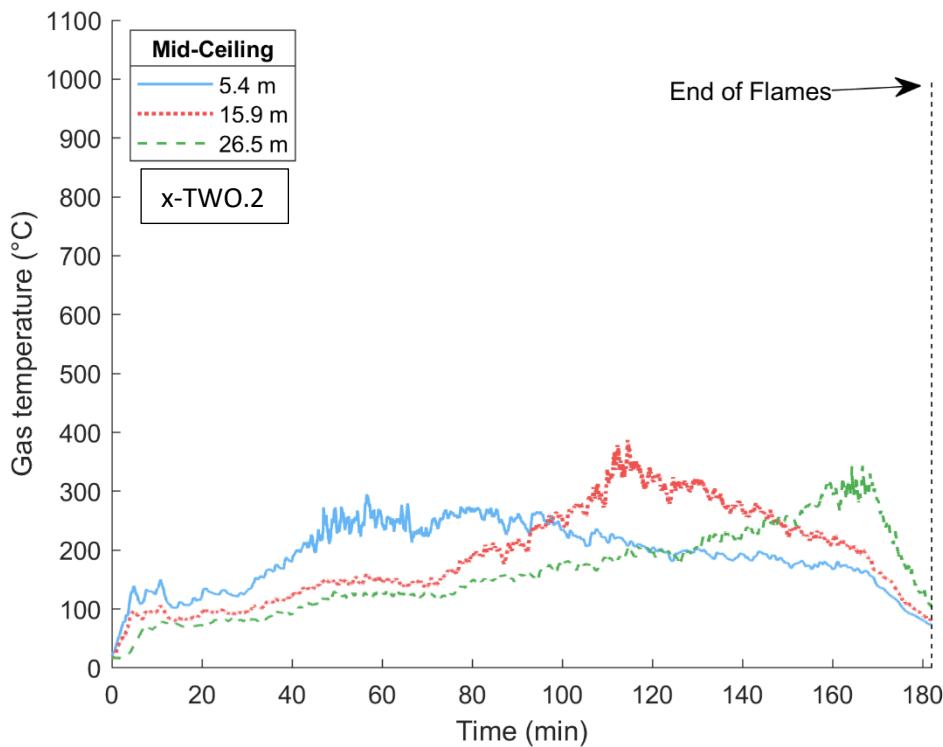
Location of near-field and far-field exposures at different times of fire can be clearly identified along the length of the compartment (Figure 5.9 and Figure 5.10). In x-ONE and x-TWO.1 (Figure 5.9 and Figure 5.10), near-field represents flames directly impinging on and extending under the ceiling, while far-field represents cooler smoke further away from the flames. In x-TWO.2, where the fuel load was decreased by 20% compared to Part 1, the maximum flame height was 1.3 m (1.60 m below the ceiling). As such, the maximum temperatures of curves for x-TWO.2 in Figure 5.9 and Figure 5.10, represent the plume temperature at the centre line of the burning area (near-field), which was travelling through the compartment floor.



(a)



(b)



(c)

Figure 5.10 Gas temperature from thermocouples at the beam soffit level at 3 locations (at 4.70 m (T3), 15.90 m (T6), and 27.10 m (T9) from ignition location towards the West entrance, for x-ONE (a), x-TWO.1 (b) and x-TWO.2 (c). Results have been corrected for radiation error. The shaded region describes the region of correction bounded using dimensionless constant β values of $1.17 \leq \beta \leq 1.25$.

In x-ONE, during the first 7 min, and x-TWO.1 during the first 13 min after ignition just the leading edge of the fire was spreading, so the near field was increasing in size. After 7.5 min in x-ONE and 14 min in x-TWO.1 both the leading and trailing edge were moving along the length of the compartment, as illustrated in Figure 5.10.

Maximum corrected gas temperatures in the near-field region reached temperatures up to $\sim 1000^\circ\text{C}$ and $\sim 325^\circ\text{C}$, in Part 1 and Part 2 of x-TWO, respectively. Part 1 reached similar maximum corrected gas temperatures compared to x-ONE, which also reached up to $\sim 1000^\circ\text{C}$. Each thermocouple in the compartment (except for T1 which was not located above the fuel bed) was subjected to near field region. Once the near-field has passed and fire has burned out, the temperatures at that location (i.e., far-field) dropped to below 900°C in Part 1 and below 250°C in Part 2. The total duration of fire was 25 min in x-ONE, 32 min in Part 1, and 182 min in Part 2. The lower temperature and longer burning duration of Part 2 were due to 20% lower fuel load compared to Part

1. x-TWO.2 was carried out on a rainy day with 94% humidity; a part of energy and compartment temperature may be absorbed by the high humidity inside the compartment.

As a reference, for x-TWO.1 in Figure 5.10 at 18 min, where for the first third of the compartment peak temperatures had almost been reached, the temperature near the far end of the compartment is still below 450 °C. The temperature near the end of the compartment then reaches a peak value of 900 °C around 23 min while the temperature at the beginning of the compartment quickly cools down to temperatures below 800 °C. The spatial evolution of the gas temperature throughout the compartment confirms the non-uniform temperature with pre-heating associated with the travelling fires methodology [27].

Vertical temperature variations for two different locations in the beginning of the compartment (i.e., at 3.90 m along the fire path from the ignition point) are shown in Figure 5.11. At different times of the experiment, vertical temperature variations are in the range of approx. 50-400°C. The temperatures near the bottom of columns (i.e., 1 m above the floor) are lower than those recorded at the top of the column (i.e., 2.4 m above the floor). Temperature variations are more obvious before the arrival of the flame front (i.e., the leading edge) and after the trailing edge has spread past it. In addition, thermocouples at the bottom of column mainly capture the flame temperatures as the flames approached and spread past it, whereas thermocouples at the top of the column were also exposed to and captured temperatures within the smoke layer.

Figure 5.11 illustrates that when the flames are burning in the proximity of the column at 27.1 m from the ignition point along the fire path, the temperature at the bottom of the column is lower than the top of the columns because the fresh air entering the compartment cooled down the air in the bottom of the column. As identified previously, the difference can go up to 200°C. In Part 2, fresh air from the West entrance cooled down the bottom column thermocouple, which was exposed to flame, as such, the temperature of the bottom of the column was equal to the recorded at top of the column in the fire plume.

The non-uniform temperature results obtained from x-ONE and x-TWO are contrary to the uniform temperature assumption of the current codes. Therefore, the experiments presented here confirm the results of previous studies [74], [88] that showed travelling fires with non-uniform temperature should be considered for the structural fire design along with the EC 1-1-2 parametric fire with uniform temperature assumption.

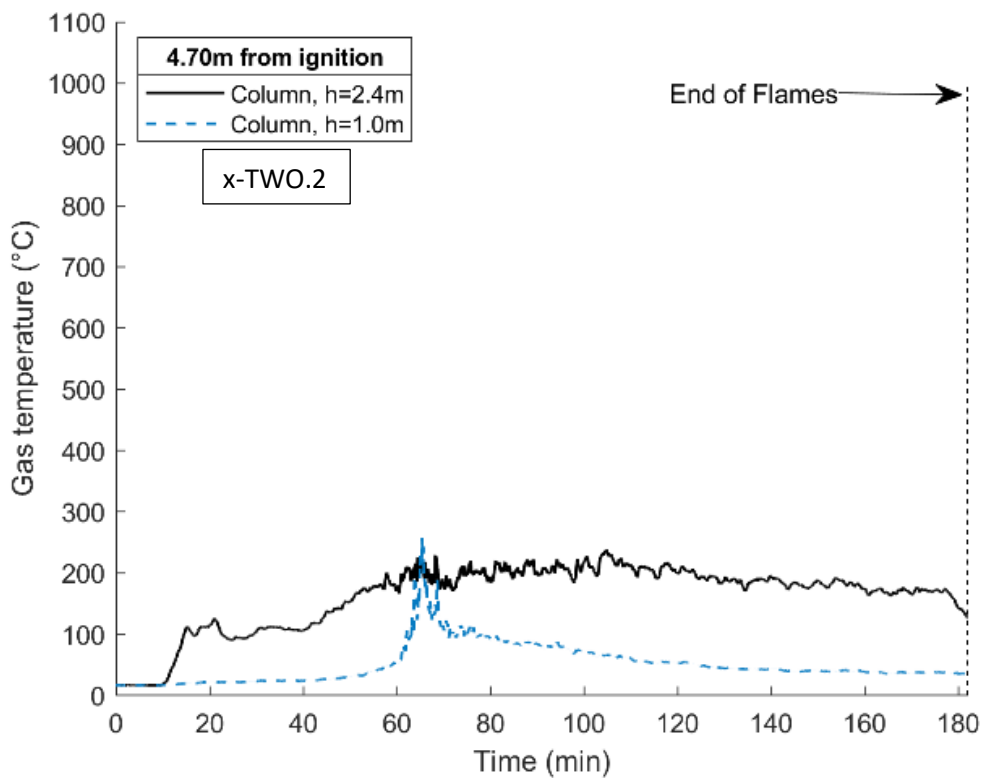
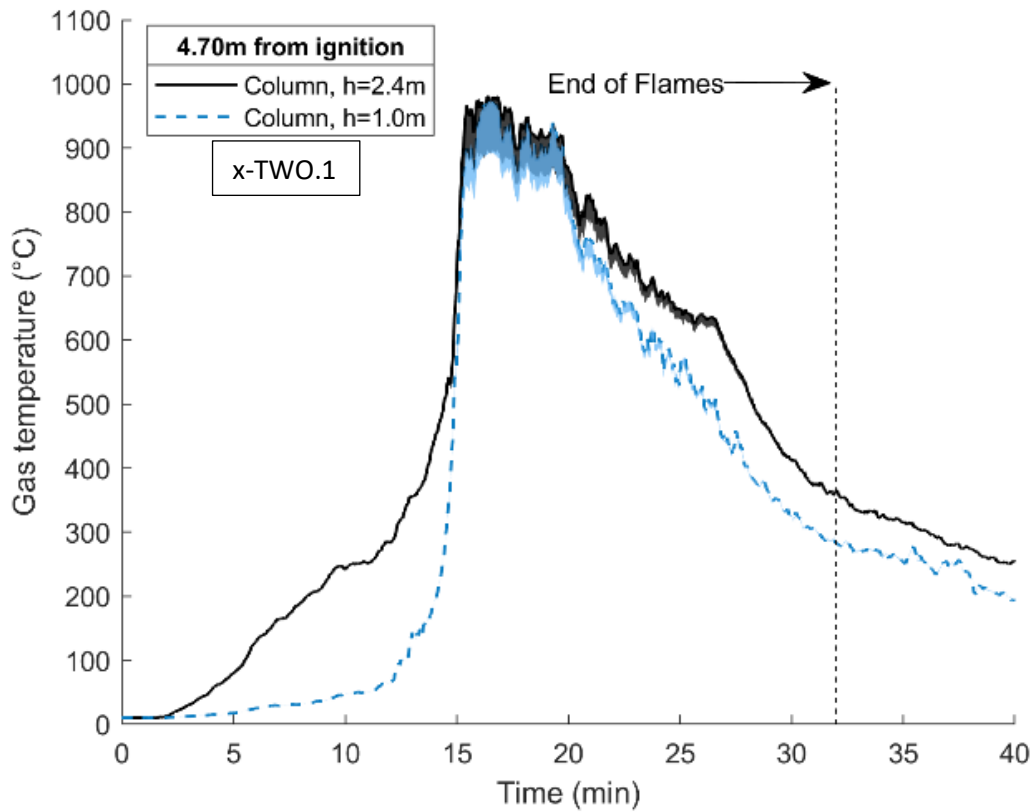


Figure 5.11 Vertical temperature variations within the compartment from x-TWO.1 (top), Part 2 (bottom). For each bay, thermocouples were located at the top of the column (~2.4 m), and the bottom of the column bottom (~1 m), respectively. Temperature is corrected for the radiation error.

5.8 Comparison Between x-TWO and Design Fires

As discussed previously the traditional design curves provide a uniform temperature for structural fire design, such as ISO standard fire and parametric fire (valid for 500 m² with a maximum 4 m height). Nevertheless, the x-TWO experiments demonstrated highly non-uniform fire behaviour, high spatial gas and smoke temperature distributions consistent with travelling fire behaviour. To fill the shortcoming of the traditional method, travelling fires methodologies [24], [27], [28], [34], [35], [86] have been developed, amongst them the iTFM and fTFM are the most recent methodologies. iTFM and fTFM account for the exposure from the near-field (flames) and the far-field (smoke) regions of the fire.

Comparison between the heat flux induced from the temperatures measured during the x-TWO.1, ISO standard fire, parametric fire, and representative travelling fire using fTFM (presented in Chapter 3 [86]) and iTFM at two different locations of the compartment (i.e., 17.77 m and 28.55 m from the ignition point) are presented in Figure 5.12.

The parametric fire curve was calculated assuming the same compartment dimensions, internal linings, and available ventilation openings as in the experimental compartment. For other models (parametric fire, ISO standard fire, iTFM), the received heat flux (gauge heat flux) was calculated assuming the surface temperature remains at ambient temperature as discussed in Chapter 3.

fTFM with the Lattimer model for the near field heat flux was used to calculate the received heat flux to the ceiling. The representative travelling fires from fTFM and iTFM assume the same fuel load density (345 MJ/m²), local burning time, and similar sizes observed during the experiment. The observed near field size when reaching the studied location, was about 55% of the area of the fire bed. For x-TWO.1, the received heat flux (gauge heat flux) was calculated from the corrected gas temperature in accordance with the methodology presented in Chapter 3. Therefore, the calculated heat fluxes for x-TWO, parametric fire, iTFM, and fTFM are coherent.

Figure 5.12 indicates significant differences in the thermal exposure between traditional models that would be used in the design of a structure and that measured in the x-TWO experiments. Peak heat flux from the experiment is up to ~120 kW/m² but increases gradually as the fire grows and travels across the compartment. On the contrary, standard fire and Eurocode parametric curves assume a sudden increase in temperature with the maximum heat flux for the parametric fire reaching ~87

kW/m² and 93 kW/m² from the ISO standard fire at 32 min, which is the time corresponding to the end of flames in the experiment.

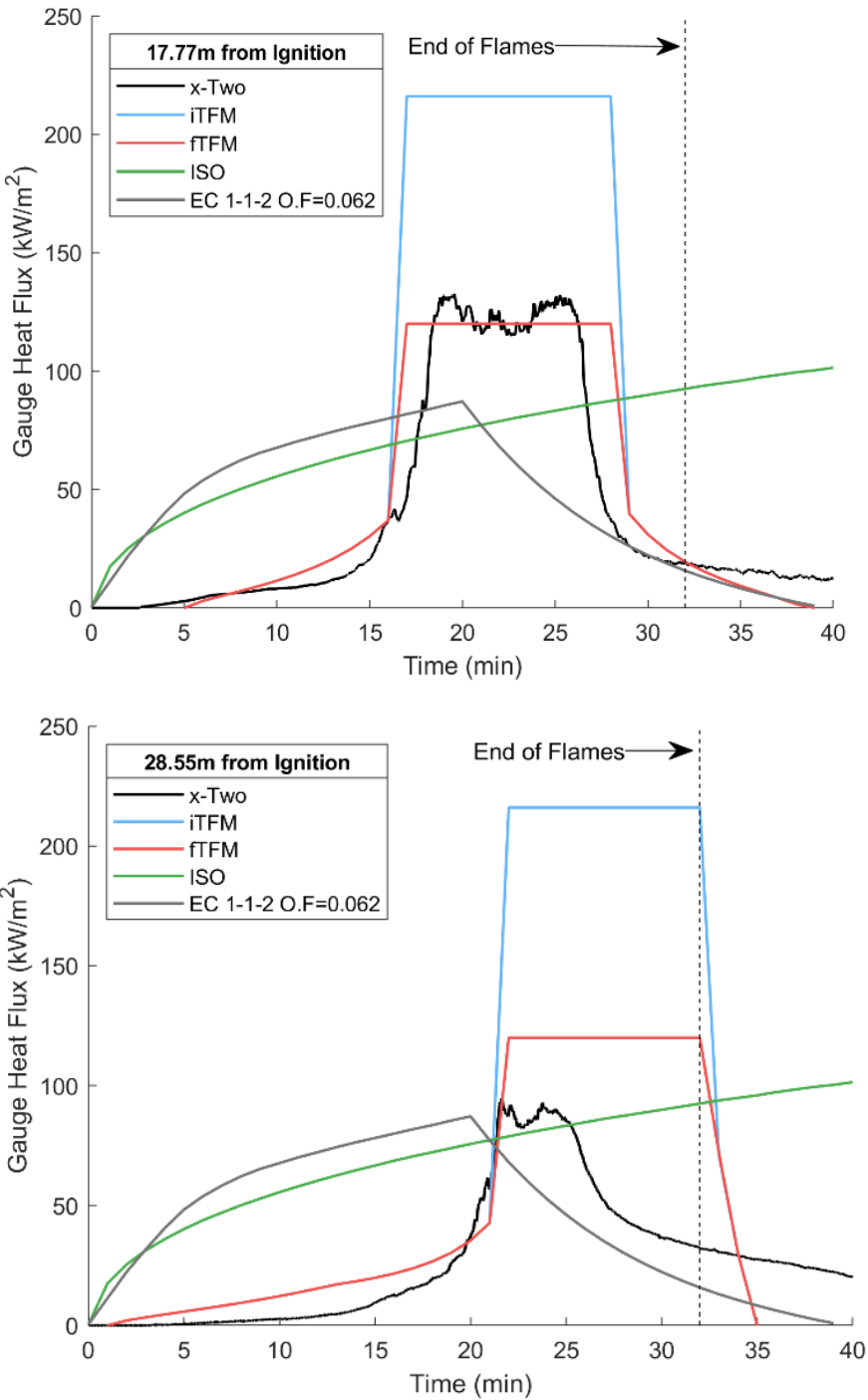


Figure 5.12 Calculated heat fluxes at two different location in the middle and far west of compartment using iTFM, fTFM, parametric fire, ISO standard fire, and corrected gas temperature of x-TWO.1. The fire size observed during the experiment at the studied locations was about 55% of the area of the compartment.

Figure 5.12 shows that both fTFM and iTFM give a good estimation for the near-field heating duration in the middle of the compartment (i.e., at 17.77 m) and overpredict it for the point close to the end of the compartment (i.e., at 28.77 m). This is because, as mentioned previously, the methodology assumes a uniform flame spread and cannot capture the changing fire size. The final fire sizes selected based on the total fire exposure is more representative of the fire size towards the middle of the experiment as the fire approached the West entrance.

Furthermore, it can be seen in Figure 5.12 that the maximum near-field heat flux induced from the experiment was well predicted by fTFM for the location in the middle of the compartment. The heat flux at the end of the compartment is lower than the models due to the cooling effect of the airflow from the West entrance.

The far field results obtained from iTFM and fTFM had almost the same trend as captured in the experiment for the middle of the compartment. For the location near the end of the compartment, the preheating of far field from models is the same as the experiment.

In general, the thermal exposure assumed in iTFM and fTFM is closer to the observed experimental results than uniform traditional design fires (i.e., standard and parametric fires) and can account for highly non-uniform temperature distributions within the compartment.

5.9 Conclusion

x-TWO consisted of two large-scale travelling fire experiments (Part 1 and Part 2), conducted in Poland in May 2019 to study fire inside a large real compartment and measure its spread characteristics. Part 1 had a fuel load density of 345 MJ/m² and Part 2 had 20% less fire load compared to Part 1 (i.e., 273 MJ/m²). The aim was to understand the impact of fuel load changes on fire dynamics and to reduce other uncertainties. The fire in both experiments was allowed to develop naturally. Observation showed a fast and accelerating fire travelling of 32 min duration in Part 1, and a longer steady-state spread travelling fire of 180 min in Part 2. The maximum recorded near-field temperature was ~1200 °C. The observations and results of the experiment further confirm that flashover does not always occur in large compartments, but fire can travel across the compartment, meaning that non-uniform heating is possible in large compartments. From a design perspective, both uniform and non-uniform heating can challenge a structure [74], [88], therefore both uniform and non-uniform fires need to be considered during design.

Comparison of fTM and iTFM with experimental results showed that in general, these methodologies provide a good prediction of travelling fire in large compartments, as long as the fire size is understood. Prediction from fTFM methodology, developed in Chapter 3, is closer to the observed experimental results than uniform traditional design fires and iTFM.

The spread rate of the fire was not constant in x-ONE (and to some degree in x-TWO) and is assumed in travelling fire methodology to be constant but was in fact gradually increasing. Reducing the fire load density shows that the accelerating nature of fire is likely related to the fuel load and its arrangement. Further experiments will facilitate estimation of the impact of other parameters (i.e., the compartment area, available ventilation, etc) on the spread rate and travelling nature of fire. The experiment presented here can be used for validation, and further development of the travelling fire methodology.

Chapter 6

Conclusions and future work

6.1 Conclusions

Prescriptive design codes are normally applied to meet the generic fire resistance requirements of a building. This approach is based on a simple fire scenario in a small compartment with specific design limitations imposed on the building (e.g., maximum compartment area), which is a challenge (or not applicable) for modern building designs with floor plates in the order of thousands square meters. Performance-based design codes lay down what safety standards need to be met by a designer, leaving scope for new materials, systems, and methods to be used in a building's design. A challenge for the performance-based design of large compartments is the characterization of the fire dynamics in large open-plan compartments.

Travelling fires methodologies were developed where a limited number of large experiments were available in large compartments of a size analogous to modern building designs (the experiments are costly and difficult). Travelling fires methodology addresses the limitation of traditional methodologies and enables innovation in design by providing a more realistic characterisation of the fire phenomena in a large open plan building.

The travelling fires methodology has been developed based on some assumptions to provide a simple and reasonable representation of travelling fires scenarios that can be used conservatively for a safe structural design. This methodology did not represent all processes related to fire dynamics in large compartments, which further research is still required to address. To this end, this thesis revisits the near field assumption of TFM and included the flame extension under the compartment ceiling. This work also applies a probabilistic model to assess the reliability of a structural element exposed to travelling fires and the uniform temperature fire.

Further development of the travelling fires methodology in this thesis was presented in Chapter 3 and labelled fTFM. fTFM considers the full extension of the near field region under the ceiling, which affects the heating exposure of the structural members. The analysis showed that including the flame extension prolongs the duration of the exposure of the structural element to the near field region. This could affect the resulting thermal response of the structural elements and therefore the structural

behavior. Therefore, the travelling fires methodology with the flame extension is more representative for structural design under a travelling fires scenario, because the time to structural failure can be earlier when the flame extension is considered (especially for smaller fire sizes of longer duration).

The travelling fires methodology with flame extension in Chapter 3 for the first time formulates the TFM in terms of heat flux rather than temperatures, thus allowing for a more formal heat transfer boundary condition between the gas and the surface of the structural element. Chapter 3 established that formulating the near field in terms of heat flux is correct and accurate. The Hasemi, Wakamatsu, and Lattimer expressions are used in fTFM to calculate the received heat flux to the ceiling in the near field region. The study showed that peak heat flux of small fire sizes, using the flame extension and the Wakamatsu model is larger than the one calculated with TFM. Comparison of the available experimental data with the three expressions showed that the Lattimer model is the most accurate in obtaining the heat flux of the localized fire impinging on the ceiling, in the absence of other experimental evidence being available to aid further analysis.

An experimental campaign in a large, open-plan compartment of 384 m² called x-ONE and x-TWO (part 1 and part 2) were carried out as a part of the framework of the research effort to study travelling fires in a very large compartment and measure basic fire characteristics such as temperature and spread rate. The fuel load was the only element that was changed between experiments to reduce other uncertainties that could affect the fire behaviour since the compartment and ventilation were fixed. x-TWO.1 repeated x-ONE. Maximum radiation corrected gas temperatures were about 1000 °C in x-ONE and x-TWO.1. The maximum recorded near-field temperature was ~1200 °C. The obvious conclusions of the experiments, presented in Chapter 5, were that: 1- flashover does not occur instead fire travels, 2- the heterogeneous temperature assumption associated with travelling fires methodology is valid for a large compartment, and; 3- the spread rate of the travelling fires is a function of the fuel when the ventilation is not changing. x-ONE and x-TWO minimised the level of complexity of travelling fires scenarios and models. Flame extension under the ceiling was observed in the experiments. Comparison of the experiment results of x-TWO with fTFM methodology showed an appropriately accurate prediction by the fTFM model. The results of the experiments could be used to justify the inclusion of travelling fires in current design methodologies for large compartments such that ultimately, they form part of best practice guidance and standards.

Figure 6.1 presents the evolution of travelling fire models, with a focus on the methodology used (iTFM) and developed methodology (fTFM) in this paper.

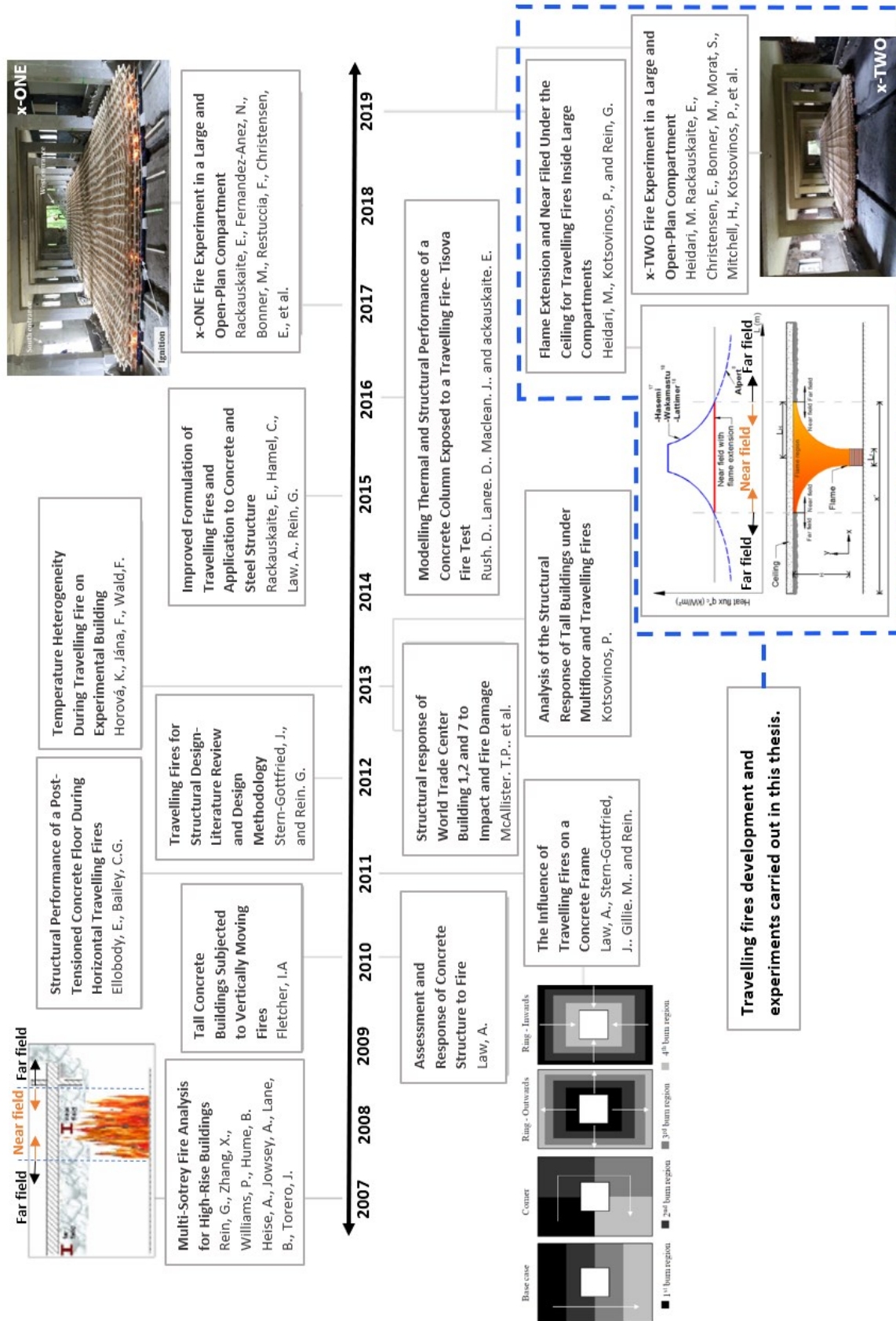


Figure 6.1. Brief background history of the Travelling Fires Methodology in literature as related to this study. The travelling fire work in this thesis is illustrated here (Post 2007- Figure adapted from [33]).

A simple, but powerful, structured methodology for sensitivity studies in Chapter 2 gives insight into the effect of varying the input parameters of parametric fire (with a uniform temperature assumption) and the heat transfer model on the thermal response of the structural element. The analysis assessed the sensitivity of structural element response to input parameter uncertainty. It was concluded that the sensitivity analysis identifies the most influential input parameters for the fire design of the structure and the range of values for each input parameter for which the design is structurally safe (i.e., to define safe and critical design fires). Such a structured approach could help to justify some of the assumptions and simplifications which are made in fire safety engineering, by identifying parameters for which more information is needed for different applications.

The probabilistic approach using Monte Carlo method in Chapter 2 and Chapter 4 quantified the reliability (or probability of the failure) of the structure when designed following EC 1-1-2 parametric fire or fTFM. It was shown that a Monte Carlo based probabilistic approach can account for the uncertainties in modelling inputs in the case of real fires, as there is the opportunity to vary input parameters within a defined range. It was demonstrated that fTFM methodology, developed in Chapter 4, is well-tailored to be applied in a probabilistic framework. The probabilistic analysis of unavailability of fire protection measures, as indicated in the EC 1-1-2 method, showed that unavailability of either sprinkler systems or detection systems resulted in a 1% probability of failure of the slab, and unavailability of sprinkler and detection systems resulted in an 8% probability of failure of the slab.

By means of the probabilistic approach, the reliability curves for a structural element based on the equivalent fire severity for parametric fire and travelling fires were determined and compared. The significant difference between the reliabilities of the structural element obtained for travelling fires and parametric fire showed that structure is being close to failure in the case of travelling fires. This study demonstrated that sensitivity and probabilistic analyses can provide a comprehensive understanding of the factors affecting the structural fire resistance and inform further fire development and detailed structural analysis. From a design perspective, the experiments campaign and probabilistic analysis conclude that both uniform and non-uniform fires need to be considered during design, as recent research [74], [88] has shown that both uniform and non-uniform heating can challenge a structure.

Travelling fires is a simplified and comprehensive tool that can express the thermal environment in large compartment. Travelling fires are not predictive, but rather generic approximations that could be used in design to test structures under a range of different heating regimes representative of

travelling fires behaviour. The findings of this thesis mitigate the uncertainty around the shortcomings of the TFM model and reinforce that it can be used for the assessment of the thermal response of structures. The development of the presented methodology (fTFM) is analogous to that of the previous versions of the travelling fires methodology [27], [28], that is already used as a complementary tool in design practice, [53], [84] and therefore fTFM could also be used for design purposes of non-combustible structures as the lining of the compartments may also contribute in various fashions.

6.2 Future Work

The experiment presented here can be used for validation, and further refinement of the travelling fires methodology (as part of future research). Further experiments will facilitate to estimation of the impact of other parameters (i.e., the compartment area, available ventilation, etc) on the spread rate and travelling nature of fire.

During the x-ONE and x-TWO experiments, fire spread rates of the leading and trailing edges were not constant and instead changed significantly during the fire. As a result of the differing leading and trailing edge behaviour, the fire size varied during the experiments. However, all TFM methodologies assume a constant fire spread rate and burning rate or movement of the fire from one bay/compartment to another. Therefore, further experimental work is needed to study the spread rates and development of travelling fires in large enclosures. A potential method for addressing this is via a probabilistic travelling fires approach, which can be used to account for different spread rates of the leading and trailing edges of the fire.

Future research should include complementary experiments, varying key influencing design parameters, including ventilation conditions, compartment size, and fuel load (for example including the combustible lining) to support the travelling fires methodology. The non-uniform heat flux and its consequences on the columns (especially for protected members where gradients can effect the protection element) in future iterations of the method can be studied.

Travelling fire methodology was considered by the International Organization for Standardization (ISO) for inclusion in an ISO technical report [38] and the UK standards PD7974-1 and -3 [36], [37]. More future works are needed through the standards process internationally to adopt these methodologies as tools in the design process.

References

- [1] Eurocode 2, "Design of concrete structures-Part 1-2: General rules — Structural fire," European Standard EN 1992-1-2,CEN,Brussels, 2004.
- [2] Eurocode 3, "Design of steel structures - Part 1-2: General rules - Structural fire design," European Standard EN 1993-1-2,CEN,Brussels, 2005.
- [3] Eurocode 1, "Actions on structures —Part 1-2: General actions — Actions on structures exposed to fire," European standard EN 1991-1-2, CEN, Brusseles, 2002.
- [4] V. Babrauskas, "A closed-form approximation for post-flashover compartment fire temperatures," *Fire Saf. J.*, vol. 4, no. 1, pp. 63–73, Aug. 1981, doi: 10.1016/0379-7112(81)90005-9.
- [5] V. Babrauskas and R. B. Williamson, "Post-flashover compartment fires: Basis of a theoretical model," *Fire Mater.*, vol. 2, no. 2, pp. 39–53, Apr. 1978, doi: 10.1002/fam.810020202.
- [6] M. Law, "A Basis for the Design of Fire Protection of Building Structures - The Institution of Structural Engineers," *Struct. Eng.*, vol. no Februar, pp. 25–33, 1983.
- [7] K. Matsuyama, T. Fujita, H. Kaneko, Y. Ohmiya, T. Tanaka, and T. Wakamatsu, "A Simple Predictive Method for Room Fire Behavior," *J. Struct. Constr. Eng.*, vol. 60, no. 469, pp. 159–164, Mar. 1995, doi: 10.3130/aijs.60.159_1.
- [8] S. E. Magnusson and S. Thelandersson, "Temperature - time curves of complete process of fire development. Theoretical study of wood fuel fires in enclosed spaces," 1970.
- [9] M. A. Delichatsios, Y. P. Lee, and P. Tofilo, "A new correlation for gas temperature inside a burning enclosure," *Fire Saf. J.*, vol. 44, no. 8, pp. 1003–1009, Nov. 2009, doi: 10.1016/j.firesaf.2009.06.009.
- [10] M. J. Hurley *et al.*, "SFPE handbook of fire protection engineering, fifth edition," in *SFPE Handbook of Fire Protection Engineering, Fifth Edition*, 2016.

- [11] D. Drysdale, *An Introduction to Fire Dynamics*. Chichester, UK: John Wiley & Sons, Ltd, 2011.
- [12] BS476-20, "Fire tests on building materials and structures —Part 20:Method for determination of the fire resistance of elements of construction," *BSI*, no. 1, 1987.
- [13] "ISO 834-1:1999(en), Fire-resistance tests — Elements of building construction — Part 1: General requirements." <https://www.iso.org/obp/ui/#iso:std:iso:834:-1:ed-1:v1:en> (accessed Feb. 06, 2019).
- [14] "ASTM E119- 08a- Standard Test Methods for Fire Tests of Building Construction and Materials," 1987.
- [15] V. Babrauskas and R. B. Williamson, "The Historical Basis of Fire Resistance Testing-Part II."
- [16] J. Gales, B. Chorlton, and C. Jeanneret, "The Historical Narrative of the Standard Temperature–Time Heating Curve for Structures," *Fire Technology*. Springer, pp. 1–30, Sep. 22, 2020, doi: 10.1007/s10694-020-01040-7.
- [17] M. Salah Dimia, M. Guenfoud, T. Gernay, and J.-M. Franssen, "Collapse of concrete columns during and after the cooling phase of a fire," *J. Fire Prot. Eng.*, vol. 21, no. 4, pp. 245–263, Nov. 2011, doi: 10.1177/1042391511423451.
- [18] B. Chorlton, B. Forrest, J. Gales, and B. Weckman, "Performance of type X gypsum board on timber to non-standard fire exposure," *Fire Mater.*, Mar. 2020, doi: 10.1002/fam.2822.
- [19] O. Pettersson, S.-E. Magnusson, and J. Thor, "Fire Engineering Design of Steel Structures, Publication 50," Stockholm:Swedish Institute of Steel Construction, 1976.
- [20] T. Lennon and D. Moore, "The natural fire safety concept--full-scale tests at Cardington," *Fire Saf. J.*, vol. 38, no. 7, pp. 623–643, 2003.
- [21] J. L. Torero, A. Law, and C. Maluk, "Defining the thermal boundary condition for protective structures in fire," *Engineering Structures*, vol. 149, Elsevier, pp. 104–112, Oct. 15, 2017.
- [22] J. Stern-gottfried, "Travelling Fires for Structural Design.Ph.D thesis," School of Engineering, The university of Edinburgh, 2011.

- [23] M. A. Khan, A. A. Khan, A. S. Usmani, and X. Huang, "Can fire cause the collapse of Plasco Building: A numerical investigation," *Fire Mater.*, p. fam.3003, Jun. 2021, doi: 10.1002/FAM.3003.
- [24] G. C. Clifton, "Fire Models for Large Firecells," *HERA Rep. R4-83*, vol. 1996, no. with proposed changes in HERA Steel Design and Construction Bulletin Issue No 54, February 2000 and updates to referenced documents, September 2008.
- [25] G. Rein, X. Zhang, P. Williams, B. Hume, and A. Heise, "Multi-Storey Fire Analysis For High-Rise Building," in *11th Interflam*, 2007, no. September, pp. 605–616, [Online]. Available: <http://hdl.handle.net/1842/1980>.
- [26] J. Stern-Gottfried and G. Rein, "Travelling fires for structural design – Part I : Literature review," *Fire Saf. J.*, vol. 54, pp. 74–85, 2012, doi: 10.1016/j.firesaf.2012.06.003.
- [27] J. Stern-Gottfried and G. Rein, "Travelling fires for structural design-Part II: Design methodology," *Fire Saf. J.*, vol. 54, pp. 96–112, Nov. 2012, doi: 10.1016/j.firesaf.2012.06.011.
- [28] E. Rackauskaite, C. Hamel, A. Law, and G. Rein, "Improved Formulation of Travelling Fires and Application to Concrete and Steel Structures," *Structures*, vol. 3, pp. 250–260, Aug. 2015, doi: 10.1016/j.istruc.2015.06.001.
- [29] R. Alpert, "Model-Based Analysis of a Concrete Building Subjected to Fire," *Fire Technol.*, vol. Vol 83, no. Issue: 3, pp. 181–195, 1972.
- [30] R. L. Alpert, "Ceiling Jet Flows," in *SFPE Handbook of Fire Protection Engineering, Fifth Edition*, New York, NY: Springer New York, 2016, pp. 429–454.
- [31] A. Law, J. Jamie Stern-Gottfried, M. Gillie, and G. Rein, "The Influence of Travelling Fires on the Response of a Concrete Frame," 2010.
- [32] E. Rackauskaite, P. Kotsovinos, and G. Rein, "Structural response of a steel-frame building to horizontal and vertical travelling fires in multiple floors," *Fire Saf. J.*, 2017, doi: 10.1016/j.firesaf.2017.04.018.
- [33] C. Jeanneret, J. Gales, P. Kotsovinos, and G. Rein, "Acceptance Criteria for Unbonded Post-

- Tensioned Concrete Exposed to Travelling and Traditional Design Fires,” *Fire Technol.*, vol. 56, no. 3, pp. 1229–1252, 2020, doi: 10.1007/s10694-019-00927-4.
- [34] D. Hopkin, “Testing the Single Zone Structural Fire Design Hypothesis,” *Interflam 2013, Proc. 13th Int. Conf.*
- [35] X. Dai *et al.*, “An extended travelling fire method framework for performance-based structural design,” *Fire Mater.*, vol. 44, no. 3, pp. 437–457, Apr. 2020, doi: 10.1002/fam.2810.
- [36] British Standards Institution, *PD 7974-1:2019 Application of fire safety engineering principles to the design of buildings. Initiation and development of fire within the enclosure of origin.* 2019.
- [37] British Standards Institution, “PD 7974-3:2019 Application of fire safety engineering principles to the design of buildings. Structural response to fire and fire spread beyond the enclosure of origin,” 2019.
- [38] International Organization for Standardization, “ISO/TS 16733-2 - Fire safety engineering — Selection of design fire scenarios and design fires — Part 2: Design fires,” 2021. <https://www.iso.org/standard/63142.html> (accessed Mar. 03, 2021).
- [39] B. J. Meacham, “The evolution of performance-based codes and fire safety design methods,” Gaithersburg, MD, 1998.
- [40] A. H. Buchanan, *Structural Design for Fire Safety*. Chichester, UK, Wiley & sons, 2002.
- [41] *SFPE Engineering Guide to Performance-Based Fire Protection, 2nd Edition.* 2006.
- [42] “ISO/TS 24679-1 - Fire safety engineering - Performance of structures in fire,” *International Organization for Standardization*, 2011. http://www.iso.org/iso/catalogue_detail.htm?csnumber=42357 (accessed Nov. 27, 2014).
- [43] C. Fleischmann, “Is Prescription the Future of Performance Based Design?,” *Fire Saf. Sci.*, vol. 10, pp. 77–94, 2011, doi: 10.3801/IAFSS.FSS.10-77.
- [44] G. Notarianni, Kathey A., Parry, “SFPE Handbook of Fire Protection Eng,” in “*Uncertainty*”, *SFPE Handbook of Fire Protection Engineering*, 5th ed., 2015, pp. 2992–3047.

- [45] J. L. Torero, A. Jowsey, A. Usmani, B. Lane, and S. Lamont, "Structure In Fire: An Overviwe Of The Boundary Condition," *Fire Struct. Conf. R. Soc. Edinburgh*, pp. 13–14, 2004.
- [46] M. A. Johann, L. D. Albano, R. W. Fitzgerald, and B. J. Meacham, "Performance-Based Structural Fire Safety," *J. Perform. Constr. Facil.*, vol. 20, no. 1, pp. 45–53, Feb. 2006, doi: 10.1061/(ASCE)0887-3828(2006)20:1(45).
- [47] D. J. Lange, "Risk and Performance Based Fire Safety Design of Steel and Composite Structures- Ph.D thesis," School of Engineering-The University of Edinburgh, 2009.
- [48] A. M. Al-Remal, "Risk-Based Design of Structures For Fire," School of Engineering-The university of Edinburgh, 2012.
- [49] D. Lange, A. Usmani, and J. L. Torero, *The Reliability of Structure in Fire*. Singapore: Proceeding of the Fifth International Conference on Structure in Fire(SiF08), 2008.
- [50] Q. Guo, K. Shi, Z. Jia, and A. E. Jeffers, "Probabilistic Evaluation of Structural Fire Resistance," *Fire Technol.*, vol. 49, no. 3, pp. 793–811, 2013.
- [51] R. Van Coile, R. Caspeele, and L. Taerwe, "Reliability-based evaluation of the inherent safety presumptions in common fire safety design," *Eng. Struct.*, vol. 77, pp. 181–192, Oct. 2014, doi: 10.1016/j.engstruct.2014.06.007.
- [52] B. R. Kirby, G. M. Newman, N. Butterworth, J. Pagan, and C. English, "A new approach to specifying fire resistance periods," *Struct. Eng.*, no. October, pp. 34–37, 2004.
- [53] A. Law, J. Stern-Gottfried, and N. Butterworth, "A Risk Based Framework for Time Equivalence and Fire Resistance," *Fire Technol.*, May 2014, doi: 10.1007/s10694-014-0410-9.
- [54] E. Nigro, A. Bilotta, D. Asprone, F. Jalayer, A. Prota, and G. Manfredi, "Probabilistic approach for failure assessment of steel structures in fire by means of plastic limit analysis," *Fire Saf. J.*, vol. 68, pp. 16–29, 2014.
- [55] S. Hostikka and O. Keski-Rahkonen, "Probabilistic simulation of fire scenarios," *Nucl. Eng. Des.*, vol. 224, no. 3, pp. 301–311, 2003, doi: 10.1016/S0029-5493(03)00106-7.

- [56] F. P. Incropera, D. P. DeWitt, T. L. Bergman, and A. S. Lavine, *Fundamentals of Heat and Mass Transfer*, vol. 6th. John Wiley & Sons, 2007.
- [57] F. Biasioli et al., “Eurocode 2: Background & Application, Design of Concrete Buildings, Worked Examples,” Publications Office of the European Union, European Union, Luxembourg, 2014. doi: 10.2788/35386.
- [58] N. Bal, “Uncertainty and complexity in pyrolysis modelling,” PhD thesis-School of Engineering, The University of Edinburgh, 2012.
- [59] S. Ulam and N. Metropolis, “The Monte Carlo Method,” *Am. Stat. Assoc.*, vol. 44, no. 247, pp. 335–341, 1949.
- [60] Eurocode 2, “Design of concrete structures-Part 1-1: General rules and rules for buildings,” European Standard EN 1992-1-1, CEN, Brussels, 2002.
- [61] Eurocode1-Annexe nationale à la NF EN 1991-1-2, “Eurocode 1 — Actions sur les structures — Partie 1-2 : Actions générales — Actions sur les structures exposées au feu,” l’Association Française de Normalisation (AFNOR), 2007.
- [62] V. Babrauskas, “Glass breakage in fires,” *Fire Sci. Technol. Inc.*, pp. 1–7, 2011, [Online]. Available: <http://doctorfire.com/GlassBreak.pdf>.
- [63] C. Thauvoye, B. Zhao, J. Klein, and M. Fontana, “Fire load survey and statistical analysis,” *Fire Saf. Sci.*, pp. 991–1002, 2008, doi: 10.3801/IAFSS.FSS.9-991.
- [64] N. E. Khorasani, M. Garlock, and P. Gardoni, “Fire load: Survey data, recent standards, and probabilistic models for office buildings,” *Eng. Struct.*, vol. 58, pp. 152–165, 2014, doi: 10.1016/j.engstruct.2013.07.042.
- [65] Y. Y. Haimes and J. H. Lambert, “When and How Can You Specify a Probability Distribution When You Don’t Know Much? II,” *Risk Anal.*, vol. 19, no. 1, pp. 43–46, Feb. 1999, doi: 10.1111/j.1539-6924.1999.tb00385.x.
- [66] M. D. Byrne, “How many times should a stochastic model be run? An approach based on confidence intervals,” *Proc. 12th Int. Conf. Cogn. Model.*, pp. 445–450, 2013.

- [67] M. Modarres and F. Joglar, "Reliability," in *SFPE Handbook of Fire Protection Engineering (3th Edition)*-P. J. Dinunno et al., National Fire Protection Association, Quincy, MA, USA, 2002, pp. 5–24.
- [68] "ISO/DTR 24679-6 Fire safety engineering -- Performance of structures in fire - Part 6: Example of an eight-storey reinforced concrete building," Geneva, Switzerland, 2015.
- [69] V. Babrauskas, "Flame lengths under ceilings," *Fire Mater.*, vol. 4, no. 3, pp. 119–126, Sep. 1980, doi: 10.1002/fam.810040304.
- [70] Y. Hasemi, S. Yokobayashi, T. Wakamatsu, and A. Ptchelintsev, "Fire safety of building components exposed to a localized fire- scope and experiments on ceiling/beam system exposed to a localized fire," 1995, Accessed: Feb. 06, 2019. [Online]. Available: https://openlibrary.org/books/OL17168996M/ASIAFLAM_'95.
- [71] B. Y. Lattimer, "SFPE Handbook of Fire Protection Engineering, Fifth Edition, Heat Transfer from Fires to Surface," in *SFPE Handbook of Fire Protection Engineering (5th Edition)*, p. 745.
- [72] J.-M. Franssen and L. Cajot, "Natural Fires in large compartment, Effects caused on the structure by localised fires in large compartments." 1998.
- [73] J. Myllymaki and M. Kokkala, "'Thermal Exposure to a High Welded I-Beam Above a Pool Fire,' First International Workshop on Structures in Fires," Copenhagen, 2000. [Online]. Available: <http://www.structuresinfire.com/corpo/conferences/sif00.pdf>.
- [74] E. Rackauskaite, P. Kotsovinos, A. Jeffers, and G. Rein, "Computational analysis of thermal and structural failure criteria of a multi- storey steel frame exposed to fire," *Eng. Struct.*, vol. 180, no. November 2018, pp. 524–543, 2019, doi: 10.1016/j.engstruct.2018.11.026.
- [75] The British Standards Institution, "BSI Standards Publication BS 7974:2019 Application of Fire Safety Engineering Principles to the Design of Buildings - Code of Practice," *Br. Stand.*, p. 34, 2019.
- [76] R. Qureshi, S. Ni, N. Elhami Khorasani, R. Van Coile, D. Hopkin, and T. Gernay, "Probabilistic Models for Temperature-Dependent Strength of Steel and Concrete," *J. Struct. Eng.*, vol. 146, no. 6, p. 04020102, Jun. 2020, doi: 10.1061/(asce)st.1943-541x.0002621.

- [77] T. Gernay, N. E. Khorasani, and M. Garlock, "Fire Fragility Functions for Steel Frame Buildings: Sensitivity Analysis and Reliability Framework," *Fire Technol.*, vol. 55, no. 4, pp. 1175–1210, Jul. 2019, doi: 10.1007/s10694-018-0764-5.
- [78] S. Ni and T. Gernay, "A framework for probabilistic fire loss estimation in concrete building structures," *Struct. Saf.*, vol. 88, p. 102029, Jan. 2021, doi: 10.1016/j.strusafe.2020.102029.
- [79] R. Felicetti, P. G. Gambarova, and P. Bamonte, "Thermal and mechanical properties of light-weight concrete exposed to high temperature," *Fire Mater.*, 2013, doi: 10.1002/fam.2125.
- [80] M. Benýšek, R. Štefan, and J. Procházka, "Effect of fire model parameter variability on determination of fire resistance of concrete structural members," in *Solid State Phenomena*, 2020, vol. 309 SSP, pp. 208–215, doi: 10.4028/www.scientific.net/SSP.309.208.
- [81] R. Van Coile, D. Hopkin, N. Elhami-Khorasani, and T. Gernay, "Demonstrating adequate safety for a concrete column exposed to fire, using probabilistic methods," *Fire Mater.*, p. fam.2835, Apr. 2020, doi: 10.1002/fam.2835.
- [82] I. Fu, I. Rickard, D. Hopkin, and M. Spearpoint, "Application of Python Programming Language in Structural Fire Engineering - Monte Carlo Simulation," *Interflam 2019 - 15th Int. Fire Sci. Eng. Conf.*, no. September, pp. 1713–1723, 2019.
- [83] T. S. Kho, F. M. Block, and T. G. Lowry, "Determining the fire rating of concrete structures: Case study of using a probabilistic approach and travelling fires," in *Applications of Structural Fire Engineering, Dubrovnik, Croatia*, 2015, pp. 15–16, doi: 10.14311/asfe.2015.015.
- [84] F. M. Block and T. S. Kho, "Engineering an Icon or the Probabilistic-based Structural Fire Engineering of the Battersea Power Station," in *9th International Conference on Structures in Fire, Princeton University, USA, 8–10 June 2016*, pp. 901–908.
- [85] F. M. Block and T. S. Kho, "Determining the fire resistance rating of buildings using the probabilistic method – a state-of-the-art," *Struct. Eng. (Special Issue)*, vol. 1, no. 96, pp. 36–40, 2018.
- [86] M. Heidari, P. Kotsovinos, and G. Rein, "Flame extension and the near field under the ceiling for travelling fires inside large compartments," *Fire Mater.*, vol. 44, no. 3, pp. 423–436, 2020, doi:

10.1002/fam.2773.

- [87] S. Lamont, A. S. Usmani, and M. Gillie, "Behaviour of a small composite steel frame structure in a 'long-cool' and a 'short-hot' fire," *Fire Saf. J.*, vol. 39, no. 5, pp. 327–357, 2004, doi: 10.1016/j.firesaf.2004.01.002.
- [88] E. Rackauskaite, P. Kotsovinos, A. Jeffers, and G. Rein, "Structural analysis of multi-storey steel frames exposed to travelling fires and traditional design fires," *Eng. Struct.*, 2017, doi: 10.1016/j.engstruct.2017.06.055.
- [89] M. Heidari, F. Robert, D. Lange, and G. Rein, "Probabilistic Study of the Resistance of a Simply-Supported Reinforced Concrete Slab According to Eurocode Parametric Fire," *Fire Technol.*, pp. 1–28, Mar. 2018, doi: 10.1007/s10694-018-0704-4.
- [90] F. Robert, L. Davenne, and L. Stoian, "Fire resistance assessment of concrete structures," Brussels. Accessed: Sep. 29, 2020. [Online]. Available: <https://www.scribd.com/document/405544325/06-ROBERT-EC-FireDesign-WS-pdf>.
- [91] E. Rackauskaite and Et. al, "Fire Experiment inside a Very Large and Open-Plan Compartment : x-ONE," *Fire Technol. Press*, pp. 1–29.
- [92] K. Kawagoe, "Fire behaviour in rooms," *Rep. No. 27 , Build. Res. Institute, Tokyo (In Japanese)*, 1958.
- [93] P. H. Thomas and A. Heselden, "Fully developed fires in single compartments; a co-operative research programme of the Conseil international du bâtiment," *Conseil Internationale du Bâtiment Report No. 20, Fire Research Note No. 923*. <https://catalog.princeton.edu/catalog/SCSB-8466674> (accessed Oct. 16, 2020).
- [94] K. D. Steckler, J. G. Quintiere, and W. J. Rinkinen, "Flow induced by fire in a compartment," *Symp. Combust.*, vol. 19, no. 1, pp. 913–920, Jan. 1982, doi: 10.1016/S0082-0784(82)80267-1.
- [95] J. M. Franssen, "Improvement of the parametric fire of Eurocode 1 based on experimental test results," in *Fire Safety Science*, 2000, pp. 927–938, doi: 10.3801/IAFSS.FSS.6-927.
- [96] V. Babrauskas and R. B. Williamson, "Post-flashover compartment fires: Basis of a theoretical

- model,” *Fire Mater.*, vol. 2, no. 2, pp. 39–53, Apr. 1978, doi: 10.1002/fam.810020202.
- [97] J. F. Cadourin and J. M. Franssen, “A tool to design steel elements submitted to compartment fires - OZone V2. Part 1: Pre- and post-flashover compartment fire model,” *Fire Saf. J.*, vol. 38, no. 5, pp. 395–427, Sep. 2003, doi: 10.1016/S0379-7112(03)00014-6.
- [98] B. Bohm and S. Hadvig, “Nonconventional Fully Developed Polyethylene and 564 Wood Compartment Fires,” *Combust. Flame*, vol. 44, pp. 201–221, 1982.
- [99] G. Rein, C. Abecassis-Empis, and R. Carvel, “The Dalmarnock Fire Tests: Experiments and Modelling | Fire Safety Engineering Applied To,” *The School of Engineering and Electronics, University of Edinburgh*, 2007. <https://www.fireseat.eng.ed.ac.uk/dalmarnock-fire-tests-experiments-and-modelling> (accessed Oct. 16, 2020).
- [100] J. Gales, “Travelling Fires and the St. Lawrence Burns Project,” *Fire Technol.*, vol. 50, no. 6, pp. 1535–1543, Oct. 2014, doi: 10.1007/s10694-013-0372-3.
- [101] D. Rush, X. Dai, and D. Lange, “Tisova Fire Test – Fire behaviours and lessons learnt,” *Fire Saf. J.*, vol. 121, p. 103261, May 2021, doi: 10.1016/j.firesaf.2020.103261.
- [102] J. P. Hidalgo *et al.*, “The Malveira fire test: Full-scale demonstration of fire modes in open-plan compartments,” *Fire Saf. J.*, vol. 108, p. 102827, Sep. 2019, doi: 10.1016/J.FIRESAF.2019.102827.
- [103] A. Nadjai *et al.*, “Travelling fire in full scale experimental building subjected to open ventilation conditions,” in *11th International Conference on Structures in Fire (SiF2020)*, 2020, no. December, doi: 10.14264/987a305.
- [104] A. Law, “The Assessment and Response of Concrete Structures Subject to Fire, Ph.D Thesis,” School of Engineering, The university of Edinburgh, 2010.
- [105] D. Rush, D. Lange, J. Machlan, and E. Rackauskaite, “Modelling the Thermal and Structural Performance of a Concrete Column Exposed to a Travelling Fire – Tisova Fire Test,” *Struct. Fire*, vol. 0, no. 0, 2016, Accessed: Oct. 16, 2020. [Online]. Available: <http://www.dpi-proceedings.com/index.php/structures-in-fire/article/view/21506>.

- [106] C. G. Bailey, I. W. Burgess, and R. J. Plank, "Analyses of the effects of cooling and fire spread on steel-framed buildings," *Fire Saf. J.*, vol. 26, no. 4, pp. 273–293, Jun. 1996, doi: 10.1016/S0379-7112(96)00027-6.
- [107] P. Kotsovinos, "Analysis of the structural response of tall buildings under multifloor and travelling fires, Ph.D thesis," The University of Edinburgh, 2013.
- [108] K. Horová, T. Jána, and F. Wald, "Temperature heterogeneity during travelling fire on experimental building," *Adv. Eng. Softw.*, vol. 62–63, pp. 119–130, 2013, doi: 10.1016/j.advengsoft.2013.05.001.
- [109] J. P. Hidalgo *et al.*, "An experimental study of full-scale open floor plan enclosure fires," *Fire Saf. J.*, vol. 89, pp. 22–40, Apr. 2017, doi: 10.1016/j.firesaf.2017.02.002.
- [110] J. Stern-Gottfried, G. Rein, L. a. Bisby, and J. L. Torero, "Experimental review of the homogeneous temperature assumption in post-flashover compartment fires," *Fire Saf. J.*, vol. 45, no. 4, pp. 249–261, Jun. 2010, doi: 10.1016/j.firesaf.2010.03.007.
- [111] P. H. Thomas, "Design Guide: Structural Fire Safety - Workshop Cib W14.," 1986.
- [112] S. Welch, A. Jowsey, S. Deeny, R. Morgan, and J. L. Torero, "BRE large compartment fire tests—Characterising post-flashover fires for model validation," *Fire Saf. J.*, vol. 42, no. 8, pp. 548–567, Nov. 2007, doi: 10.1016/j.firesaf.2007.04.002.

Appendix

The results from the OAT sensitivity analysis for the some of the parameters in are illustrated in Table 2.1 and Table 2.2 are illustrated in Figure A 2.1 to Figure A 2.8. The results demonstrate the effects of varying the input parameters on the maximum rebar temperature and corresponding time.

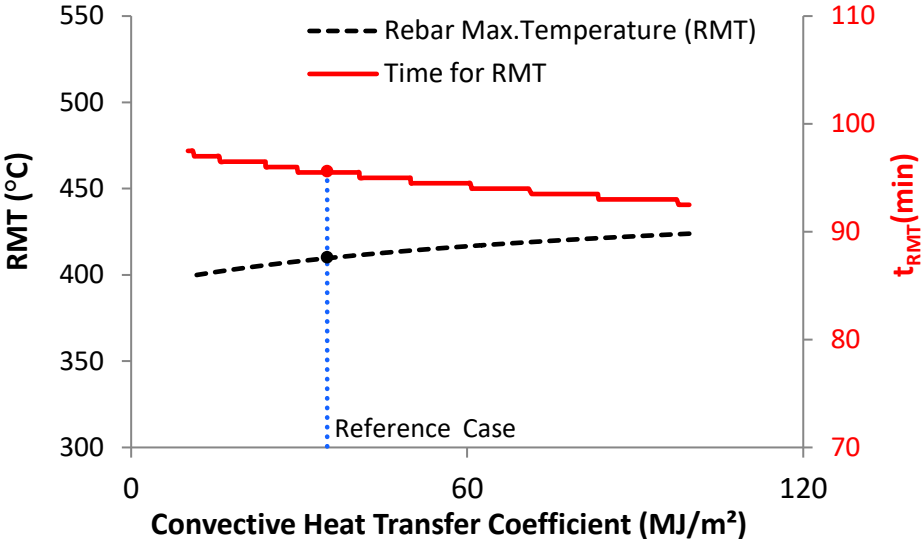


Figure A 2.1 Maximum rebar temperature and corresponding time vs. the convective heat transfer Coefficient of exposed surface. No critical case is found in this range of the parameters.

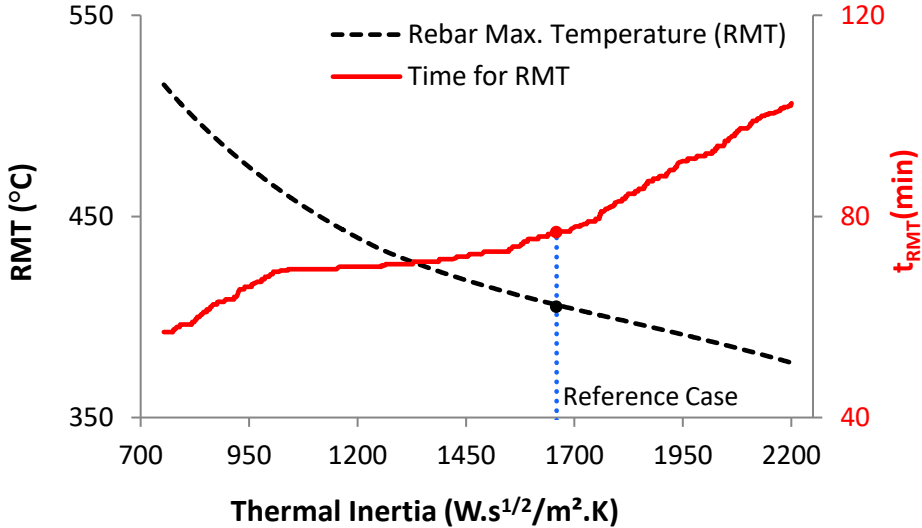


Figure A 2.2 Maximum rebar temperature and corresponding time vs. concrete thermal inertial characteristic. No critical case is found in this range of the parameters.

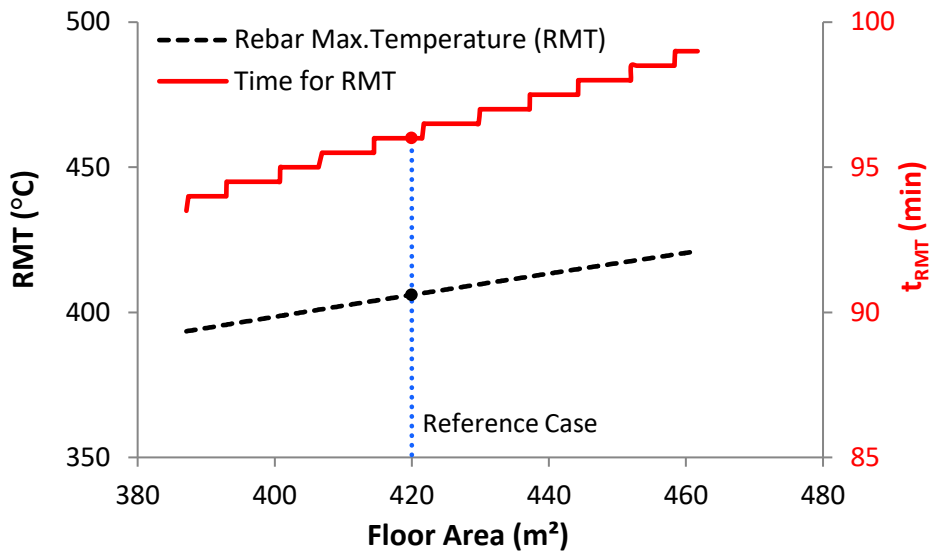


Figure A 2.3 Maximum rebar temperature and corresponding time vs. coefficient in the time. No critical case is found in this range of the parameters.

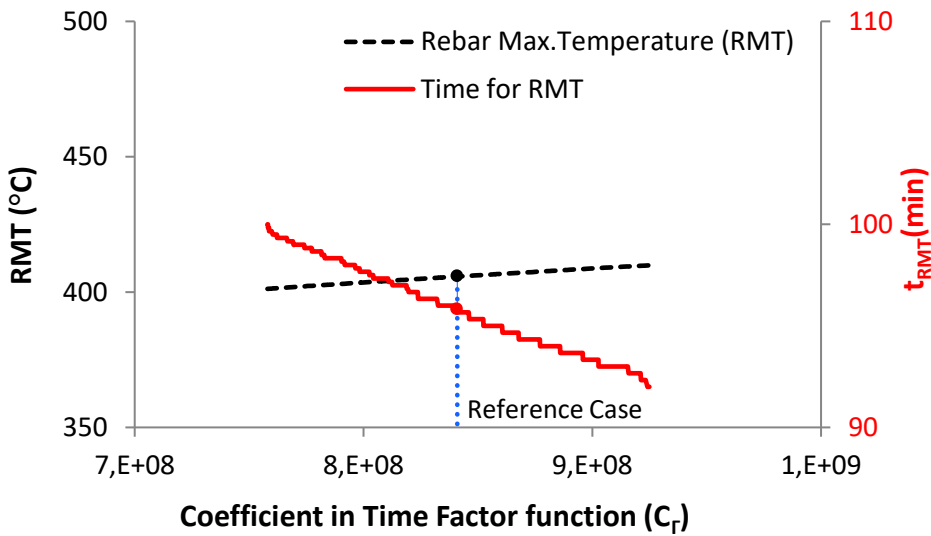


Figure A 2.4 Maximum rebar temperature and corresponding time vs. Coefficient in time factor function Γ . No critical case is found in this range of the parameters.

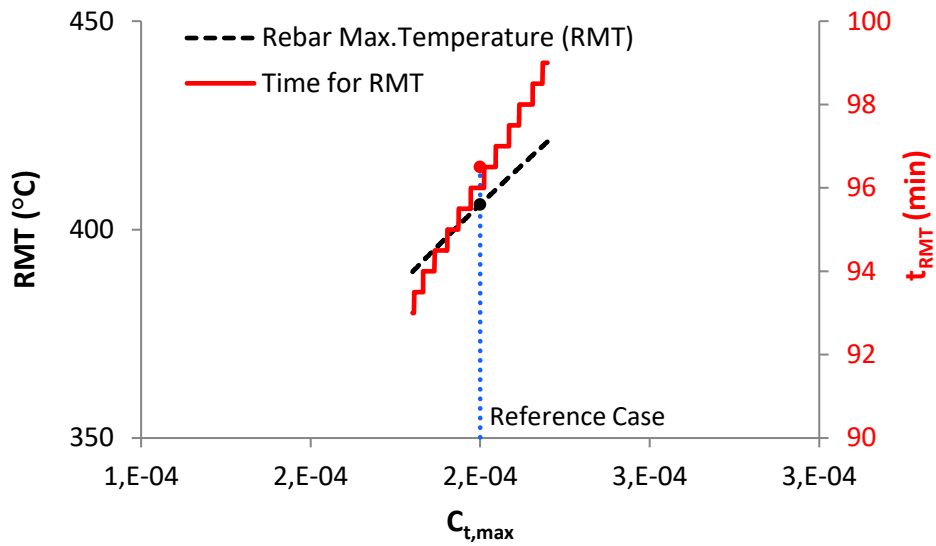


Figure A 2.5 Peak bay temperature and corresponds time vs. coefficient in the time t_{max} . No critical case is found in this range of the parameters.

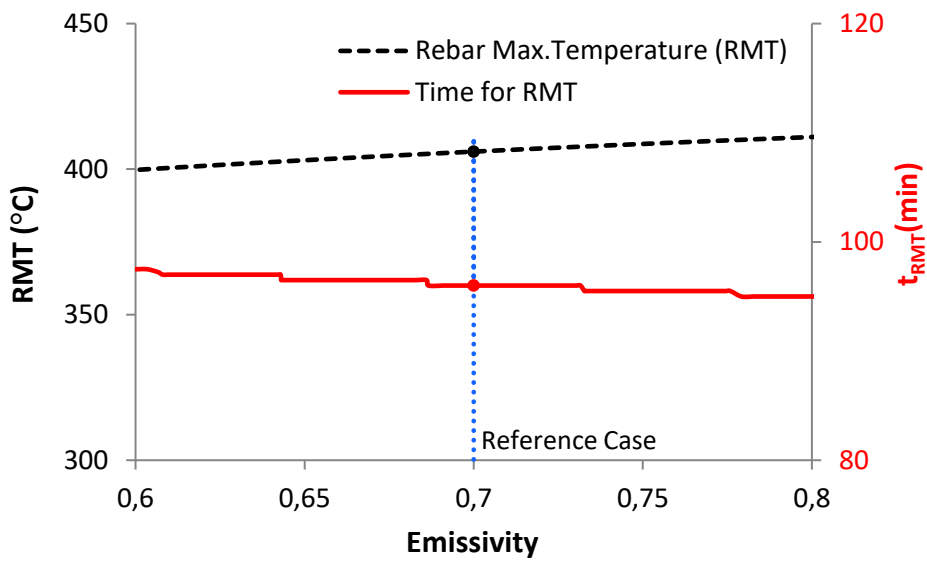


Figure A 2.6 Maximum rebar temperature and corresponding time vs. the emissivity of concrete. No critical case is found in this range of the parameters.

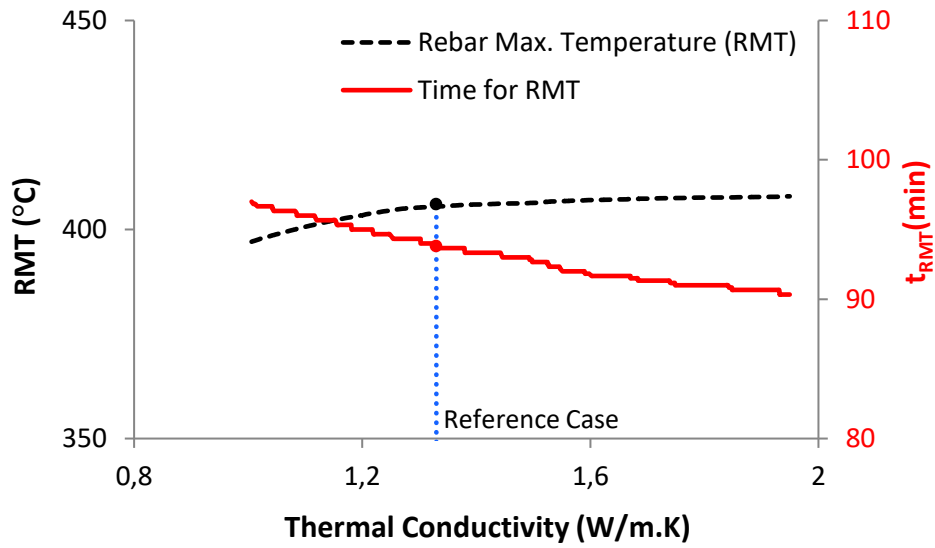


Figure A 2.7 Maximum rebar temperature and corresponding time vs. thermal conductivity of concrete. No critical case is found in this range of the parameters.

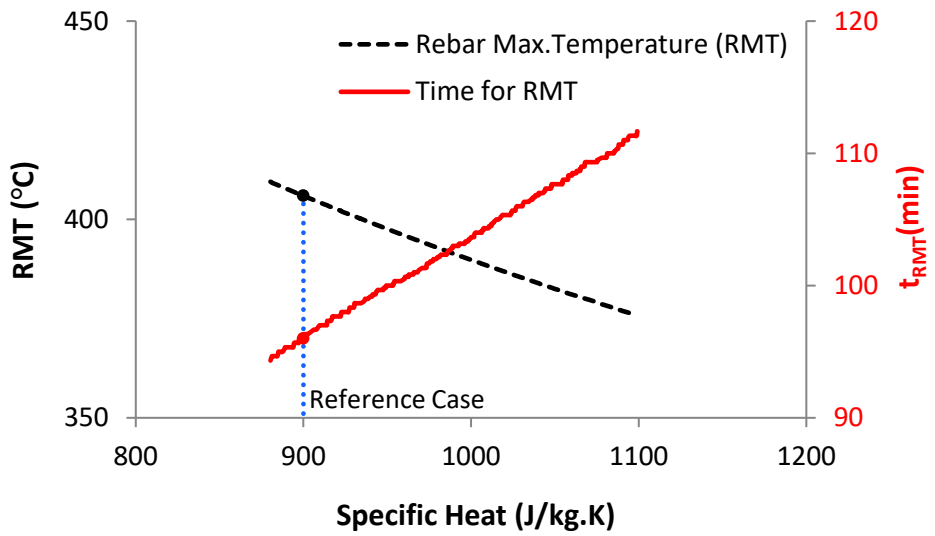


Figure A 2.8 Maximum rebar temperature and corresponding time vs. specific heat of boundary of enclosure. No critical case is found in this range of the parameters.